Applications of high-aspect-ratio gold nanowires fabricated by nanoskiving

Zhao, Zhiyuan

Applications of High-Aspect-Ratio Gold Nanowires Fabricated by Nanoskiving

Zhiyuan Zhao

Applications of High-Aspect-Ratio Gold Nanowires Fabricated by Nanoskiving

Zhiyuan Zhao

PhD thesis

University of Groningen
The Netherlands

Zernike Institude PhD thesis series 2016-05
ISSN: 1570-1530
ISBN: 978-90-367-8898-4 (Printed version)
ISBN: 978-90-367-8897-7 (Electronic version)

This Ph.D. Project was carried out in the research group Chemistry of (Bio) Molecular Materials and Devices part of the Stratingh Institute for Chemistry and Zernike Institute for Advanced Materials, University of Groningen, The Netherlands.

university of groningen / faculty of mathematics and natural sciences

university of groningen

Applications of High-Aspect-Ratio Gold Nanowires Fabricated by Nanoskiving

PhD thesis

to obtain the degree of PhD at the
University of Groningen
on the authority of the
Rector Magnificus Prof. E. Sterken
and in accordance with
the decision by the College of Deans.

This thesis will be defended in public on

Friday 27 May 2016 at 11.00 hours

by

Zhiyuan Zhao

born on 27 February 1986
in Liaoning, China

Supervisor

Prof. R.C. Chiechi

Assessment Committee

Prof. J.T.M. de Hosson
Prof. J. Ye
Prof. H. Zhang

谨以此书献给我最深爱的妻子

Dedicated to my beloved wife

Table of Contents

Chapter 1

Introduction

1.1 From nanoscience to nanotechnology

How small is nanometer? One nanometer (nm) is equivalent to one billionth of a meter (10^{-9} m). A few illustrative examples as followed: there are 25,400,000 nanometers in an inch; the width of a pinhead is around one million nanometers; most atoms are 0.1 to 0.2 nm wide; red blood cells are about 7000 nm in diameter; if a marble were one nanometer, then one meter would be the size of the Earth. Figure 1.1 shows the illustration of three examples of the size and the scale. When structures are made in the nanometer size range, they can display interesting and unusual properties.

What is nanoscience? The study of objects that occur in this range of sizes, which begins with molecules, and ends with the smallest structures that can be fabricated (by lithography), is known as nanoscience.[1-3] It comprises the overlap between the chemistry of materials, solid-state physics, biology, engineering and other fields. Nano-structured materials exhibit properties that cannot be found in bulk materials, which include statistical mechanical effects, as well as quantum mechanical effects, for example "quantum size effect" where materials at the nanoscale display enhanced properties, such as higher strength, lighter weight, increased control of light spectrum, and greater chemical reactivity, and special optical, electronic, chemical and thermal properties. For

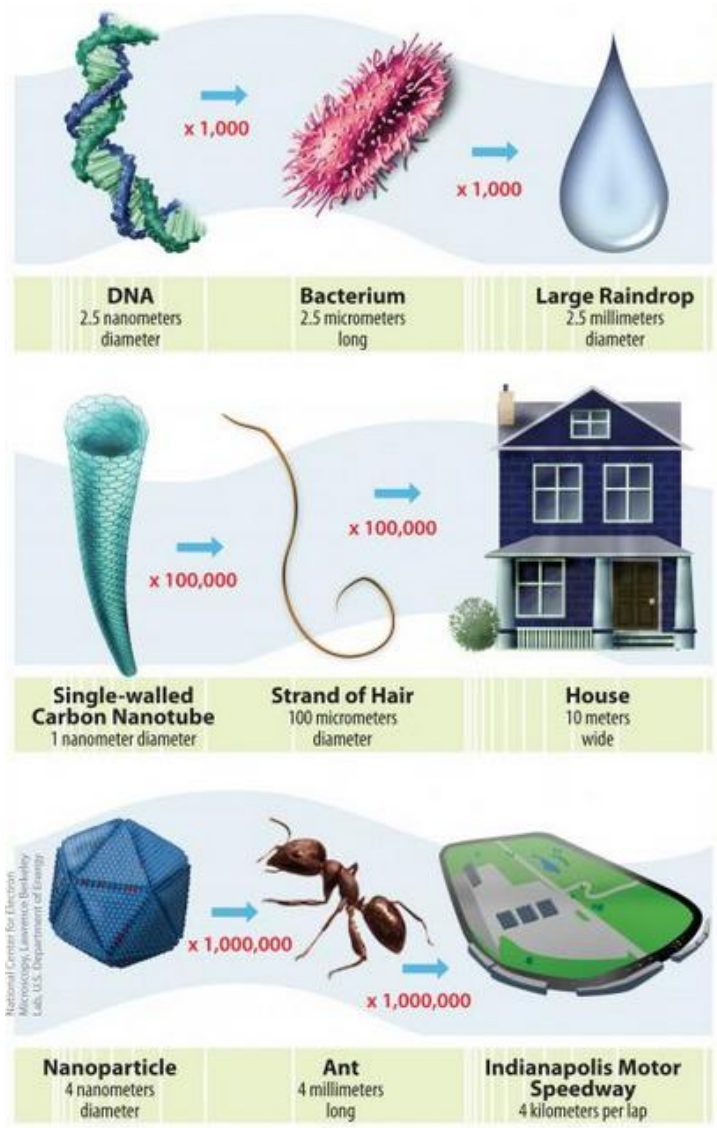

Figure 1.1 An illustration of the size and the scale of nanotechnology, showing how small things at the nanoscale are. Source from the official website of the United States National Nanotechnology Initiative.

example, the melting point of a solid material will be greatly reduced when the material is fabricated to nanostructures, which is necessary for the synthesis of defect-free nanowires, and it is possible to purify nanostructures at a modest temperature.[4] Nanostructures are in a range of sizes in which quantum phenomena are the ultimate basis of the properties of atoms and molecules such as electron confinement,[5-7] near-field optical effects,[8-10] quantum entanglement,[11,12] electron tunneling,[13-17] and ballistic charge transport.[18]

After modern nanotechnology came into its own with the development of the scanning tunneling microscope in 1981, Eric Drexler popularized the word “nanotechnology”. Scientific research really expanded over the last decades. Nanotechnology refers to manipulating and controlling atoms or molecules to construct nanoscale objects, and fabricating nanoscale-widgets from bulk materials. It involves the engineering of functional systems at the nanoscale, and is more than just mixing nanomaterials together. One important advantage of nanotechnology is access to very high surface-area to volume ratios (*e.g.*, nanowire). Nanotechnology is helping to improve, even revolutionize, information technology, energy, environmental science, medicine, national security, food safety, and transportation, among many others. Nanotechnology can be used to greatly extend the well-used toolkits of materials science, and there already exists in over 800 everyday commercial products that rely on nanoscale materials and processes. Nanotechnology has already being used in computing, communications, and other electronics applications to fabricate faster, cheaper, and more efficient devices.[19,20] Nanotechnology has the potential to revolutionize medical and biotechnology tools and procedures so that they are more portable, cheaper, safer, and easier to administer. Figure 1.2 lists an impressive array of applications of zero-dimensional (0D) nanoparticles.[21] The applications cover an extremely broad range of markets and industries including biomedical and cancer treatment, surface coatings, electronics, and building materials, *etc.* Meantime, one-dimensional (1D) nanostructures are also expected to play an important role in various applications, specially, in electronic, photonic, mechanical, biological, sensing, and energy-conversion applications. Thus, the ability to develop methods for manufacturing nanostructures, devices and systems is

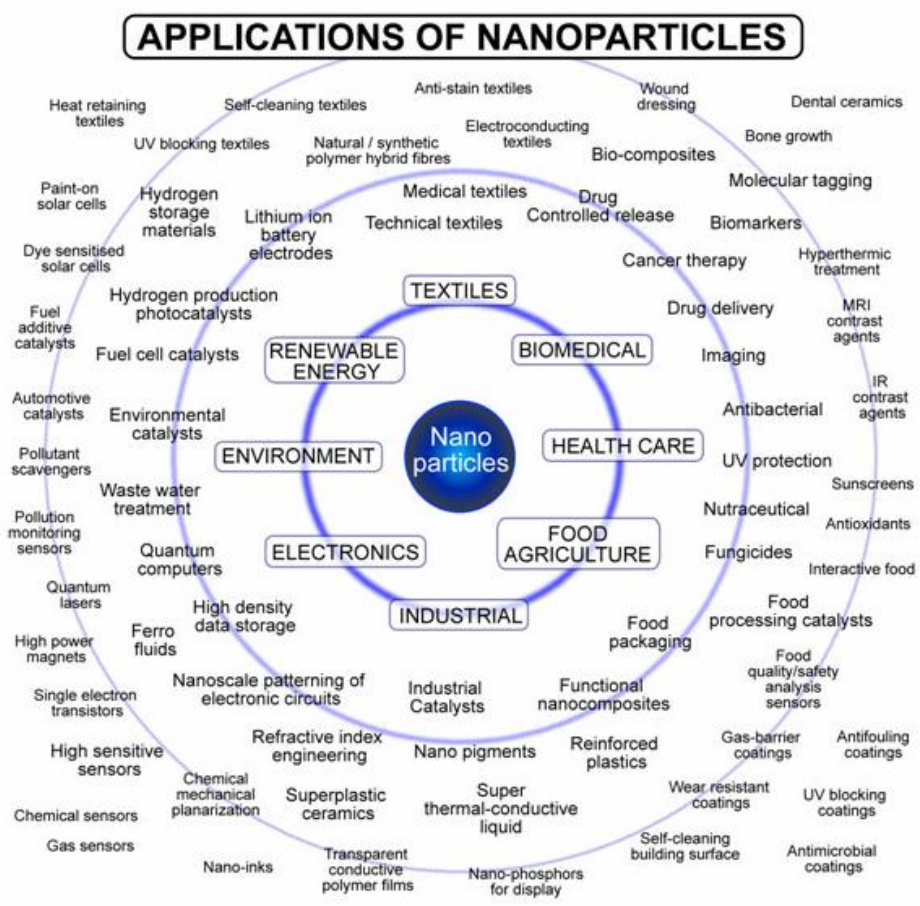

Figure 1.2 Major applications of nanoparticles.[21]

essential to modern nanoscience and nanotechnology, with the potential for low-cost, high-throughput production.

1.2 Nanofabrication

With the development of nanotechnology, nanofabrication, the patterning a material into nanoscale structures, is becoming an increasingly important part of modern scientific and technological fields, such as the production of integrated circuits, information storage devices, display units, sensors, actuators, and microfluidic devices.[22] Nanofabrication generates patterns that have minimum dimensions defined to be below 100 nm.[23] The ability to fabricate nanoscale structures is a key element for creating functional nanoscale devices and novel materials. In this regard, a number of techniques have been invented and engaged in producing nanostructures. Fabrication and investigation of patterned surfaces are active areas of research in chemistry, physics, materials science, and biology. Methods of nanofabrication used to generate nanoscale structures and nanostructured materials are commonly summarized as “top-down” and “bottom-up”.[24] In the “top–down” approach, the nanoscale features are written directly or transferred onto a substrate by various methods of lithography. The “bottom-up” approach uses interactions between molecules or colloidal particles to assemble discrete nanoscale structures in two and three dimensions.

The fabrication of nanostructures from bulk materials acts as a bridge between the macroscopic world and the nanoscopic world, and becomes the escalating demand. Obviously, the low-throughput and expensive conventional technique for nanofabrication are largely restricted to planar or very small substrates, and are incompatible with many organics, biologics, and other materials.[25-27] The limitations of these conventional approaches motivate the exploration and development of new, or “unconventional”, nanofabrication techniques. A tremendous effort has been devoted to develop unconventional approaches to nanofabrication in research.[28] These techniques create opportunities to fabricate nanostructures on nonplanar surfaces and over large areas. They are probably the only techniques that are applicable to biological and organic materials. The ability of any technique to generate nanoscale structures rapidly and

inexpensively will be a key factor that influences the acceptance of that technique. Unconventional techniques have the potential to be an operationally simple, low-cost method for nanofabrication. Many new applications for nanostructures require structures that are simpler, extend over larger areas, and that are less expensive than integrated circuits. Thus, unconventional approaches help to explore a wide range of applications of nanoscience and nanotechnology, especially connecting to electrical and optical engineering.[24]

1.3 One-dimensional nanowires

A type of nanostructures such as wires, rods, belts, and tubes, which have been called one-dimensional nanostructures, have received extensive attention duo to their unique applications in chemistry, physics, and fabrication of nanoscale devices.[29] The lateral dimensions of these one-dimensional nanostructures are in the range of 1 to 100 nm. They are expected to play an important part as functional units in the fabrication of electronic, optical, and electrochemical devices.[30] Among the various one-dimensional nanostructures, nanowires possess unique characteristics. They have high surface-to-volume ratio, large tolerance for mechanical deformations, and abilities to be integrated into electronic devices and interface with other microscopic and nanoscopic systems, which have led to an explosion of applications using nanowires. Nanowires have been explored as building blocks to fabricate nanoelectronic devices including p-n junctions, field-effect transistor (FET), and resonant tunneling diodes, *etc*. For example, semiconductor nanowires were assembled into cross-bar p-n junctions with controllable electrical characteristic integrated nanoscale FET arrays.[31] Furthermore, nanowires as photonic components provide a versatile platform for optical and optoelectronic devices. Nanowires are natural one-dimensional optical waveguides for optical cavities due to photons propagating along their longitudinal axes.[32] For nanowires made of noble metal or semiconductor materials, they have surface plasmon resonance properties that can, for example, be used to enhance the efficiency of solar cells.[33-35] Another major application for nanowires is the sensing of molecules, either for chemical, biological medical, or environmental detection.[36,37] The extremely high surface-to-volume ratios

make them extremely sensitive to species on surfaces. In addition to photovoltaics, nanowires can convert solar energy into chemical fuels for photosynthesis.[38] Although a number of advanced nanolithographic techniques can be used to fabricate 1D nanowires,[39] such as focus-ion-beam (FIB), electron-beam (e-beam), and deep UV lithography, further achievement of large quantities 1D nanostructures through cost-effect approaches for a range of materials, still requires great ingenuity. In contrast, unconventional methods might be exploited as an alternative strategy to generate 1D nanostructures in terms of cost, throughput, and material diversity.[23]

1.4 Strategies of fabricating nanowires

For developing a suitable method to generate 1D nanowires, the simultaneous control over dimensions, morphology and uniformity needs to be adequately considered. In the past decades, a variety of strategies have been demonstrated for achieving nanowires growth (Figure 1.3): dictation by the anisotropic crystallographic structure of a solid, confinement of a liquid droplet as in the vapor-liquid-solid process, direction through the use of a template, kinetic control provided by a capping reagent, self-assembly of 0D nanostructures, and size reduction of a 1D microstructure.[40]

1.4.1 Highly anisotropic crystallization

The formation of 1D nanowires from crystallization is the evolution of a solid from a vapor, a liquid, or a solid phase that involves two fundamental steps: nucleation and growth.[41] The building blocks of a solid can aggregate into small nuclei through nucleation, as the concentration of them becomes high. Then these nuclei can serve as seeds for further growth with the more building blocks. Many solid materials can grow into 1D nanowires through highly anisotropic crystallographic structure. One of the best known examples is poly(sulphur nitride) due to its metallic and superconducting properties.[42] Its uniform nanowires of hundreds of micrometers in length can be grown from the vapor phase. Many polymeric and biological systems exist in fibrous form such as cellulose, and collagen. Furthermore, there are two ideal inorganic systems for producing nanowires: molybdenum chalcogenides and chalcogens. Molybdenum chalcogenides, with the

formula $M_2Mo_6X_6$ (M=Li, Na; X=Se, Te), contain hexagonal close-packed linear chains.[43] Chalcogens (Se and Te) can be packed into hexagonal lattice through van der Waals interaction.[44] As shown in Figure 1.4, uniform nanowires of t-Se were synthesized with lateral dimensions in the range of 10 nm to 100 nm.

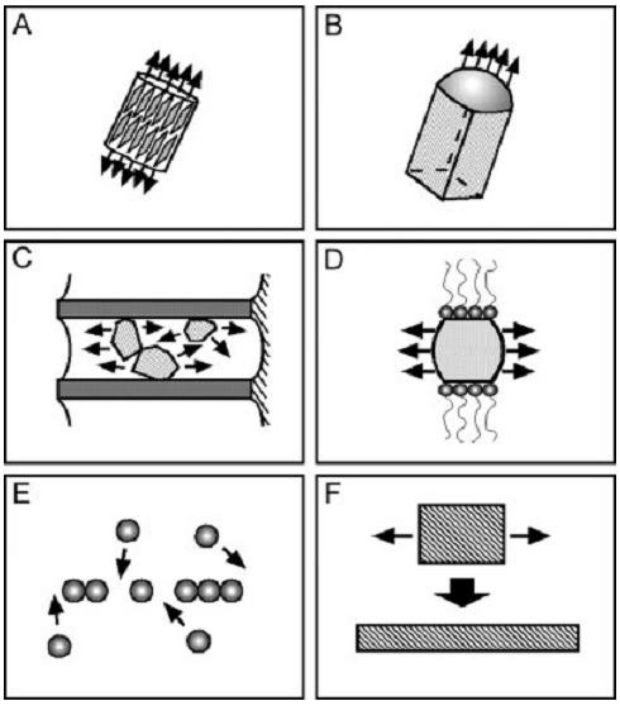

Figure 1.3 Schematic illustrations of six different strategies have been demonstrated for achieving 1D growth: (A) dictation by the anisotropic crystallographic structure of a solid; (B) confinement of a liquid droplet as in the vapor-liquid-solid process; (C) direction through the use of a template; (D) kinetic control provided by a capping reagent; (E) self-assembly of 0D nanostructures; and (F) size reduction of a 1D microstructure.[40]

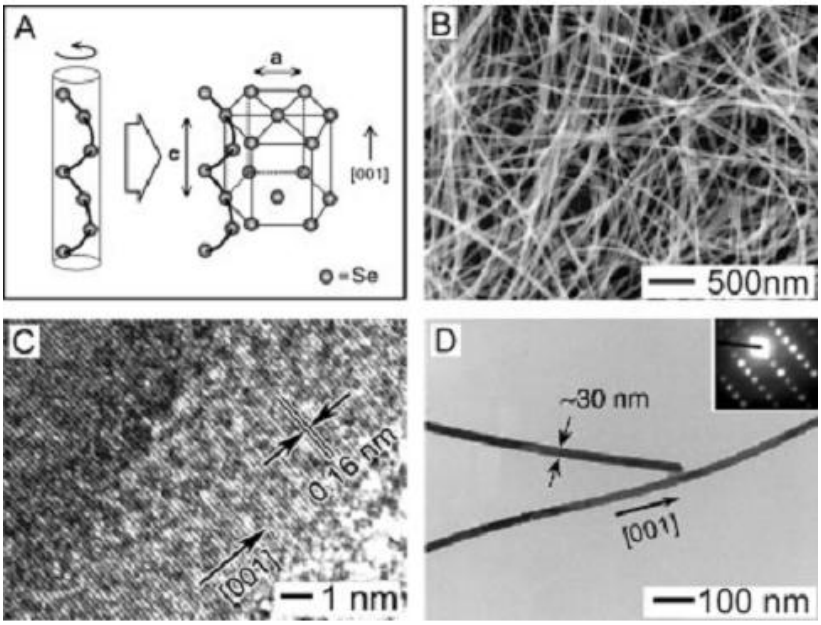

Figure 1.4 (A) An illustration of the crystal structure of t-Se composed of hexagonally packed, helical chains of Se atoms parallel to each other along the c-axis. (B) A scanning electron microscopy (SEM) image t-Se nanowires with a mean diameter of 32 nm. (C) A high-resolution transmission electron microscopy (TEM) image recorded from the edge of an individual nanowire showing well-resolved interference fringe spacing of 0.16 nm that agrees well with interplanar distance between {003} lattice planes. (D) A TEM images of two t-Se nanowires, indicating the dimensional uniformity along each wire. The inset shows an electron diffraction pattern obtained from the middle portion of an individual nanowire, confirming that the growth direction was along the <001> axis.[44]

1.4.2 Template-directed synthesis

In template-directed synthesis approach, the template simply induces different materials to be produced and shaped into 1D nanowires. When the template only serves as a scaffold physically, it is often removed using an etching method in order to obtain the nanowires. For example, metal and metal oxide materials were deposited onto a rotating anodized aluminum oxide membrane template using collimated electron beam evaporation to fabricate arrays of nanotubes.[45] In a chemical process, the template is usually removed as the reaction proceeds to directly obtain the nanowires. A number of templates have been successfully utilized, including templating against features on the surfaces of solid substrates (Figure 1.5);[46] channels within a porous material;[47] self-assembled structures from organic surfactants, block copolymer or biological macromolecules;[48] and existing nanostructures as template.[49] The strategy of template-directed synthesis provides a simple, high-throughput and cost-effective procedure that allows the 1D nanowires produce on the surface of a template in a single step.

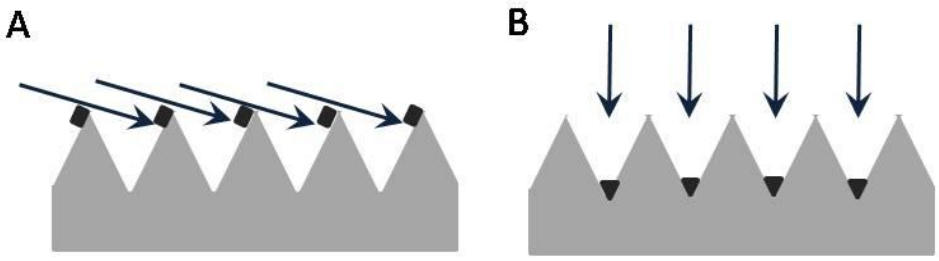

Figure 1.5 Schematic illustrations of procedures that generated 1D nanowires by (A) shadow evaporation and (B) reconstruction at the bottom of V-grooves;

1.4.3 Generic methods suitable for all solid materials

If a solid material has a highly anisotropic crystal structure, the growth of 1D nanowires is relatively simple. However, many solids have isotropic crystal structures and breaking symmetry is necessary to generate nanowires. The vapor-liquid-solid (VLS) process is an elegant method to lower symmetry to produce nanowires through introducing a solid-liquid interface. As shown in Figure 1.6, the nucleation and growth of nanowire

through a typical VLS process happens after gaseous reactants dissolve into nanoscale liquid droplets of catalyst metals.[50,51] By controlling the supersaturation at a relatively low level, solvothermal processes can be used to induce any solid material into nanowires.[52] Capping reagents have been introduced to change the free energies of the various facets of a solid to kinetically control growth rate of nanowires.[53] In principle, these methods are suitable for all types of solid materials, no matter whether they have an anisotropic or isotropic crystalline structure.

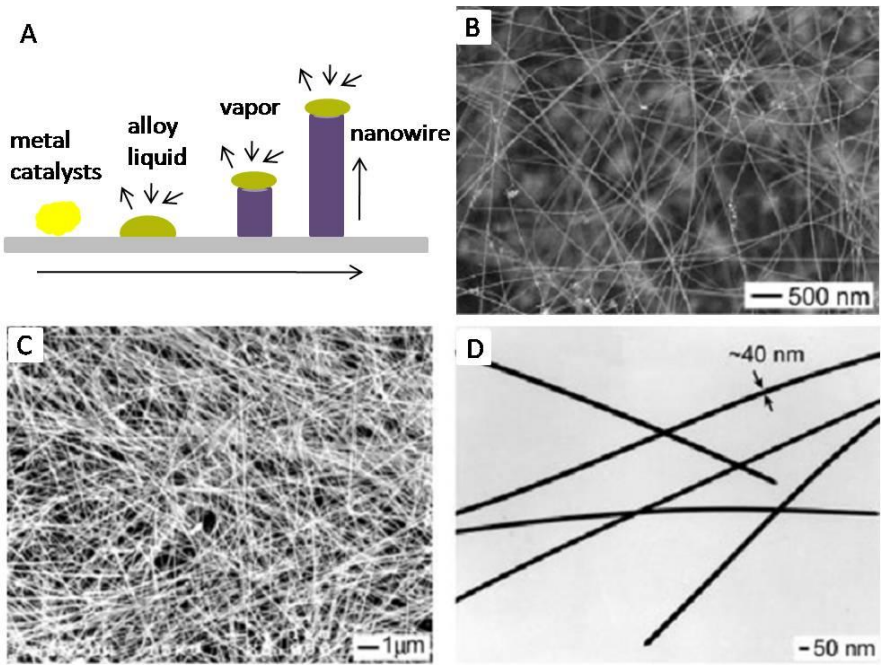

Figure 1.6 (A) Schematic illustration showing the growth of a nanowire via the vapor-liquid-solid mechanism. (B) SEM image of Ge nanowires prepared using the chemical vapor-transport method.[50] (C) SEM and (D) TEM images of silver nanowires (after purification and centrifugation) that were synthesized at 160 °C.[53]

1.4.4 Self-assembly of nanoparticles and size reduction

Self-assembly has been extensively used as a bottom-up approach to generate complex nanostructures with different scales. Colloid particles as building blocks can form wire-like structure through self-assembly. Gold nanoparticles were filled in the pores of an alumina or polymer membrane, or were manipulated by a field or a mechanical probe to induce the formation of 1D linear chains.[54] In addition, nanoparticles could be assembled into nanostructures by templating against features on the surface of solid substrates.[55] The

size of 1D microstructures, which can be fabricated using conventional microfabrication techniques, can be reduced to 1D nanostructures below 100 nm. The use of isotropic deformation of a polycrystalline or amorphous material, anisotropic etching of a single crystal, and near-field optical lithography with a phase-shift mask are three of the most promising methods for size reduction.[56-58]

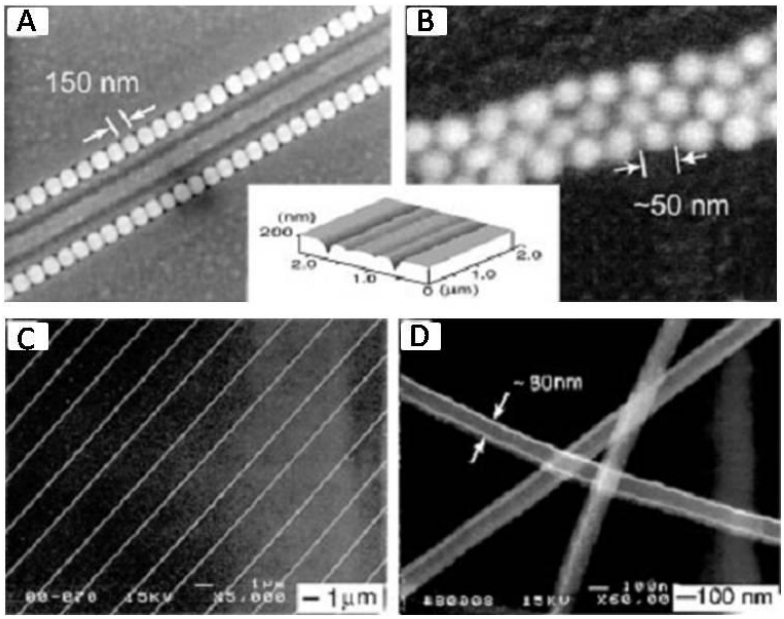

Figure 1.7 SEM images of nanowire structures that were assembled from 150 nm polystyrene beads (A), and 50 nm Au colloids (B), by templating against 120 nm-wide channels patterned in a thin photoresist film.[55] (C) The scanning electron diffraction image of a 2D parallel array of nanobelts (130 nm wide and 100 nm thick) that were fabricated from single-crystalline silicon using near-field optical lithography. (D) An SEM image of these silicon nanobelts after they had been oxidized in air at 850 ^{o}C for 1h, and then lifted-off in HF solution. These nanowires had lateral dimension of ~80 nm and lengths up to ~2 cm.[58]

Although a variety of approaches have been developed to achieve the synthesis and growth of 1D nanowires, it is still difficult to produce ultra-long nanowires with precise control over each dimension and manipulate single-nanowire. A low-cost technique of nanofabrication, nanoskiving, can simply and fast produce a number of high-aspect-ratio (>10000:1) nanowires directly from sectioning thin films. All three dimensions of these nanowires can be controlled accordingly. At the meantime, each nanowire is able to be transferred onto any substrate with accurate manipulation and alignment.

1.5 Nanoskiving

The ultramicrotome can be used by itself, or combination with soft lithography to achieve greater flexibility. This process is known as “nanoskiving” and is one of the thriving methods in the field of nanofabrication. Developed by Whitesides and coworkers, nanoskiving is a form of edge lithography used to fabricate nanostructures that are difficult or impossible to generate using other approaches. This technique combines the deposition of thin film with sectioning thin film embedded in a polymer matrix using an ultramicrotome.[59,60] Compared to conventional methods for nanofabrication, nanoskiving is of efficiency, simplicity and is compatible with soft materials such as conjugated polymers and organic compounds, requiring no special associated tools and clean rooms.

1.5.1 Description of the procedure

Nanoskiving involves three major steps: (1) depositing a thin metallic, semiconducting, or polymeric film onto a substrate; (2) embedding the film in an epoxy or thiol-ene polymer block;[61] and (3) sectioning the block into slabs using an ultramicrotome. As shown in Figure 1.8, an ultramicrotome has a stereomicroscope, sample arm that holds the sample to be sectioned, and a movable stage that holds the diamond knife.[60] The diamond knife is fixed on a knife holder that is like boat-like and filled with water for sections floating on the surface. In preparation for sectioning, a face of the block of epoxy will be trimmed to the width of the diamond knife using a razor blade. The sample arm advances in controlled steps towards the diamond knife and is forced against the edge of the diamond knife. After each advance, the sample arm returns to its starting position to generate successive sections that float on the surface of the water in the boat.[59] The rate of cutting produces about one section per 2 s. One block can be sectioned to produce hundreds of thousands of sections by nanoskiving. There are two general mechanisms proposed for the process of sectioning: true sectioning, in which the edge of the knife remains in contact with both the facet of block and the nascent slab; and in crack initiation and propagation, the knife splits or cleaves the block.[62] The two mechanisms dominate, respectively, in soft materials such as metals and alloys, and brittle materials such as minerals and ceramics.[63]

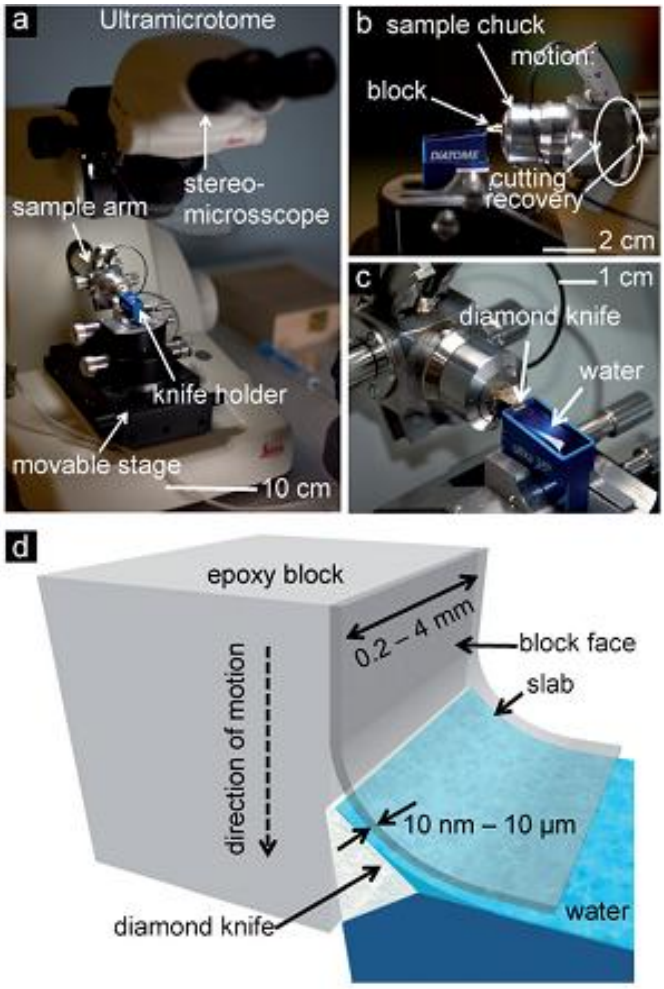

Figure 1.8 Photographs and schematic drawings of the tools of ultramicrotomy and nanoskiving. (a) A photograph of a Leica UC6 ultramicrotome. (b) A side wiew of the sample chuck and knife holder as the epoxy block impringes upon the knife. (c) A top view of the single-crystalline diamond blade and the water-filled trough. (d) A schematic drawing of the sectioning process. The epoxy block contacts the diamond knife, and the slab slides onto the surface of water.[60]

The simplest structure that can be produced by sectioning thin film using nanoskiving is nanowire. Figure 1.9 is a schematic drawing of the procedure to fabricate nanowire by nanoskiving. The first step is a polymeric substrate obtained by curing a prepolymer on a flat or topographical poly(dimethylsiloxane) (PDMS) stamp formed by soft lithography.[64] The low free energy of the surface of PDMS enables the two polymers to be separated easily. A thin gold film is deposited onto the epoxy substrate by a number of deposition methods. This epoxy-supported metal film can be cut in thin strips using a saw and placed into an embedding mold, which is then filled with more epoxy. Prior to sectioning, a face of the block of epoxy must be trimmed to the width of the diamond knife using a razor blade. The resulting block is sectioned with ultramicrotome to generate epoxy slabs that float on the surface of the water in the boat, and that can be collected and transferred all together (submerging a substrate below the floating epoxy slabs and pulling the substrate toward the slabs) or one by one using a collection loop. After collection of the sections to a substrate, the embedding epoxy resin can be removed by exposure to oxygen plasma to produce free-standing gold nanowires. The dimensions of the nanowire are determined by the width of strips by rough cutting, the thickness of the deposited thin film, and the thickness of the epoxy slabs generated by ultramicrotome. A number of different materials have been successfully formed nanostructures with nanoskiving.[65] As shown in Figure 1.10, there are four kinds of materials that are sectioned into nanowires: gold (metal), silicon dioxide (ceramic), germanium (semiconductor), and poly(3-hexylthiophene) (polymer).

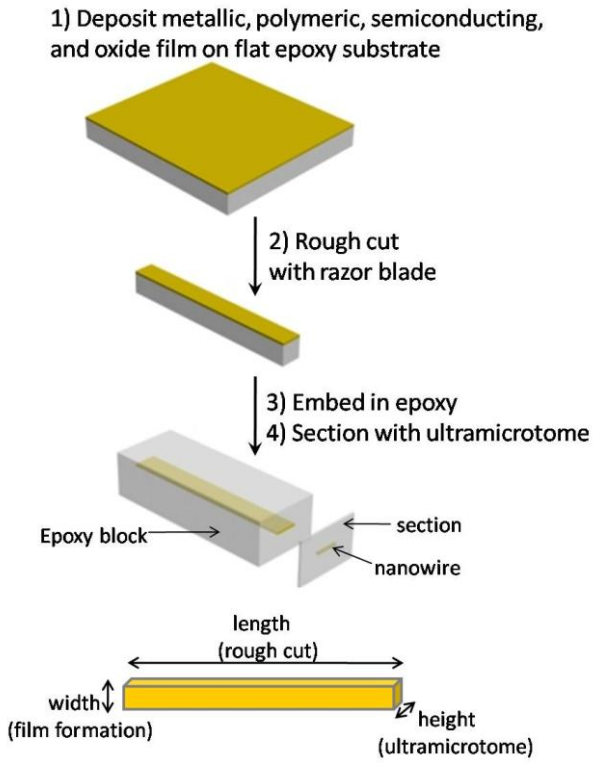

Figure 1.9 Summary of the process used for fabricating nanowires of loosely defined length (>100 μm) by sectioning thin films. 1) A piece of flat epoxy served as the substrate for deposition of a metallic, polymeric, semiconducting, or oxide film. 2) A rough cut provided a strip of this film supported by epoxy, 3) which we embedded in additional epoxy. 4) Ultrathin sectioning and removal of the epoxy matrix formed nanowires in which each dimension was controlled by a different step of the process.

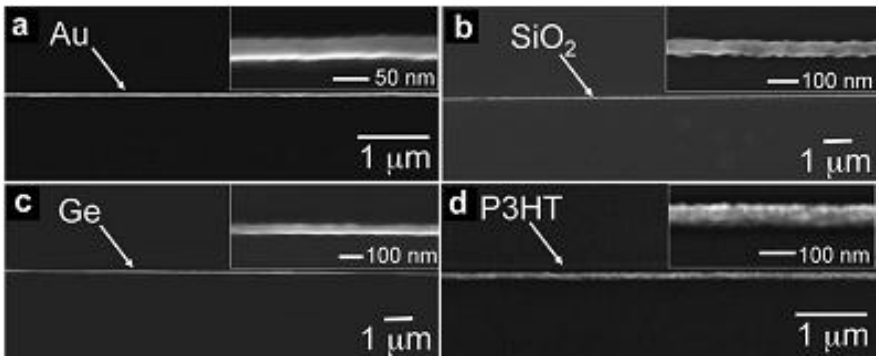

Figure 1.10 Examples of representative spans of nanowires of four classes of materials formed by obtaining sections of the metallic, ceramic, semiconducting, and polymeric thin films. Each nanowire is physically continuous over >100 μm.[65]

1.5.2 Fabrication of complex nanostructures

Sectioning a thin film generates nanowires that are the simplest structure by nanoskiving, can be millimeters in length. Nanoskiving clearly has the ability to fabricate more complex nanostructures by incorporating topographically patterned substrate and selecting the sectioning orientation, which would be difficult or impossible to be fabricated by conventional approaches.[59] As combination with nanoskiving, the patterned film can be formed by photolithography, soft lithography or electron-beam lithography, *etc*. Some examples of complex gold nanostructures fabricated using nanoskiving are shown in Figure 1.11. Sectioning of epoxy replicas formed by photolithographically patterned strips resulted in a free-standing, step-shaped nanostructure.[66] A multilayer, composite Au/SiO_2 film prepared using successively depositing could be sectioned by nanoskiving to generate parallel gold nanowires with spacing.[66] free standing gold nanostructures (*e.g.*, rings or double loop-shaped structures) with high aspect ratios were generated based on sectioning with a microtome.[67] Magnetic mooring can be used to manipulate and position nanowires of different types on a surface.[68] Addressable, sub-3 nm gold gaps were fabricated by nanoskiving using SAMs as templates to construct metal-molecule-metal tunneling junctions.[69] Thus, to establish the versatility of nanoskiving, epoxy slabs containing arrays of multicomponent nanostructures in arbitrary patterns can be readily placed even on any substrate.

1.5.3 Applications of nanostructures

Nanostructures fabricated by nanoskiving have extensive applications in electronics and optics. An array of metallic nanowires as nanoelectrodes embedded in an epoxy slab was fabricated and placed on a conductive substrate, so that only the top facet of the nanowires were plated for electrochemistry.[70] Arrays of polymer nanowires formed by sectioning could act as an ordered bulk heterojunction solar cell.[71] Parallel nanowires separated by a nanogap were fabricated using nanoskiving, which are electrically addressable are useful for a number of applications.[72] Single-crystal gold microplates prepared using chemical synthesis could be sectioned by nanoskiving to generate gold nanowires for plasmonic waveguiding.[73] Two-dimensional arrays of nanostructures

formed by combination of replica molding with sectioning could have plasmonic properties to excite localized surface plasmon resonances and integrate with optical fibers.[74,75]

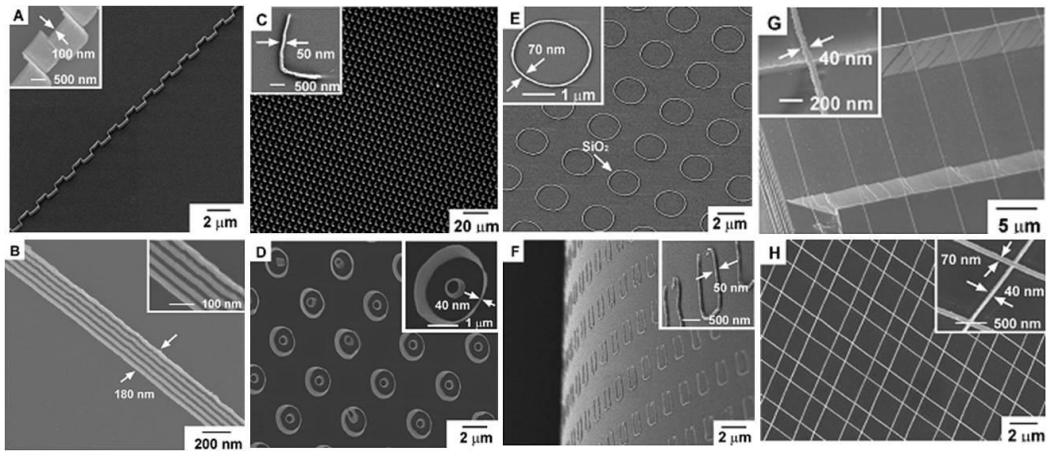

Figure 1.11 A) SEM image of 100 nm wide, 1 μm high step-shaped nanostructures fabricated by nanoskiving a metal-coated epoxy substrate prepatterned with 1 μm wide lines with 1 μm spacing.[66] B) SEM image of parallel gold nanowires with 20 nm spacing, by nanoskiving a flat epoxy substrate coated with a multilayer, composite Au/SiO_2 film, followed by complete etching of the SiO_2 spacing layers using reactive ion etching.[66] C) Dark-field optical microscopy image of "L-shaped" nanostructures patterned over a ~3 mm^2 area by nanoskiving in a direction parallel to the patterned substrate.[74] D) SEM image of double loop-shaped gold nanostructures.[67] E) SEM image of loop-shaped SiO_2 nanostructures on a SiO_2/Si(100) substrate by using gold loop-shaped nanostructures as a physical mask during reactive ion etching with CF_4. F) SEM image of an array of "U-shaped" gold nanostructures positioned on the curved surface of a glass rod.[66] G) SEM image of parallel gold nanowires draped over 20 μm wide truncated-V-shaped, etched in a Si(100) surface.[66] H) Cross-bar nanostructures fabricated by the orthogonal stacking of two epoxy slabs containing arrays of gold nanowires on top of each other. The insets are high-magnification SEM images of the nanostructures.

1.6 Outline of the thesis

The goal of this thesis is to integrate ultra-long gold nanowires fabricated by nanoskiving, which was introduced in this chapter, into various functional devices that are applicable for electronics, optics, and sensing of chemical or biological species. We focus on extending the range of the applications of nanoskiving.

By applying aluminum sacrificial layer, in chapter 2, air-nanogap electrodes composed of two high-aspect-ratio gold nanowires are fabricated by nanoskiving. They are addressable and controllable. Large gaps are readily accessible by this method, while molecule-gaps focus on the order of the length scale of those molecules. Thus, the air-gap forms metal/air/metal tunneling junction to be investigated electrical measurements, and length-dependence also is measured.

Nanometric gaps between noble metals constitute one of the most explored structures. Especially for sub-10 nm gaps, they can serve as “hot spots” to generate highly confined energy. The fabrication of a series of 1D, millimeter-long nanogaps with tunable sub-10 nm gap-widths based on nanoskiving is demonstrated in chapter 3. These nanogaps are optimized by simulation and experiment. Further, 2D nanogap arrays were rapidly generated by introducing surface patterning techniques. Notably, novel 3D nanogap arrays that are hard to achieve by conventional nanofabrication via a unique stacking procedure were successively built, possessing higher integration and much enhanced plasmonic coupling.

In chapter 4, the millimeter-long gold nanowires fabricated by nanoskiving were integrated into microfluidic devices. To demonstrate the utility of integrating discrete nanowires into microfluidic channels, two device architectures were designed, one active and one passive. The active device demonstrates a two-terminal, hot-wire anemometer that samples flow in the center of the channel in which the entire surface area of the wire is in contact with the fluid being measured. The passive device uses the nanowires as substrates for the attachment of long DNA molecules for the study of elongation.

In chapter 5, a transfer approach is developed to use a film of polymer as carrier layer and aluminum as sacrificial layer to transfer and manipulate sections that are fabricated

by nanoskiving. This transfer process enables the preparation of sections at one-time to be used many times. Meantime, the manipulation and positioning of sections can construct 2D or 3D structures, even heterostructures that can improve the potential applications of nanoskiving. In addition, this process is applicable to other structures or arrays of structures as well.

Bibliography

1. A. Dowling, R. Clift, N. Grobert, D. D. Hutton, R. Oliver, B. O. O'Neill, J. Pethica, N. Pidgeon, J. Porritt, J. Ryan, A. Seaton, S. Tendler, M. Welland, and R. Whatmore, Nanoscience and nanotechnologies: Opportunities and uncertainties, A Report by The Royal Society & The Royal Academy of Engineering, London, July 2004.

2. C. P. Poole Jr., and F. J. Owens, Introduction to Nanotechnology, Wiley-Interscience, Hoboken, NJ, 2003.

3. C. M. Lieber, Nanoscale science and technology: Building a big future from small things. MRS Bull. 2003, 28(77): 486-491.

4. P. Buffat, and J. P. Borel, Size effect on the melting temperature of gold articles. Phys. Rev. A 1976, 13(6): 2287-2298.

5. P. M. Petroff, A. Lorke, and A. Imamoglu, Epitaxially self-assembled quantum dots. Phys. Today 2001, 54(5): 46-52.

6. S. A. Empedocles, R. Neuhauser, K. Shimizu, and M. G. Bawendi, Photoluminescence from single semiconductor nanostructures. Adv. Mater. 1999, 11(15): 1243-1256.

7. F. H. Julien, and A. Alexandrou, Controlling artificial atoms. Science 1998, 282(5393): 1429-1430.

8. M. M. Alkaisi, R. J. Blaikie, and S. J. McNab, Nanolithography in the evanescent near field. Adv. Mater. 2001, 13(12-13): 877-887.

9. J. Jiang, K. Bosnick, M. Maillard, and L. Brus, Single molecule Raman spectroscopy at the junctions of large Ag nanocrystals. J. Phys. Chem. B 2003, 107(37): 9964-9972.

10. M. J. Levene, J. Korlach, S. W. Turner, M. Foquet, H. G. Craighead, and W. W. Webb, Zero-mode waveguides for single-molecule analysis at high concentrations. Science 2003, 299(5607): 682-686.

11. J. Bao, A. V. Bragas, J. K. Furdyna, and R. Merlin, Optically induced multispin entanglement in a semiconductor quantum well. Nat. Mater. 2003, 2(3): 175-179.

12. A. N. Cleland, J. S. Aldridge, D. C. Driscoll, and A. C. Gossard, Nanomechanical displacement sensing using a quantum point contact. Appl. Phys. Lett. 2002, 81(9): 1699-1701.

13. J. A. Stroscio, and D. M. Eigler, Atomic and molecular manipulation with the scanning tunneling microscope. Science 1991, 254(5036): 1319-1326.

14. D. Fracasso, H. Valkenier, J. C. Hummelen, G. C. Solomon, and R. C. Chiechi, Evidence for Quantum Interference in SAMs of Arylethynylene Thiolates in Tunneling Junctions with Eutectic Ga-In (EGaIn) Top-Contacts. J. Am. Chem. Soc. 2011, 133(24): 9556-9563.

15. H. B. Akkerman, P. W. M. Blom, D. M. de Leeuw, and B. de Boer, Towards molecular electronics with large-area molecular junctions. Nature, 2006, 441 (7089): 69-72.

16. J. M. Beebe, V. B. Engelkes, L. L. Miller, and C. D. Frisbie, Contact resistance in metal-molecule-metal Junctions based on aliphatic SAMs: Effects of surface linker and metal work function. J. Am. Chem.Soc. 2002, 124(38): 11268-11269.

17. E. A. Weiss, R. C. Chiechi, G. K. Kaufman, J. K. Kriebel, Z. Li, M. Duati, M. A. Rampi, and G. M. Whitesides. Influence of defects on the electrical characteristics of mercury-drop junctions: Self-assembled monolayers of n-alkanethiolates on rough and smooth silver. J. Am. Chem. Soc. 2007, 129(14): 4336-4349.

18. A. I. Yanson, G. Rubio Bollinger, H. E. Van Den Brom, N. Agrait, and J. M. Van Ruitenbeek, Formation and manipulation of a metallic wire of single gold atoms. Nature 1998, 395(6704): 783-785.

19. A. V. Akimov, A. Mukherjee, C. L. Yu, D. E. Chang, A. S. Zibrov, P. R. Hemmer, H. Park, and M. D. Lukin, Generation of single optical plasmons in metallic nanowires coupled to quantum dots. Nature 2007, 450(7168): 402-406.

20. R. F. Pease, and S. Y. Chou, Lithography and other patterning techniques for future electronics. Proc. IEEE 2008, 96(2): 248-270.

21. T. Tsuzuki, Commercial scale production of inorganic nanoparticles. Int. J. Nanotechnol. 2009, 6(5-6): 567-578.

22. M. Geissler, and Y. N. Xia, Patterning: Principles and some new developments. Adv. Mater. 2004, 16(15): 1249–1269.

23. Y. Xia, J. A. Rogers, K. E. Paul, and G. M. Whitesides, Unconventional methods for fabricating and patterning nanostructures. Chem. Rev. 1999, 99(7): 1823-1848.

24. B. D. Gates, Q. Xu, M. Stewart, D. Ryan, C. G. Willson, and G. M. Whitesides, New Approaches to nanofabrication: molding, printing, and other techniques. Chem. Rev. 2005, 105(4): 1171-1196.

25. B. J. Wiley, D. Qin, and Y. Xia, Nanofabrication at high throughput and low cost. ACS Nano 2010, 4(7): 3554-3559.

26. Y. Xia, E. Kim, X. M. Zhao, J. A. Rogers, M. Prentiss, and G. M. Whitesides, Complex optical surfaces formed by replica molding against elastomeric masters. Science 1996, 273(5273): 347-349.

27. E. J. Smythe, M. D. Dickey, G. M. Whitesides, and F. Capasso, A technique to transfer metallic nanoscale patterns to small and non-planar surfaces. ACS Nano 2009, 3(1): 59-65.

28. B. D. Gates, Q. Xu, J. C. Love, D. B. Wolfe, and G. M. Whitesides, Unconventional nanofabrication. Annu. Rev. Mater. Res. 2004, 34(1): 339-371,.

29. J. Hu, T. W. Odom, and C. M. Lieber, Chemistry and physics in one dimension: Synthesis and properties of nanowires and nanotubes. Acc. Chem. Res. 1999, 32(5): 435-445.

30. N. P. Dasgupta, J. Sun, C. Liu, S. Brittman, S. C. Andrews, J. Lim, H. Gao, R. Yan, and P. Yang, 25th Anniversary article: Semiconductor nanowires-synthesis, characterization, and applications. Adv. Mater. 2014, 26(14): 2137-2184.

31. Y. Huang, X. Duan, Q. Wei, and C. M. Lieber, Directed assembly of one-dimensional nanostructures into functional networks. Science 2001, 291(5504): 630-633.

32. D. J. Sirbuly, M. Law, P. Pauzauskie, H. Yan, A. V. Maslov, K. Knutsen, C. Z. Ning, R. J. Saykally, and P. Yang, Optical routing and sensing with nanowire assemblies. Proc. Natl. Acad. Sci. USA 2005, 102(22): 7800-7805.

33. R. F. Oulton, V. J. Sorger, T. Zentgraf, R. M. Ma, C. Gladden, L. Dai, G. Bartal, and X. Zhang, Plasmon lasers at deep subwavelength scale. Nature 2009, 461(7264): 629-632.

34. W. U. Huynh, J. J. Dittmer, and A. P. Alivisatos, Hybrid nanorod-polymer solar cells. Science 2002, 295(5564): 2425-2427.

35. J. Wallentin, N. Anttu, D. Asoli, M. Huffman, I. Aberg, M. H. Magnusson, G. Siefer, P. Fuss-Kailuweit, F. Dimroth, B. Witzigmann, H. Q. Xu, L. Samuelson, K. Deppert, and M. T. Borgstrom, InP nanowire arrays solar cells achieving 13.8% efficiency by exceeding the ray optics limit. Science 2013, 339(6123): 1057-1060.

36. M. Law, H. Kind, F. Kim, B. Messer, and P. Yang, Photochemical sensing of NO_2 with SnO_2 Nanoribbon nanosensors at room temperature. Angew. Chem. Int. Ed. 2002, 41(13): 2405-2408.

37. G. Zheng, F. Patolsky, Y. Cui, W. U. Wang, and C. M. Lieber, Multiplexed electrical detection of cancer markers with nanowire sensor arrays. Nat. Biotechnol. 2005, 23(10): 1294-1301.

38. Y. Tachibana, L. Vayssieres, and J. R. Durrant, Artificial photosynthesis for solar water-splitting. Nat. Photonics 2012, 6(8): 511-518.

39. F. Cerrina, and C. Marrian, A path to nanolithography. MRS Bull. 1996, 21(12): 56-62.

40. Y. Xia, P. Yang, Y. Sun, Y. Wu, B. Mayers, B. Gates, Y. Yin, F. Kim, and H. Yan, One-Dimensional Nanostructures: Synthesis, characterization, and applications. Adv. Mater. 2003, 15(5): 353-389.

41. E. I. Givargizov, Highly Anisotropic Crystals. Reidel, Dordrecht, The Netherlands 1987.

42. J. Stejny, R. W. Trinder, and J. Dlugosz, Preparation and structure of poly(sulphur nitride) whiskers. J. Mater. Sci. 1981, 16(11): 3161-3170.

43. J. Song, B. Messer, Y. Wu, H. Kind, and P. Yang, MMo_3Se_3 ($M=Li^+$, Na^+, Rb^+, Cs^+, NMe_4^+) nanowire formation via cation exchange in organic solution. J. Am. Chem. Soc. 2001, 123(39): 9714-9715.

44. B. Gates, Y. Yin, and Y. Xia, A solution-phase approach to the synthesis of uniform nanowire of crystalline selenium with lateral dimensions in the range of 10-30 nm. J. Am. Chem. Soc. 2000, 122(50): 12582-12583.

45. M. D. Dickey, E. A. Weiss, E. J. Smythe, R. C. Chiechi, F. Capasso, and G. M. Whitesides, Fabrication of arrays of Metal and Metal oxide nanotubes by shadow evaporation, ACS Nano, 2008, 2, 800-808

46. J. Jorritsma, M. A. M. Gijs, J. M. Kerkhof, and J. G. H. Stienen, General technique for fabricating large arrays of nanowires. Nanotechnology 1996, 7(3): 263-265.

47. G. Meng, Y. J. Jung, A. Cao, R. Vajtai, and P. M. Ajayan, Controlled fabrication of hierarchically branched nanopores, nanotubes, and nanowires, Proc. Natl. Acad. Sci. USA 2005, 102, 7074-7078.

48. M. A. El-Sayed, Some interesting properties of metals confined in time and nanometer space of different shapes. Acc. Chem. Res. 2001, 34(4): 257-264.

49. Y. Yin, Y. Lu, Y. Sun, and Y. Xia, Silver nanowires can be directly coated with amorphous silica to generate well-controlled coaxial nanocables of silver/silica. Nano Lett. 2002, 2(4): 427-430.

50. Y. Wu, and P. Yang, Germanium nanowire growth via simple vapor transport. Chem. Mater. 2000, 12(3): 605-607.

51. T. Kuykendall, P. J. Pauzauskie, Y. Zhang, J. Goldberger, D. Sirbuly, J. Denlinger, and P. Yang, Crystollographic alignment of high density gallium nitrude nanowire arrays, Nat. Mater. 2004, 3, 524-528.

52. X. Wang, and Y. Li, Selected-control hydrothermal synthesis of α-and β-MnO_2 single crystal nanowires. J. Am. Chem. Soc. 2002, 124(12): 2880-2881.

53. Y. Sun, Y. Yin, B. T. Mayers, T. Herricks, and Y. Xia, Uniform silver nanowire synthesis by reducing $AgNO_3$ with ethylene glycol in the presence of seeds and poly(vinyl pyrrolidone). Chem. Mater. 2002, 14(11): 4736-4745.

54. G. Hornyak, M. Kroll, R. Pugin, T. Sawitowski, G. Schmid, J. O. Bovin, G. Karsson, H. Hofmeister, and S. Hopfe, Gold clusters and colloids in alumina nanotubes. Chem. Eur. J. 1997, 3(12): 1951-1956.

55. Y. Yin, Y. Lu, B. Gates, and Y. Xia, Temple-assisted self-assembly: a practical route to complex aggregates of monodispersed colloids with well-defined sizes, shapes, and structures. J. Am. Chem. Soc. 2001, 123(36): 8718-8729.

56. R. M. Penner, M. J. Heben, T. L. Longin, and N. S. Lewis, Fabrication and use of nanometer-sized electrodes in electrochemistry. Science 1990, 250(4984): 1118-1121.

57. J. L. Wilbur, E. Kim, Y. Xia, and G. M. Whitesides, Lithographic molding: a convenient route to structures with sub-micrometer dimensions. Adv. Mater. 1995, 7(7): 649-652.

58. Y. Yin, B. Gates, and Y. Xia, A soft lithography approach to the fabrication of nanostructures of single crystalline silicon with well-defined dimensions and shapes. Adv. Mater. 2000, 12(19): 1426-1430.

59. Q. Xu, R. M. Rioux, M. D. Dickey, and G. M. Whitesides, Nanoskiving: A new method to produce arrays of nanostructures. Acc. Chem. Res. 2008, 41(12): 1566-1577.

60. D. J. Lipomi, R.V. Martinez, and G. M. Whitesides, Use of thin sectioning (nanoskiving) to fabricate nanostructures for electronic and optical applications. Angew. Chem. Int. Ed. 2011, 50(37): 8566-8583.

61. R. L. Mays, P. Pourhossein, D. Savithri, J. Genzer, R. C. Chiechi, and M. D. Dickey, Thiol-containing polymeric embedding materials for nanoskiving. 2013, 1(1): 121-130.

62. J. D. Acetarin, E. Carlemalm, E. Kellenberger and W. Villiger, Correlation of some mechanical properties of embedding resins with their behavior in microtomy. J. Electron Microsc. Tech. 1987, 6(1): 63-79.

63. T. F. Malis, and D. Steele, Ultramicrotomy for materials science. Mater. Res. Soc. Symp. Proc. 1990, 199: 3-50.

64. Y. Xia, and G. M. Withesides, Soft lithography. Angew. Chem. Int. Ed. 1998, 37(5): 550-575.

65. D. J. Lipomi, R.V. Martinez, R. M. Rioux, L. Cademartiri, W. F. Reus, and G. M. Whitesides, Survey of materials for nanoskiving and influence of the cutting process on the nanostructures produced. ACS Appl. Mater. Interfaces 2010, 2(9): 2503-2514.

66. Q. Xu, R. M. Rioux, and G. M. Whitesides, Fabrication of complex metallic nanostructures by nanoskiving. ACS Nano 2007, 1(3): 215-227.

67. Q. Xu, R. Perez-Castillejos, Z. F. Li, and G. M. Whitesides, Fabrication of high-aspect-ratio metallic nanostructures using nanoskiving. Nano Lett. 2006, 6(9): 2163-2165.

68. D. J. Lipomi, F. Ilievski, B. J. Wiley, P. B. Deotare, M. Loncar, and G. M. Whitesides, Integrated fabrication and magnetic positioning of metallic and polymeric nanowires embedded in thin epoxy slabs. ACS Nano 2009, 3(10): 3315-3325.

69. P. Pourhossein, and R. C. Chiechi, Directly addressable, sub-3 nm gold nanogaps fabricated by nanoskiving using self-assembled monolayers as templates. ACS Nano 2011, 6(6): 5566-5573.

70. Q. Xu, B. D. Gates, and G. M. Whitesides, Fabrication of metal structures with nanometer-scale lateral dimensions by sectioning using a microtome. J. Am. Chem. Soc. 2004, 126(5): 1332-1333.

71. D. J. Lipomi, R. C. Chiechi, W. F. Reus, and G. M. Whitesides, Laterally ordered bulk heterojunction of conjugated polymers: Nanoskiving a jelly roll. Adv. Funct. Mater. 2008, 18(21): 3469-3477.

72. M. D. Dickey, D. J. Lipomi, P. J. Bracher, and G. M. Whitesides, Electrically addressable parallel nanowires with 30 nm spacing from micromolding and nanoskiving. Nano Lett. 2008, 8(12): 4568-4573.

73. B. J. Wiley, D. J. Lipomi, J. M. Bao, F. Capasso, and G. M. Whitesides, Fabrication of surface plasmon resonators by nanoskiving single crystalline gold microplates. Nano Lett. 2008, 8(9): 3023-3028.

74. Q. Xu, J. Bao, R. M. Rioux, R. Perez-Castillejos, F. Capasso, and G. M. Whitesides, Fabrication of large-area patterned nanostructures for optical applications by nanoskiving. Nano Lett. 2007, 7(9): 2800-2805.

75. D. J. Lipomi, R. V. Martinez, M. A. Kats, S. H. Kang, P. Kim, J. Aizenberg, F. Capasso, and G. M. Whitesides, Patterning the tips of optical fibers with metallic nanostructures using nanoskiving. Nano Lett. 2011, 11(2): 632-636.

Chapter 2

Fabrication of Air-gap Electodes Composed of Two Ultra-long Gold Nanowires by Nanoskiving

2.1 Introduction

In the 20th century, the electronic revolution sustained the advances of integrated circuit technologies that have given us computers and consumer electronics with powerful processing capabilities for changing life.[1,2] Nanometer-sized devices as the next generation electronic circuit elements possess lower power consumption and a higher level of integration. However, the relatively slow pace of the miniaturization of electronic devices limits the rapid development of semiconductor technology in the practical application of electronics. The fabrication of nanodevices and circuits is important for the examination of material properties at the nanometer, even molecular scale.[3] Because of the excellent characteristics and promising potential, nanogap electrodes that have the potential to serve as building blocks for electronic devices and have attracted extensive attention for several decades. They can exhibit various characteristic phenomena. The integration of nanogap electrodes and organic molecules or other nanometer-sized components (small molecules,[4] biomolecules,[5,6] polymers,[7] and carbon nanotubes,[8] *etc*.) can effectively function as memory, switches, and transistors for investigating resistance-switching effects,[9,10] detection of DNA or proteins,[11-13] and sensing hydrogen gas,[14] *etc*.

For the precise control over the spacing of nanogaps, several effective methods of fabricating nanogap electrodes have been reported: mechanical break junctions,[15,16] electron-beam lithography,[17] electromigation,[18] electrochemical plating,[19] focused ion beam lithography,[20] shadow mask evaporation,[21] scanning probe and atomic force microscopy lithography,[22] on-wire lithography,[23] *etc*. Despite their own characteristics and promising results, there remain many challenges to making nanogaps with precise and controllable manner that are electrically addressable, specifically, for conventional lithography. The fabrication of nanogap electrodes conveniently and efficiently in large numbers is a key step for the construction of nanodevices.

One way of utilizing nanogap electrodes is the formation of metal/insulator/metal tunneling junctions, which are barriers between two electrically conductive materials.[24-26] Electrons pass through the barriers by the process of quantum tunneling. At molecular length scales (<10 nm), quantum behavior may provide basis for electronic devices.[27] A number of studies focused on a single molecules or self-assembly monolayers (SAMs) as constituent components of junctions for molecular electronics that are supposed to achieve nanometer resolution with low-costs and while integrating complex functions at the same time.[16,28-31] Much of the work on molecular junctions is to investigate electrical characteristics in terms of the molecular structure.[32-37] The first report based on measurement of current through molecular junctions of fatty acids reproduced the theoretical concept of a rectangular tunneling-barrier model.[38] Since the molecular rectifier was proposed to predict the feasibility of constructing a functional molecular device in 1974, the field of molecular electronics has attracted significant interest.[39] Tunneling currents decrease exponential with increasing molecular length (the width of barrier). By measuring the dependence of current-voltage (*I*-*V*) characteristics on molecular length, charge transport through molecular junctions is mainly studied in such systems.[40-42]

A simply and low-cost approach to fabricate nanogap is nanoskiving, which has been introduced in Chapter 1. These nanogap were fabricated without a clean room or

lithographic processes using vacuum-deposited aluminum as a sacrificial spacer layer to separate nanowires of gold followed by nanoskiving.[43] If combination with photolithography, nanoskiving has produced electrically addressable nanowire separated by 30 nm-thick layer of SiO_2.[44] Recently, sub-3 nm gaps were fabricated by nanoskiving using self-assembled monolayer as templates. Length-dependent electrical measurements on alkanedithiols demonstrated that the SAM-templated addressable nanogaps (STAN) are defined by the lengths of the molecules in the SAMs.[45] But when air serves as insulator instead of molecules to form air-gap junction, what are their electrical characteristics? In this chapter, air-nanogap electrodes composed of two high-aspect-ratio gold nanowires by nanoskiving are presented. They are addressable and controllable. These nanogaps were defined using aluminum as spacers that could be removed by acid to achieve precise tuning for the width of gaps on-demand, requiring no additional lithographic steps. The large gaps are readily accessible by this method, while molecule-gaps focus on the order of the length scale of those molecules. The air-gap forms metal/air/metal tunneling junction to be investigated electrical measurements, and length-dependence also is measured.

2.2 Experimental section

A silicon wafer was treated in an air plasma cleaner and then exposed to (tridecafluoro-1,1,2,2,-tetrahydrooctyl)trichlorosilane vapor for 1 h to passivate the surface of the silicon wafer. After a 100 nm-thick film of gold was deposited through a Teflon master onto the silicon wafer, 8 mL of Epofix epoxy prepolymer (from Electron Microscopy Science) was used to cover the entire wafer. After curing epoxy for 3 h at 60 ^{o}C, the gold layer was template-stripped by peeling the epoxy from the wafer so that the gold features remain adhered to the epoxy. The same Teflon mask was placed back over the gold features, but laterally offset by 67% of the gold features. A 5 nm, 10 nm, 15 nm or 20 nm aluminum layer was first deposited followed by a second 100 nm-thick layer of gold deposition through the mask and entire Au/Al/Au sandwich structure was embedded in epoxy prepolymer, which was then cured for 3 h at 60 ^{o}C. The gold features were cut

using a jeweler's saw into small pieces and placed into separate wells in a polyethylene microtome mold, which was then filled with epoxy prepolymer, and cured 3 h at 60 ^{o}C to form epoxy blocks.

To prepare for sectioning, a prepared block was mounted in the sample chuck of the ultramicrotome (Leica EM UC-6), and its top was trimmed to the width of the diamond knife (4 mm Diatome Ultra 35^{o}) in a trapezoid shape around the embedded structure using a razor blade (Figure 2.1). The block was first pre-cutting with the ultramicrotome using a glass knife to make a smooth surface on the top of the block. After alignment of the flat mold face with the diamond knife edge, diamond knife was utilized to section the block to 100 nm at 1 mm/s to produce epoxy sections containing the sandwich structures. The resulting sections were collected from the surface of the water in the boat to a glass substrate by placing the substrate under the surface of the water and raising it slowly. These sections were dried at 60 ^{o}C to improve adhesion to the substrate. To remove aluminum layer, the sections were immersed into 2 M HCl. After 2 h, the sections were removed from the HCl, rinsed with ethanol, and dried at 60 ^{o}C.

Figure 2.1 A diagram of ultramicrotome. The epoxy block containing the thin-film structures is mounted to the sample arm, which holds the block above the diamond knife. The knife is wetted on one side by water of a boat, onto which the sections float as the block is pushed against the edge of the knife.

The nanogap structures were observed by scanning electron microscope (SEM) measurements using a Jeol JSM 7000F scanning electron microscope operating at 30 kV and a working distance of 10 mm. All electrical measurements were performed in a home-built Faraday cage using a Keithley 6430 source meter. Sections were positioned on a piece of glass and held in place with a gold tip. The low and high inputs were connected to a metal probe and a syringe filled with eutectic Ga-In (EGaIn), respectively.[46]

2.3 Results and Discussion

2.3.1 Fabrication

For constructing metal/insulator/metal tunneling junctions, we successively deposited a thin film of aluminum and a second layer of gold on a film of gold to form a gold/aluminum/gold sandwich, which then was sectioned into thin slabs perpendicular to the plane of films by nanoskiving. With the remove of sacrificial layers, the resulting structures are air-nanogaps of various sizes between two ultra-long nanowires. It is different with SAM-based junctions that direct deposition of top metal contact damages the SAM, and a protective layer is used. Figure 2.2 illustrates the entire procedure to generate air-nanogap structures which are controllable. Gold films are deposited through a Teflon mask on a clean and passivated silicon wafer to form rectangular patterns of gold (1-2 mm in width). Epofix epoxy prepolymer is used to cover the whole wafer. After the epoxy is cured, gold features adhered to the epoxy are separated from the silicon wafer via template-stripping. Then the same Teflon mask is placed over the gold features with an offset of about 500 μm for depositing a layer of aluminum with desired thickness, followed by a second layer of gold. The sacrificial layers of aluminum will define the width of nanogaps. All sandwich structures are separated by rough cut using a high-precision saw, and then embedded into more epoxy to form blocks for sectioning with an ultramicrotome.

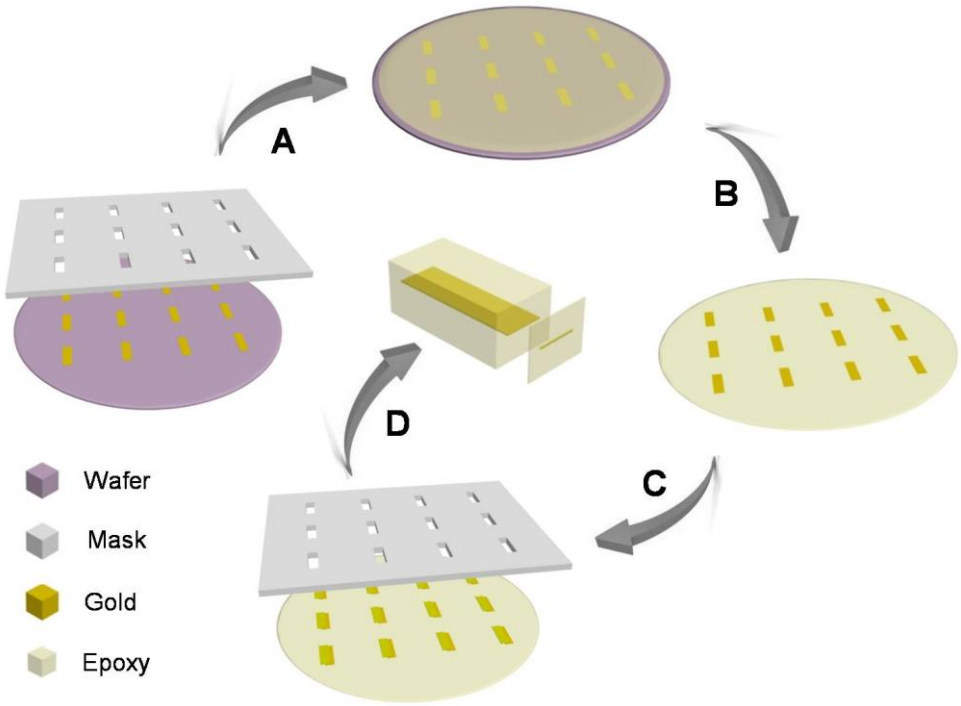

Figure 2.2 The schematic illustration of the fabrication of air-nanogap electrodes. A) A layer of gold is deposited on a clean silicon wafer through a Teflon mask to generate millimeter-scaled patterns of gold. Then epofix epoxy prepolymer is poured on the entire wafer to cover the gold features. B) After curing the epoxy, the gold features are template-stripped by peeling the cured epoxy from the wafer. C) After turnover of the epoxy substrate, the same Teflon mask is placed back over the gold features with laterally offset of 67%. A layer of aluminum then is deposited through the mask followed by a second layer of gold to form sandwich structures. D) The gold features are cut into small pieces, and embedded in more epoxy prepolymer to produce blocks for sectioning.

The resulting sections contain two gold nanowires, and an aluminum spacer. To get air-gap structures, the aluminum layer is etched away by acid. For precisely controlling the structure of the air-gap junctions, Figure 2.3 illustrates how each dimension is defined. The width of gaps is defined by the thickness of aluminum layer; and the length, the width, and the height of nanowires is defined by the shadow mask, the deposition of gold, and the ultramicrotome, respectively.

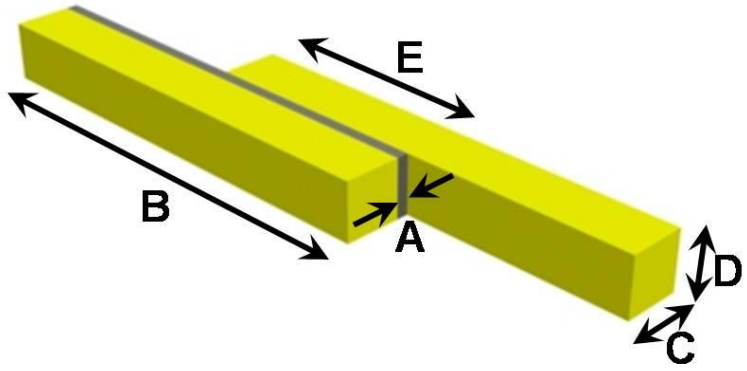

Figure 2.3 The schematic illustration of the dimension of an air-nanogap electrode. A) The width of gap between the two gold nanowire, is defined the thickness of aluminum spacer. B) The length of the gold nanowire, which is the longest dimension, is defined by the shadow mask. C) The width of the nanowire is defined by the deposition of gold. D) The height is defined by the sectioning of the ultramicrotome. E) The length of gap is determined by the offset between the two layers of gold along the longitude dimension.

The preparation of blocks through embedding the films into resins is the basis of nanoskiving to fabricate various nanostructures before sectioning. Epoxy-based resins are the most commonly used to fabricate blocks, and thiol-ene polymers are new resins that have been developed for nanoskiving gold structures.[47] Here we used epofix epoxy as resin. Figure 2.4 shows the images of the procedure of preparing blocks. The film of gold is deposited on a silicon wafer through a Teflon mask to form gold features. After epoxy prepolymer is cured, the gold features are template-stripped with an epoxy substrate from the silicon wafer. All sandwich structures are cut to strips that are placed in a polyethylene microtome mold to form blocks can be formed. Figure 3.3D shows the final block.

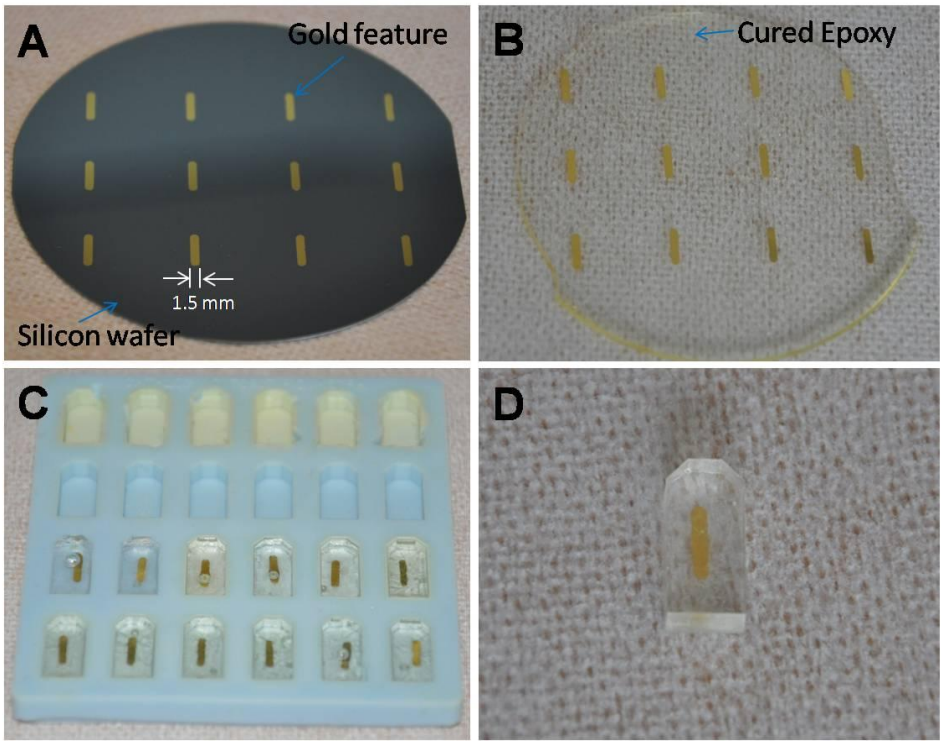

Figure 2.4 The graphic images of the procedure of fabricating the epoxy blocks. A) The gold features are deposited on silicon wafer, B) and then template-stripped to epoxy substrate. C) The entire structures are embedded in a microtome mold. D) A final block is ready for sectioning.

2.3.2 Electron Microscopy

Four air-gap junctions were prepared with different gap-widths that are defined by the thickness of aluminum layers. The layers of depositing aluminum are 5 nm, 10 nm, 15 nm, and 20 nm in thickness, respectively. After sectioning, these structures were exposed to acid to etch away the sacrificial layers of aluminum. For observing the gap structures as-fabricated, we had to etch the epoxy using oxygen plasma before imaging by SEM. Figure 2.5 shows SEM images of nanogap structures with different gap-widths after etching aluminum (from A to D, they are two nanowires of gold separated by 5 nm, 10 nm, 15 nm, and 20 nm gaps). The gaps are clearly visible, and the width of the gaps is corresponding to the thickness of aluminum.

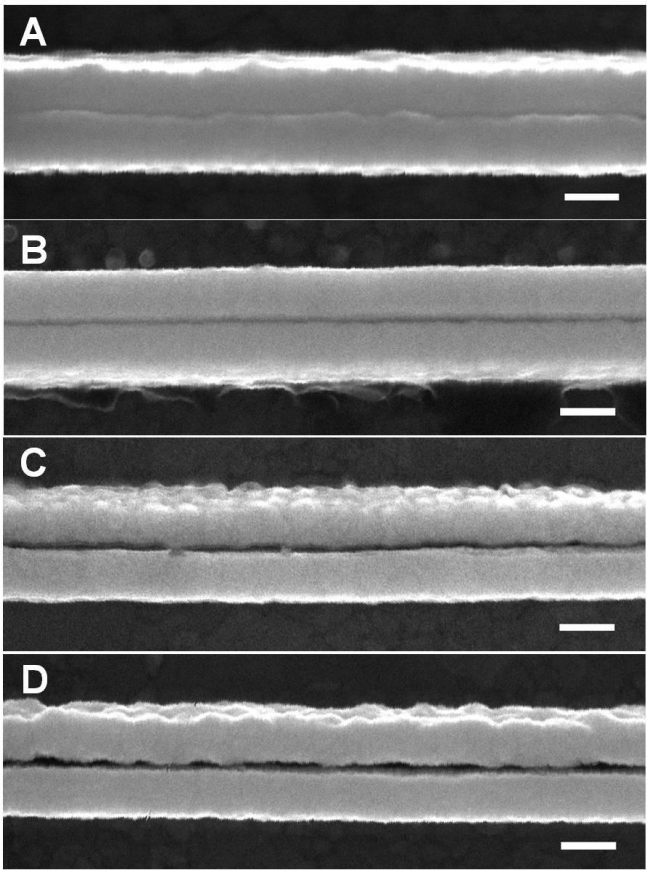

Figure 2.5 SEM images of the air-gaps of four electrodes with A) 5 nm, B) 10 nm, C) 15 nm, and D) 20 nm gap in width. After sectioning, the aluminum spacer was removed by acid followed by etching the epoxy resin using oxygen plasma. Scale bar: 100 nm.

2.3.3 Electrical Measurements

According to dimensions shown in Figure 2.3, the length of the gold nanowire and the gap (dimension B and E) can be measured; they are about 1.5 mm and 500 μm, respectively, so approximate 1 mm of each gold wire is available for electrical contact. Before applying droplets of silver paste on the end of each gold wire to form electrical contact pads by hand, we positioned sections containing air-gap electrodes on clean glass substrates, and dried them in oven to improve their adhesion to the substrates. It is worth mentioning, the silver paste was dropped on both ends of a line that is in the epoxy slab, can be clearly seen under a light microscope. To measure electrical characteristics of air-gap junctions, two electrodes were then contacted by placing the sharp tip of EGaIn formed at the tip of a syringe on one pad of silver paste, and connecting a tungsten probe with a droplet of EGaIn to the other pad of silver paste in a home-made Faraday cage.

As a working air-gap junction, the *I-V* curves should be S-shaped that refers to tunneling junctions, and low-noise currents are in the nA regime. For no-contact and shorts junctions, they can be characterized by noisy current in the pA regime and linear, ohmic curves with current in the μA regime, respectively. Figure 2.6 shows the short junction with linear *I-V* curve. If the distance between two conductive materials is short enough, a tunneling current exists without any contact between the two electrodes. With decreasing distance or increasing voltage, the wave functions of the electrodes overlap increasingly near to Femi energy. So an electron is to pass through the perpendicular distance between the two electrodes by tunneling as the dominate mechanism. Tunneling is independent on temperature and dependent on the width of the junctions.

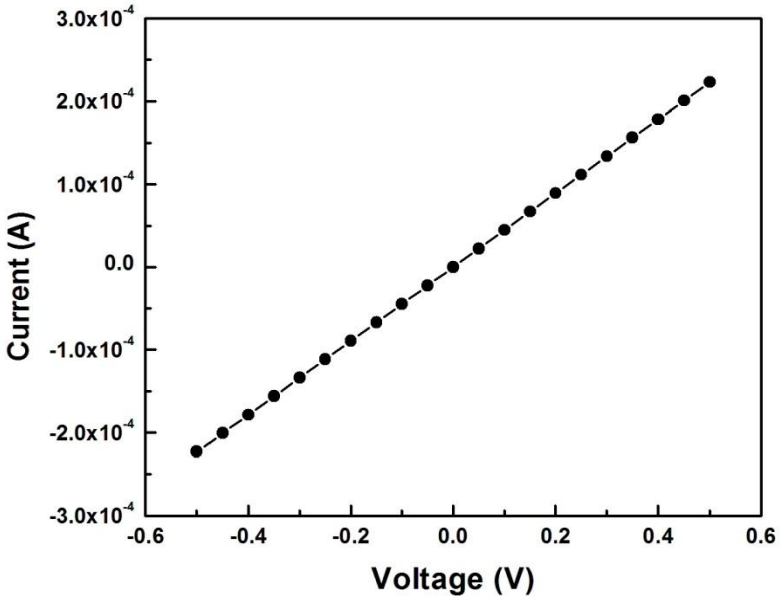

Figure 2.6 The linear plot of current versus voltage for a short contact of the air-gap junction. The current is in the μA regime.

For these air-gap electrodes, all dimensions are kept as constant except the width of gaps. Current density *J* (A/cm^2) was used to characterize air-gap junctions instead of current *I* (A). We can directly measure the length and height of gaps using a microruler before embedding the entire structure to calculate the emission area. The length is defined by the offset of the shadow mask, and the height is defined by ultramicrotome (shown in Figure 2.3). Figure 2.7 shows the plots of *J*-*V* data for 5 nm, 10 nm, 15 nm and 20 nm gaps. With the increasing of the width of gaps, the *J* decreases at the same voltage. As a tunneling junction, the dependence of *J*-*V* characteristics on the width of gap is fit to a simple approximation of Simmons equation:[48]

$$J=J_0e^{-d\beta} \qquad (1)$$

where β is the tunneling decay constant that can be estimated by linear plot of Ln *J* versus *d* from the slope, *d* is the width of gap, and J_0, which is the current density lacking a gap at *d*=0, can be extracted from the zero width intercept of the plot. Figure 2.8 shows a plot of Ln *J* at 500 mV as a function of the width of gap for air-gap junctions with 5 nm, 10 nm, 15 nm, and 20 nm gaps. The β value determined from the slope of plot is 0.26 nm^{-1}. The

current density through the air-gap junctions depends exponentially on the bias in low-bias regime, and linearly on the width of the gap. These observations indicate that the mechanism of charge transport is tunneling, when an electron delocalizes from one electrode to the other electrode.

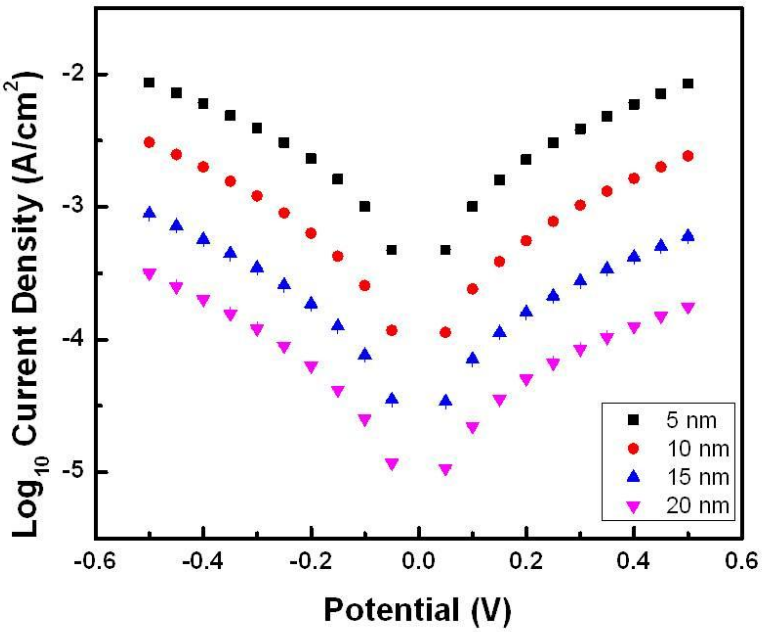

Figure 2.7 The plots of log current density as a function of voltage for air-gap junctions with 5nm, 10 nm, 15 nm, and 20 nm gaps in width. The current density of each junction is average of different electrodes.

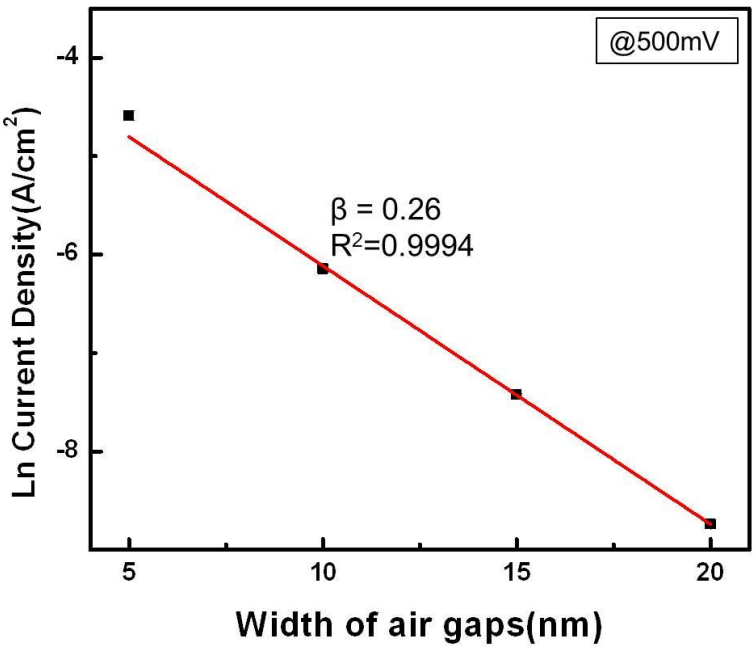

Figure 2.8 The plot of *Ln* current density against the width of gap used in the junctions at 0.5 V. The straight line shows Equation 1 with the parameter β determined from a linear fit of *Ln J*.

2.4 Conclusion

Nanogap electrodes are fabricated in this work by multi-layered deposition followed by process of nanoskiving. It is simple and efficient. A sacrificial layer of aluminum is applied to form air-gaps to achieve metal/insulator/metal junctions. The width of the gaps can be precisely controlled by the thickness of aluminum spacer that can be etched away using acid. It breaks the limitation of molecule-gap focused on the order of their length scale. For these air-nanogap junctions with different width of gap, the electrical measurements demonstrate that the current density through the junctions depends exponentially on the bias, and linearly on the width of the gap. These data indicate that the mechanism of charge transport is tunneling. Comparing to existing methods, we offer an exceedingly simple approach to fabricate air-gap electrodes that are directly addressable, requiring no addition lithography steps. No special equipment is needed to fabricate them—only an ultramicrotome that is much cheaper than conventional infrastructure (clean room, e-beam/photolithography, etc.). They can be made in large number with short time

consuming (at the rate of about one per second). It is of high efficiency and precision with wide operating window, and also has the ability to fabricate nanoelectrodes over large area. In addition to providing precise control over all three dimensions of the electrodes, many identical air-gap electrodes can be produced at a time, thus eliminating the need to image each individual electrode.

Bibliography

1. G. E. Moore, Cramming more components onto integrated circuits, *Electronics*, **1965**, 38, 114-117.

2. D. J. Frank, R. H. Dennard, E. J. Nowak, P. M. Solomon, Y. Taur, and H. S. Philip Wong, Device scaling limits of Si MOSFETs and their application dependencies. *Proc. IEEE* **2001**, 89, 259-288.

3. T. Li, W. Hu, and D. Zhu, Nanogap Electrodes. *Adv. Mater.* **2010**, 22, 286-300.

4. Z. K. Keane, J. W. Ciszek, J. M. Tour, and D. Natelson, Three-terminal devices to examine single molecule conductance switching, *Nano Lett.* **2006**, 6, 1518-1521

5. G. Maruccio, A. Biasco, P. Visconti, A. Bramanti, P. P. Pompa, F. Calabi, R. Cingolani, R. Rinaldi, S. Corni, R. Di Felice, E. Molinari, M. R. Verbeet, and G. W. Canters, Towards protein field-effect transistors: Report and model of a prototype, *Adv. Mater.* **2005**, 17, 816-822.

6. D. Porath, A. Bezryadin, S. de Vries, and C. Dekker, Direct measurement of electrical transport through DNA molecules, *Nature* **2000**, 403, 635-638.

7. W. Hu, J. Jiang, H. Nakashima, Y. Luo, Y. Kashimura, K. Chen, Z. Shuai, K. Furukawa, W. Lu, Y. Liu, D. Zhu, and K. Torimitsu, Electron transport in self-assembled polymer molecular junctions, *Phys. Rev. Lett.* **2006**, 96, 027801

8. R. V. Seidel, A. P. Graham, J. Kretz, B. Rajasekharan, G. S. Duesberg, M. Biebau, E. Unger, F. Kreupl, and W. Hoenlein, Sub-20 nm short channel carbon nanotube transistors, *Nano Lett.* **2005**, 5, 147-150.

9. T. Mizukami, Y. Miyato, K. Kobayashi, K. Matsushige, and H. Yamada, Resistive switching effects in single metallic tunneling junction with nanometer-scale gap, *Appl. Phys. Lett.* **2011**, 98, 083120.

10. J. Yao, L. Zhong, Z. Zhang, T. He, Z. Jin, P. J. Wheeler, D. Natelson, and J. M. Tour, Resistive switching in nanogap systems on SiO_2 substrates, *Small*, **2009**, 5, 2910-2915.

11. H. Cho, S. K. Kim, Y. jung, J. Jung, and B. H. Chung, Electric detection of target DNA by fabricating gold nanowire bridges on planar nanogap electrodes, *Chem. Commun.* **2011**, 47, 5756-5758.

12. L. Lesser-Rojas, P. Ebbinghaus, G. Vasan, M. L. Chu, A. Erbe, and C. F. Chou, Low-copy number protein detection by electrode nanogap-enabled dielectrophiretic trapping for surface-enhanced Raman spectroscopy and electronic measurements, *Nano Lett.* **2014**, 14, 2242-2250.

13. X. Chen, Z. Guo, G. M. Yang, J. Li, M. Q. Li, J. H. Liu, and X. J. Huang, Electrical nanogap

devices for biosensing, *Mater. Today* **2010**, 13, 28-41.

14. J. Lee, W. Shim, E. Lee, J. S. Noh, and W. Lee, Highly mobile palladium thin films on an elastomeric substrate: Nanogap-based hydrogen gas sensors, *Angew. Chem. Int. Ed.* **2011**, 50, 5301-5305.

15. M. A. Reed, C. Zhou, C. J. Muller, T. P. Burgin, and J. M. Tour, Conductance of a molecular Junction, *Science*, **1997**, 278, 252-254.

16. D. Xiang, H. Jeong, T. Lee, and D. Mayer, Mechanically controllable break junctions for molecular electronics, *Adv. Mater.* **2013**, 25, 4845-4867.

17. W. Chen, H. Ahmed, and K. Nakazoto, Nanoscale metallic islands in a lateral nanostructure, *Appl. Phys. Lett.* **1995**, 66, 3383-3384.

18. J. Park, A. N. Pasupathy, J. I. Goldsmith, C. Chang, Y. Yaish, J. R. McEuen, and D. C. Ralph, Coulomb blockade and the Kondo effect in single-atom transistors, *Nature* **2002**, 417, 722-725.

19. A. F. Morpurgo, C. M. Marcus, and D. B. Robinson, Controlled fabrication of metallic electrodes with atomic separation, *Appl. Phys. Lett.* **1999**, 74, 2084-2086.

20. T. Nagase, T. Kubota, and S. Mashiko, Fabrication of nano-gap electrodes for measuring electrical properties of organic molecules using a focused ion beam. *Thin Solid Films*, **2003**, 438-439, 374-377.

21. S. Kubatkin, A. Danilov, M. Hjort, J. Cornil, J. L. Brédas, N. Stuhr-Hansen, P. Hedegård, and T. Bjørnholm, Single-electron transistor of a single organic molecule with access to several redox states, *Nature* **2003**, 425, 698-701.

22. A. Notargiacomo, V. Foglietti, E. Cianci, G. Capellini, M. Adami, P. Faraci, F. Evangelisti, and C. Nicolini, Atomic force microscopy lithography as a nanodevice development technique, *Nanotechnology* **1999**, 10, 458-463.

23. L. Qin, S. Park, L. Huang, and C. A. Mirkin, On-wire lithography, *Science* **2005**, 309, 113-115.

24. M. A. Reed, Molecular-scale electronics, *Proc. IEEE* **1999**, 87, 652-658.

25. R. M. Metzger, Electrical rectification by a molecule: The advent of unimolecular electronic devices, *Acc. Chem. Res.* **1999**, 32, 950-957.

26. E. W. Wong, C. P. Collier, M. Behloradsky, F. M. Raymo, J. F. Stoddart, and J. R. Heath, Fabrication and transport properties of single-molecule-thick electrochemical junctions, *J. Am. Chem. Soc.* **2000**, 122, 5831-5840.

27. C. H. Bennett, and D. P. DiVincenzo, Quantum information and computation, *Nature* **2000**, 404, 247-255.

28. H. Song, M. A. Reed, and T. Lee, Single molecule electronic devices, *Adv. Mater.* **2011**, 23, 1583-1608.

29. Y. Zhang, Z. Zhao, D. Fracasso, and R. C. Chiechi, Bottom-up molecular tunneling junctions formed by self-assembly, *Isr. J. Chem.* **2014**, 5-6, 513-533.

30. G. S. McCarty, Molecular lithography for wafer-scale fabrication of molecular junctions, *Nano Lett.* **2004**, 4, 1391-1394.

31. T. Li, J. R. Hauptman, Z. Wei, S. Petersen, N. Bovet, T. Vosch, J. Nygård, W. Hu, Y. Liu, T. Bjørnholm, K. Nørgaard, and B. W. Laursen, Solution-processed ultrathin chemically derived grapheme films as soft top contacts for solid-state molecular electronic junctions, *Adv. Mater.* **2012**, 24, 1333-1339.

32. D. Fracasso, H. Valkenier, J. C. Hummelen, G. C. Solomon, and R. C. Chiechi, Evidence for quantum interference in SAMs of arylethynylene thiolates in tunneling junctions with eutectic Ga-In (EGaIn) top-contacts, *J. Am. Chem. Soc.* **2011**, 133, 9556-9563.

33. S. Seo, M. Min, S. M. Lee, and H. Lee, Photo-switchable molecular monolayer anchored between highly transparent and flexible grapheme electrodes, *Nat. Commun.* **2013**, 4, 1920-1926.

34. B. Kim, S. H. Choi, X. Y. Zhu, and C. D. Frisbie, Molecular tunnel junctions based on π–conjugated oligoacene thiols and dithiols between Ag, Au, and Pt contacts: Effect of surface linking group and metal work function, *J. Am. Chem. Soc.* **2011**, 133, 19864-19877.

35. H. B. Akkerman, P. W. M. Blom, D. M. de Leeuw, and B. de Boer, Towards molecular electronic with large-area molecular junctions, *Nature*, **2006**, 441, 69-72.

36. Z. Li, T. H. Park, J. Rawson, M. J. Therien, and E. Borguet, Quasi-ohmic single molecule charge transport through highly conjugated meso-to-meso ethyne-bridged porphyrin wires, *Nano Lett.* **2012**, 12, 2722-2727.

37. W. F. Reus, M. M. Thuo, N. D. Shapiro, C. A. Nijhuis, and G. M. Whitesides, The SAM, not the electrodes, dominates charge transport in metal-monolayer//Ga_2O_3/ gallium-indium eutectic junctions, *ACS Nano* **2012**, 6, 4806-4822.

38. B. Mann, and H. Kuhn, Tunneling through fatty acid salt monolayers, *J. Appl. Phys.* **1971**, 42, 4398-4405.

39. A. Aviram, M. A. Ratner, Molecular rectifiers, *Chem. Phys. Lett.* **1974**, 29, 277-283.

40. M. M. Thuo, W. F. Reus, C. A. Nijhuis, J. R. Barber, C. Kim, M. D. Schulz, and G. M. Whitesides, Odd-even effects in charge transport across self-assembled monolayers, *J. Am. Chem. Soc.* **2011**, 133, 2962-2975.

41. K. Slowinski, H. K. Y. Fong, and M. Majda, Mercury-mercury tunneling junctions: Electron tunneling across symmetric and asymmetric alkanethiolate bilayers, *J. Am. Chem. Soc.* **1999**,

121, 7257-7261.

42. C. A. Nijhuis, W. F. Reus, J. R. Barber, M. D. Dickey, and G. M. Whitesides, Charge transport and rectification in arrays of SAM-based tunneling junctions, *Nano Lett.* **2010**, 10, 3611-3619.

43. P. Pourhossein, and R. C. Chiechi, Fabricating nanogaps by Nanoskiving, *J. Vis. Exp.* **2013**, 75, e50406.

44. M. D. Dickey, D. J. Lipomi, P. Bracher, and G. M. Whitesides, Electrically addressable parallel nanowires with 30 nm spacing from micromolding and nanoskiving, *Nano Lett.* **2008**, 8, 4568-4573.

45. P. Pourhossein, and R. C. Chiechi, Directly addressable sub-3 nm gold nanogaps fabricated by nanoskiving using self-assembled monolayers as templates, *ACS Nano*, **2012**, 6, 5566-5573.

46. R. C. Chiechi, E. A. Weiss, M. D. Dickey, and G. M. Whitesides, Eutectic Gallium-Indium (EGaIn): A moldable liquid metal for electrical characterization of self-assembled monolayers, *Angew. Chem. Int. Ed.* **2008**, 47, 142-144.

47. R. L. Mays, P. Pourhossein, D. Savithri, J. Genzer, R. C. Chiechi, and M. D. Dickey, Thiol-containing polymeric embedding materials for nanoskiving, *J. Mater. Chem. C*, **2013**, 1, 121-130.

48. J. G. Simmons, Generalized formula for the electric tunnel effect between similar electrodes separated by a thin insulating film, *Appl. Phys. Lett.* **1963**, 34, 1793-1803.

Chapter 3

Multiple-Dimensional, Ultra-long, Plasmonic Sub-10 nm Gaps in Large Area Devices

3.1 Introduction

The fabrication of nanostructures for large electric field enhancements has become increasingly attractive over the last several years duo to outstanding performance in applications of sensing and imaging.[1-6] In particular, nanometric gaps between noble metals constitute one of the most explored structures.[7-12] Especially for sub-10 nm gaps, squeezing light through them can generate extreme subwavelength confinement of electromagnetic energy.[13] Thus, subwavelength "hot spots" with highly confined energy are easily generated in the gaps, leading to dramatically enhanced signals from adsorbates. This intriguing capability was essential to enable applications in nonlinear optics,[14,15] optical trapping,[16,17] and surface-enhanced spectroscopies.[10, 18, 19] In view of the remarkable advantages and broad application prospects, many efforts have been made to fabricate various nanogaps. Gap-separated gold nanoparticle chains in silica nanopeapods,[20] self-aligned sub-1 nm gaps between gold electrodes,[21] and nano-star dimers with sub-10-nm gaps[18] were fabricated and exhibit hallmarks of exceedingly high Raman sensitivity. Plasmonic nanogaps have been fabricated by aggregates of

*This chapter has been published in: Adv. Mater., 2016, 28, 2956-2963. I would like to thank Ziwei Zhou, Ye Yu, Bin Ai, Helmuth Möhwald, and Joel K. W. Yang for the fruitful collaboration.

nanoparticles,[1,16] self-assembled particle chains,[20,22,23] electromigration,[10,21] electron-beam lithography (EBL),[8, 18, 24] focused ion beam (FIB) bombardment,[25, 26] nanosphere lithography,[9, 27-29] and on-wire lithography.[30,31] However, simple and efficient manufacturing of sub-10 nm gaps remains a challenge. For broader dissemination, improved sensitivity, higher reproducibility and relaxed requirements on intense sources for spectroscopies, however, it is necessary to fabricate large-area nanogaps in parallel and at low cost.

Moreover, with the rapid development of nano-optics and nanoelectronics, devices with a high level of integration are in great demand.[19, 32, 33] Nevertheless, conventional point-like nanogaps only provide a few dominant “hot spots” contributing to the overall signal, in which the field distribution varies with position.[34] In addition, the amount of light that can be coupled into these gaps is limited due to the mismatch with optical wavelengths.[13] In contrast, for those one-dimensional (1D) nanogaps composed of two close flat-sided metals, it is straightforward to generate well-defined, high-density hotspots along the entire length.[35-37] Thus, 1D nanogaps are robust against local defects or impurities, enabling more reliable and reproducible SERS (Surface-enhanced Raman Scattering) spectroscopy. Further, fabricating a two-dimensional (2D) array on a plane will largely increase the throughput and gap density.[32, 38] This approach can integrate nanogap devices with the required geometries over a large area that is suitable for modern planar lithography technologies.[39, 40] Likewise, 3D nanogap arrays with high integration by adequately utilizing stereoscopic space, which are hard to realize through conventional methods, will be of great significance in the future.

The approach based on nanoskiving introduced in Chapter 1 provides a feasible strategy to meet these criteria.[41-45] The resulting structures embedded in epoxy slabs are free-standing and can be transferred to flat or curved surfaces and various kinds of substrates, skirting the substrate-dependence problem of nanofabrication in conventional techniques. Recently, nanoskiving has been utilized to fabricate linear nanogaps with ultra-small, stationary gap-widths by Chiechi[46] and Lipomi[35] using self-assembled

monolayers (SAM) and single-layer graphene as templates respectively. And, fabricating width-tunable ultrathin nanogaps is imperative to systematically investigate the gap-width dependence of the nanogaps.

In this chapter, we demonstrate a scalable nanofabrication approach based on nanoskiving to create a series of 1D, millimeter-long nanogaps with tunable sub-10 nm gap-widths. These structures are optimized by simulation and experiment to obtain the strongest plasmonic coupling with 5 nm gap-widths, enabling a 250 times greater enhancement compared to an individual gold nanowire. A mechanistic explanation is provided to the non-monotonic electric field dependence on gap-width. Further, 2D nanogap arrays were rapidly generated by introducing surface patterning techniques. Notably, novel 3D nanogap arrays that are hard to achieve by conventional nanofabrication via a unique stacking procedure were successively built, possessing higher integration and much enhanced plasmonic coupling.

3.2 Experimental Section

3.2.1 The procedure of fabricating the nanogap arrays.

Fabrication of the epoxy block with flat metal films. Silicon wafers were cleaned by piranha solution (H_2SO_4:H_2O_2=3:1) and then washed with ethanol. After drying by a stream of nitrogen gas, a 90 nm-thick layer of gold was deposited by thermal evaporation onto the clean wafers. After curing Epofix epoxy prepolymer on the surface of the gold film, the film of gold was template-stripped by peeling the epoxy from the wafer. A 2 nm, 3 nm, 5 nm, 6 nm, or 8 nm aluminum layer was deposited on the surface of the gold-covered epoxy substrate followed by a second 90 nm-thick film of gold to form Au/Al/Au sandwich structures. These epoxy-supported sandwich structures were cut into thin strips (~2 mm in width × ~10 in length) using a jeweler's saw and then formed blocks of cured epoxy.

Fabrication of the epoxy block with patterned metal films. A 2 μm-thick layer of

photoresist (BP212-37 positive photoresist, Kempur Microelectronics, Inc., Beijing, China) was spin-coated on clean silicon wafers at 3000 rpm and patterned using conventional photolithography with a stripe-patterned mask, and then the patterned surface was passivated with trichloro-(1H,1H,2H,2H-perfluorooctyl) silane (PFS, purchased from Aldrich). The poly(dimethylsiloxane) (PDMS) prepolymer (Dow Corning Sylgard 184, prepolymer and curing agent in 10:1 w/w ratio) was cast onto the stripe mold and cured in oven at 60 °C for 3 hours, before the PDMS mold was peeled off from the patterned photoresist substrate. After a patterned epoxy substrate was obtained by curing epofix epoxy prepolymer for 3 h at 60 °C against the PDMS master, a 90 nm-thick layer of gold, a layer of aluminum, and a second 90 nm-thick layer of gold were successively deposited on the patterned epoxy substrate at a glancing angle of 45^{o}. This epoxy-supported sandwich structures were cut in thin strips (~2 mm in width × ~10 mm in length) and then formed blocks of cured epoxy.

Ultramicrotome sectioning. An epoxy block was mounted in the sample chuck of the ultramicrotome (Leica EM UC 7) and trimmed to the width of the diamond knife (3 mm Diatome Ultra 35^{o}) After alignment of the flat mold face with the diamond knife edge, the block was sectioned to 150 nm at 1 mm/s to produce epoxy sections containing the sandwich structures in a plane perpendicular or parallel to the metal films. The sections were collected by directly immersing the solid substrate into water below the epoxy slabs and raising it slowly. After these sections were dried at 60 ^{o}C, the sections were immersed into 2 M HCl for 2 h to remove the sacrificial aluminum layers. The epoxy resin was then dry-etched with oxygen plasma.

3.2.2 FDTD simulation.

A commercial software package (FDTD Solutions v8.6.3, Lumerical Solutions Inc.) was used to perform simulations of electromagnetic fields with the same structural dimensions as extracted from the actual fabricated samples. The structure was excited by a normally incident, unit magnitude plane wave propagating in the z direction with an

electric field polarization along the x-axis. The mesh refinement is the conformal variant 2. Monitors of frequency-domain field profile and frequency domain field and power were placed to calculate the distributions of surface plasmon (SP) energy and the transmission spectra in the continuous wave normalization state. The magnitude of the incident electric fields was taken to be unity, and the enhancement of electromagnetic fields evaluated. The optical parameter of Au was taken from Palik's handbook.

3.2.3 Raman spectroscopy analysis.

A 1 mM solution of p-aminothiophenol (PATP, Sigma-Aldrich) was prepared in ethanol. The nanogap samples were then soaked in this solution for 12 hours to allow PATP monolayer formation on the metal surface and on the sidewall inside the gap. Before measurement, the samples were cleaned with a flow of ethanol for 2 minutes to remove unbound PATP molecules. To obtain the Raman spectra of as-sectioned 1D, 2D and 3D nanogaps, a Raman microscope (LabRAM HR Evolution) with a 633 nm excitation source and a 1 μm beam spot was used. The exposure time was set to 15 seconds at 5% transmittance.

3.2.4 Scanning electron microscope (SEM) imaging

The nanostructures were measured by a Nova Nano (FEI) scanning electron microscope 450 field emission scanning electron microscope with primary electron energy of 15 kV and a working distance of 10 mm.

3.3 Results and Discussion

3.3.1 Fabrication of 1D nanogaps

As illustrated in Figure 3.1a, to build the basic 1D linear nanogaps, gold (90 nm thick)/aluminum/gold (90 nm thick) sandwich films were successively deposited on a flat epoxy substrate.[47] The entire structure was cut into individual stripes (~2 mm × 10 mm

pieces), which were then embedded in more epoxy. With sectioning, ultrathin epoxy slabs with the thickness of 150 nm were generated and then transferred onto a silicon wafer bearing a 90 nm-thick gold mirror. After the removal of aluminum template and epoxy each individual 1D nanogap, consisting of two parallel gold nanowires with sub-10 nm spacing was formed. The gap-width can be tuned by the thickness of the sacrificial aluminum layer; It is well known that techniques of thin film deposition such as physical/chemical vapor deposition can provide a level of nanometric precision.[39] Here, thermally-deposited aluminum was used as a spacer to template the nanogap precisely because aluminum tends to form precise, ultrathin films and its etching process is fast and highly uniform. Moreover, the gap-width can be continuously tuned by controlling the evaporation of aluminum during fabrication. In addition, using this method, insulators (e.g. silica, alumina) could also be deposited between gold films without etching to construct metal-insulator-metal (MIM) wave-guides.

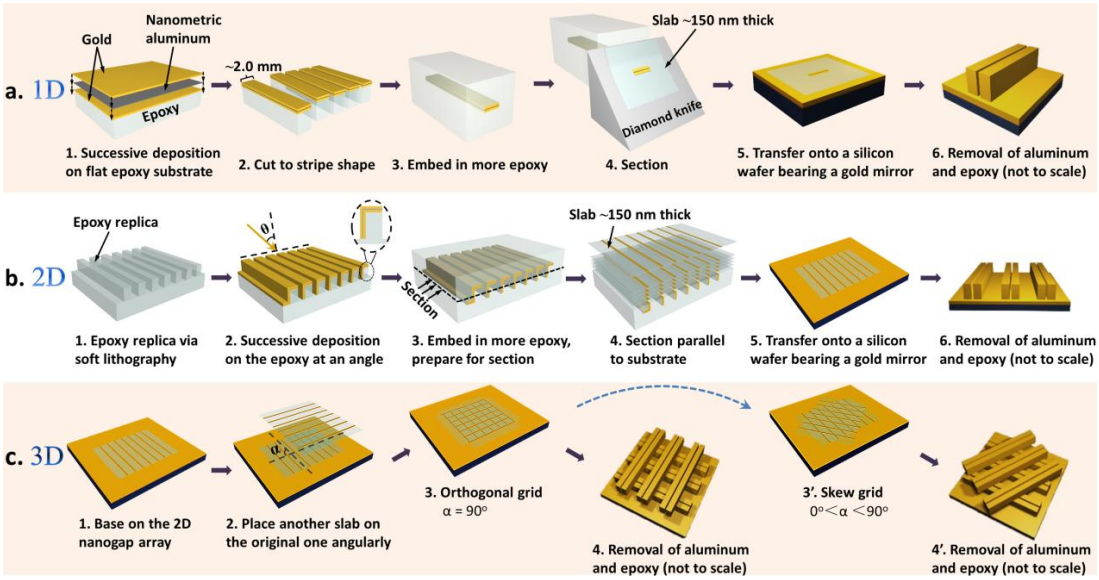

Figure 3.1 Schematics of the process of fabricating size-tunable nanogaps from 1D to 3D. (a) For a 1D nanogap: gold/aluminum/gold sandwich films are formed on a flat epoxy substrate followed by ultrathin sectioning and transfer. (b) For a 2D nanogap array: successive gold/aluminum/gold films are deposited on the sidewall of the shaped epoxy substrate. After embedding, parallel sectioning is conducted along the substrate. (c) For a 3D nanogap grid: based on the 2D nanogap array, a second epoxy slab is stacked on the original one angularly. Varying the stacking angle (α) contributes to differently shaped nanogrids. All epoxy slabs are transferred to silicon wafers bearing a gold mirror. The 1D/2D/3D nanogap (array) forms after removal of spacer and epoxy.

As the gap-width is one of the crucial parameters that determines the magnitude of the local electromagnetic field,[48] we first demonstrate that 1D nanogaps with well-controlled gap-widths were successfully fabricated. Figure 3.2a illustrates the geometric parameters of the final 1D nanogap structure, where the wire width (W) = 90 nm, height (H) = 150 nm, length (L) ≈ 2 mm and gap-width (G) are varied from 2 nm to 8 nm. The wire-width is determined by the thickness of deposited gold. The height is determined by the thickness of the sectioning processes, which is programmed on the ultramicrotome, while the length is determined by the rough sectioning process of cutting the film sample into 2-2.5 mm-wide stripes, which is limited by the width of the diamond knife (in this work, a diamond knife of 3.0 mm in width was used). By controlling the deposition thickness of aluminum, the gap-width can be precisely tuned. Figures 3.2b-f show scanning electron microscope (SEM) images of the linear nanogaps with different gap-widths. The gaps can be clearly seen in the SEM images indicating that the aluminum spacers have been etched. Also the gap-widths differ from each other, commensurate with the thickness of the respective aluminum templates, demonstrating that the evaporated aluminum is a suitable spacer material for nanogaps to tune the gap-width with nanometer precision. The intact spans of the 1D nanogaps could be millimetric depending on the width of the diamond knife. Corresponding voltage-current curve of a 5 nm gap behaving as nano-electrodes indicates the intactness of the nanogap as nano-electrodes with no short-out or broken points (Chapter 2). However, for small gap-width (*e.g.*, 2 or 3 nm), it is difficult to maintain the two nanowires completely separated along their entire length. The intact span could last for several microns, but do touch at points but this isn't a problem to SERS measurements because >90% of the gaps are intact (Figure 3.3).

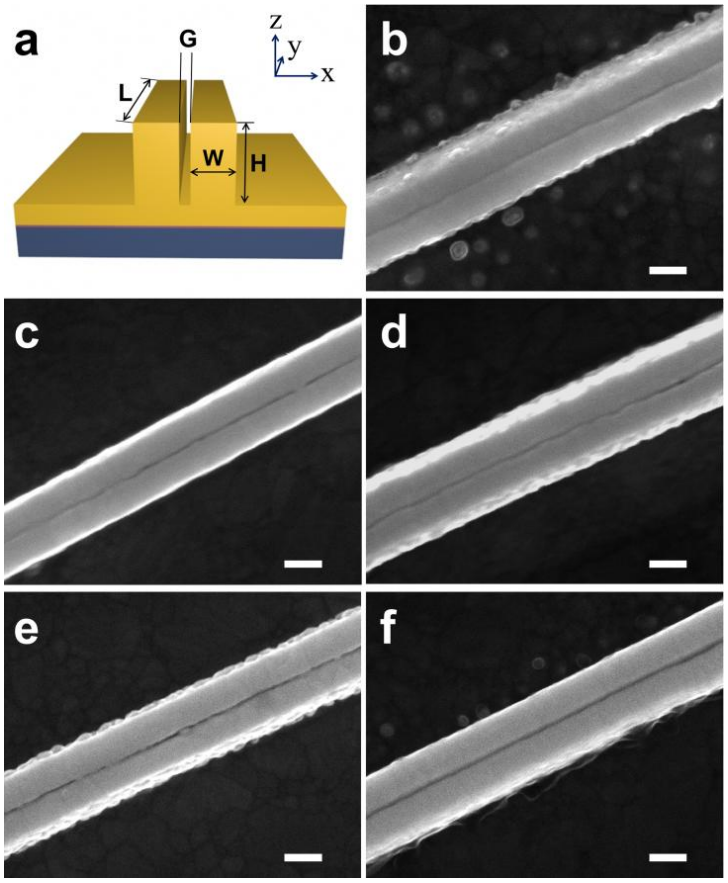

Figure 3.2 (a) Sketch of a 1D nanogap structure, illustrating the geometric parameters. (b-f) SEM images of 1D gold nanogaps with increasing gap-widths of 2, 3, 5, 6 and 8 nm, respectively. The height of the structures in the inset is 150 nm, and the wire width is 90 nm. Scale bar: 100 nm.

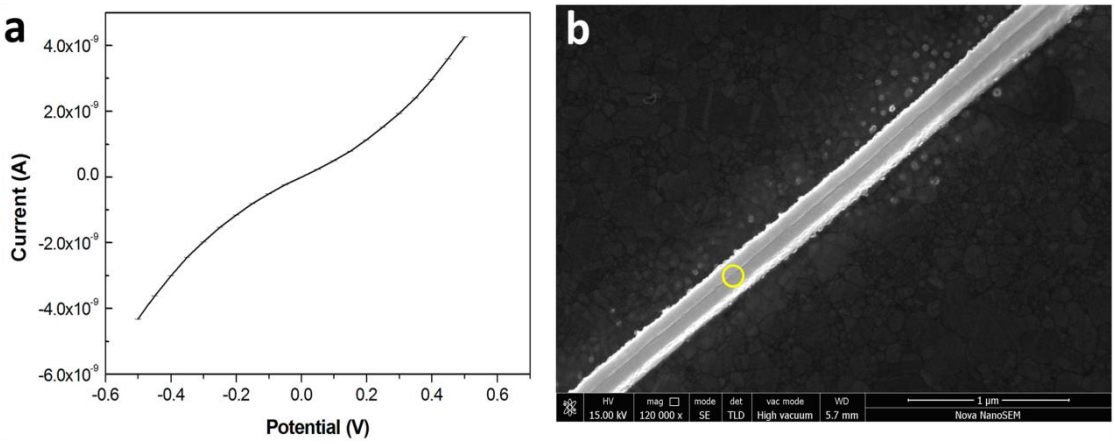

Figure 3.3 a) The voltage-current curve of a 5 nm gap. b) A zoom-out SEM image of a 2 nm gap, illustrating that the wires maintain gaps for several microns, but do touch at points (as yellow-circled) but this isn't a problem to the SERS measurements because >90% of the gaps are intact.

3.3.2 Analysis of Raman spectroscopy for 1D nanogaps

A gap at sub-10 nm scale provides a strongly coupled plasmonic device, which is an attractive candidate for sensing and imaging. As the gap-widths are precisely tuned, the gap-width dependence of the nanogaps can be systematically investigated. We acquired SERS spectra on the 1D nanogaps with varied gap-width from 2 to 8 nm, while keeping the wire width and height constant (W = 90 nm, H = 150 nm, L ≈ 2 mm) and all wires residing on a gold mirror. A schematic diagram of this SERS workbench principle for a 1D nanogap is illustrated in Figure 3.4a. The nonresonant molecule p-aminothiophenol (PATP) was used as the analyte due to its capability of forming self-assembled monolayers (SAMs) on gold surfaces.[49] Figure 3.4b shows SERS spectra in the range of 800-1800 cm^{-1} for SAMs of PATP molecules that were assembled on the 1D nanogap structures with different gap-widths and on a single gold nanowire. The incident laser wavelength, laser transmission, and accumulation time were set to 633 nm, 5%, and 15 s, respectively (the laser was non-polarized). Distinct features of PATP are clearly identifiable as strong bands center at 1077 and 1590 cm^{-1} and many other low-intensity bands can be observed in the spectra. The SERS intensities of the C–S stretch at 1077 cm^{-1} was used to illustrate the impact of the gap-width on the enhancement of the electric field (Figure 3.4c). As the

gap-width increases from 2 to 5 nm, the SERS intensity increases sharply and reaches its maximum at a 5 nm gap-width. However, if the gap continues enlarging, the SERS intensity begins to drop. The maximum intensity of the signal originating from PATP, obtained with the 5 nm nanogap (as the blue line plotted in Figure 3.4b), is 250 times greater compared with that obtained with the single gold nanowire 90 nm-wide (Figure 3.4d) under the same test conditions. As a reference, compared to the nanogap structures, the Raman spectrum recorded on the sandwich nanowires without removal of aluminum spacer shows a weak Raman signal similar to that of the single gold nanowire (Figure 3.5), indicating the necessity of the gap in generating strong plasmonic coupling. The reference Raman spectrum recorded from PATP on a flat gold film is also shown in Figure 3.5, with a weak signal of the Raman bands at 1077 and 1590 cm^{-1}, only slightly above the noise level. From these observations, we conclude that the nanometric gap between two spaced gold nanowires is the dominant cause of the strong enhancement of the Raman signal; gold cuboid nanowire only yields a weak enhancement resulting from the outside edges. Interestingly, among the sub-10 nm gap-widths, neither the smallest nor the largest gap-width can generate the strongest enhancement; the maximum was obtained at the 5 nm gap-width, showing a non-monotonic dependence on the gap-widths.

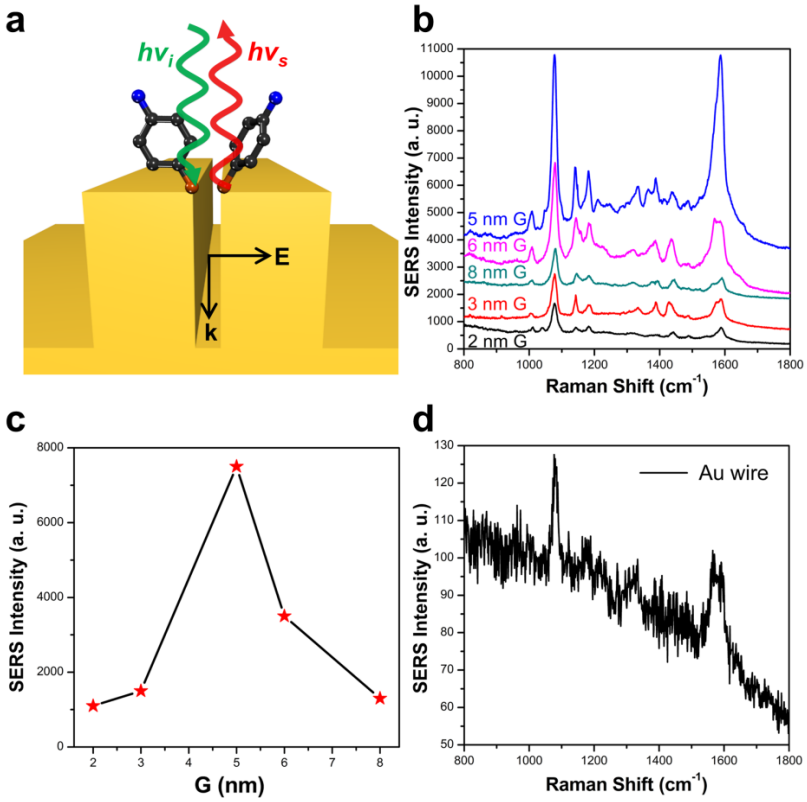

Figure 3.4 (a) Illustration of the SERS workbench principle for the standing nanogap. *E* and *k* indicate the direction of electric field and wave vector, respectively. hv_i and hv_s represent the incoming and scattered photon energy, respectively. (b) Experimentally recorded dependence of the SERS intensity versus G from 2 nm to 8 nm. (c) SERS intensity at 1077 cm^{-1} for different-sized nanogaps in (b). (d) Raman spectrum produced by an individual 90 nm-wide gold nanowire on a gold mirror.

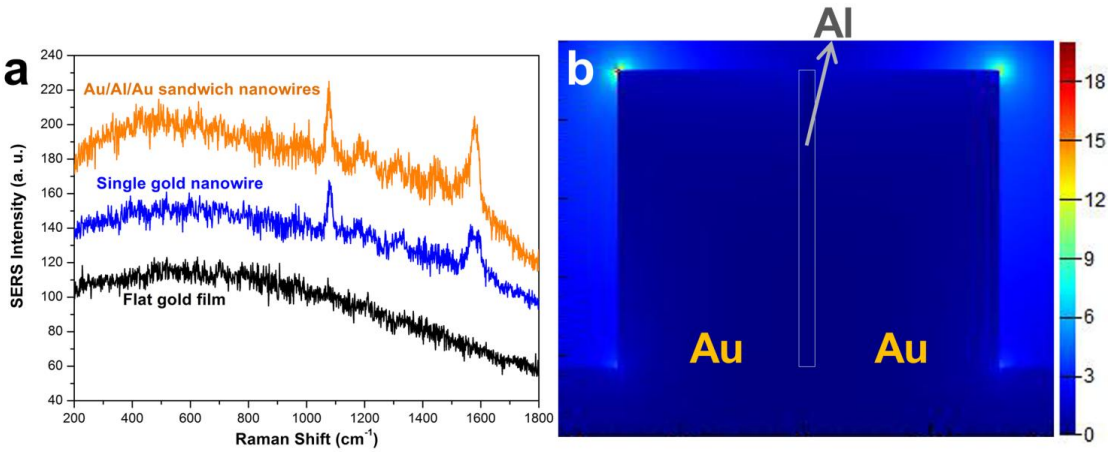

Figure 3.5 (a) Raman signals of p-aminothiophenol (PATP) obtained from the Au/Al/Au sandwich nanowires (yellow line), single gold nanowire of 90 nm wire width (blue line) and the flat gold film (black line). (b) The FDTD simulation of the electric field distribution in the cross-section of the Au (90 nm)/Al (5 nm)/Au (90 nm) sandwich nanowires without etching the aluminum spacer. The scale bar represents E/E_0.

3.3.3 Simulation of the field distribution for 1D nanogaps

Precise control over all dimensions, particularly by tuning the gap-width, allows us to obtain superb near-field generation. To further understand the origin of this unusually non-monotonic phenomenon, FDTD simulations of the near-field distribution for the 1D nanogaps with varied gap-width from 2 to 8 nm and the single gold nanowire are performed as shown in Figure 3.6. The wire width and height are kept constant (W = 90 nm, H = 150 nm) with all wires residing on a gold mirror. The excitation wavelength was set at 633 nm with the electric field polarized along the x-axis.[38] The FDTD simulation with y-polarized light is depicted in Figure 3.7, showing extremely weak coupling. If two parallel gold nanowires are close enough, a prominent near-field interaction occurs between the nanowires, owing to the strong coupling of the localized surface plasmon resonance (LSPR) supported by each nanowire. This coupling enables the enhancement of highly localized electric fields (hot spots) in the gap area that decays rapidly outside the gap. From the calculations, a 2 nm gap results in a slight field enhancement and localization in the gap, comparable with that which is induced by the outside edges of each nanowire (Figure 3.6a). As the gap-width increases, the gap plasmon plays a more important role than that of the corners of the wire, enabling strong confinement of the

optical field to the nanometric gap. Notably, while the gap-width reaches 5 nm, the enhancement of the local electric field in the nanogap approaches the maximum compared to nanogaps of other sizes, as shown Figure 3.6c, which may result from the generation of a strong standing wave. However, the electric-field enhancement begins to weaken with the further increase of the gap-width as shown in Figures 3.6d-e. The maximum of calculated E/E_0 also shows a non-monotonic dependence on gap-width (Figure 3.8). In comparison, from the electric field simulation for the single 90 nm wide nanowire ($G \rightarrow \infty$) on a gold mirror (Figure 3.6f), a weak electric-field enhancement induced just by the outside edges of the wires is observed, which can be regarded as two gold nanowires separated too far to establish plasmonic coupling. The electric-field dependence on gap-height was also simulated, showing very weak sensitivity of the plasmonic response compared with the change of gap-width. These simulation results are highly consistent with the SERS measurements, confirming the non-monotonic dependence on gap-width experimentally and theoretically.

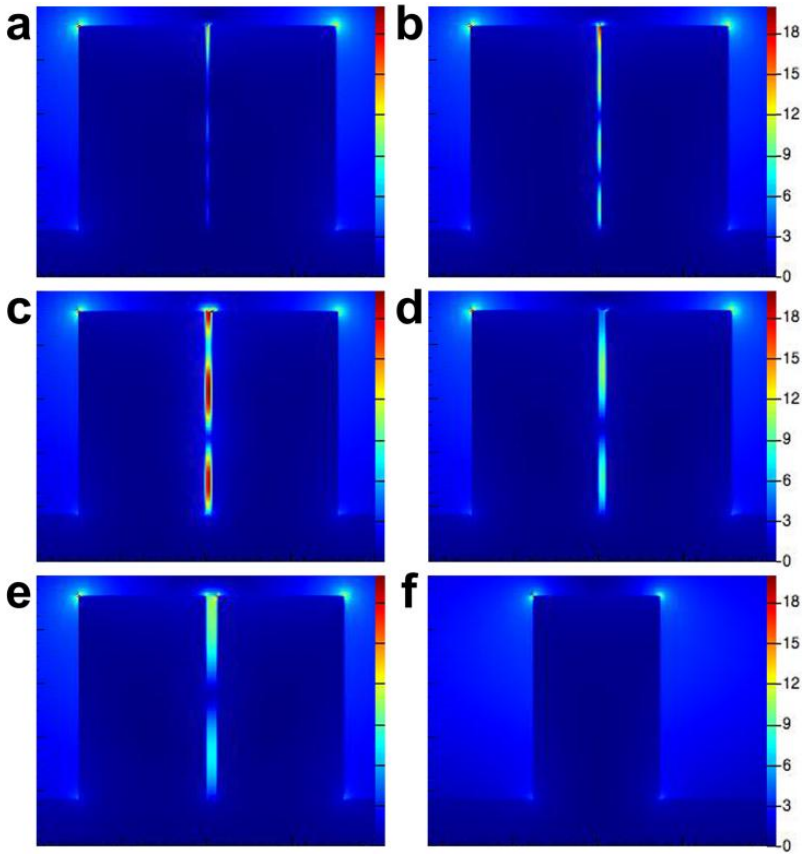

Figure 3.6 (a-e) FDTD simulations of the electric field distribution in cross-section between gold wires with 2 nm, 3 nm, 5 nm, 6 nm, 8 nm gap-widths, constant wire width (90 nm) and height (150 nm). (f) Calculated electric-field distribution of a single 90 nm-wide gold nanowire ($G \rightarrow \infty$) with a 150 nm-height. The scale represents E/E_0.

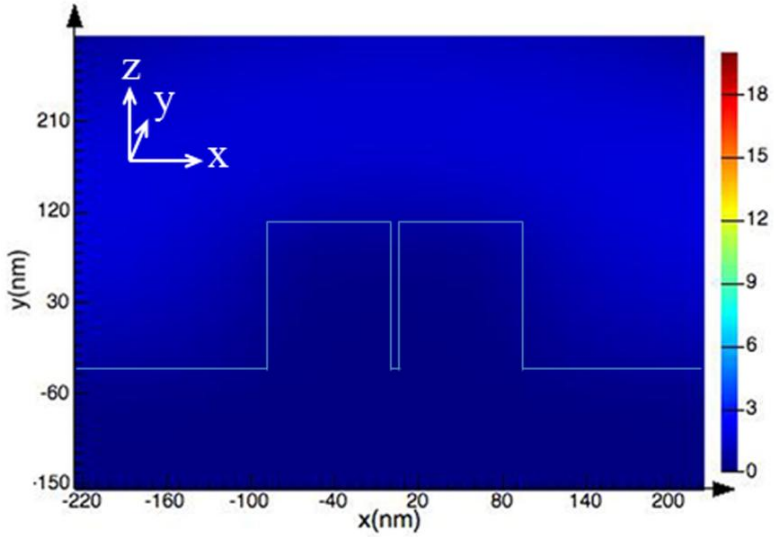

Figure 3.7 FDTD simulation of the electric field distribution in a cross-section of the 1D nanogap (5 nm gap-width) with the electric field polarized along the y-axis. The scale bar represents E/E_0.

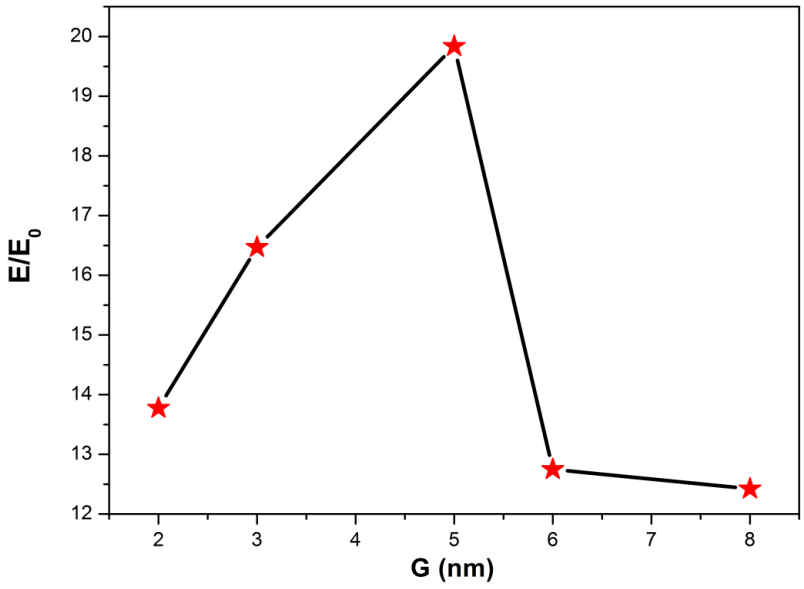

Figure 3.8 Maximum of the calculated electric-field intensity as a function of gap-width.

Unlike conventional nanogaps, which are usually “flat” with a short gap-height, the nanogaps in this work are relatively “tall” and uniform with a tunable height-to-width ratio (H/W) of greater than 18. Thus, the propagation of surface plasmon polariton (SPP) waves along the long-and-narrow gaps cannot be ignored. To confirm the non-monotonic dependence of electric field on gap-width, we investigated the formation of a strong standing wave produced by the 5 nm gaps, which greatly reduces the loss of waves and therefore enhances the plasmonic coupling. This standing wave is formed by the resonance of the SPP waves generated by the two closed edges of the gold nanowires and the SPPs reflected by the gold mirror on the substrate. The standing wave cannot form if the gap resides directly on the silicon substrate without a gold mirror due to lack of the effective reflected waves (Figure 3.9). The first requirement for forming a standing wave is two sufficiently strong waves with the same wavelength and speed, but opposite directions. The second requirement is that the wave path (the gap-height, H = 150 nm here) fits the equation:

$$H = n(\lambda/2),\ n \in N\ (\lambda \text{ refers to the wavelength of SPPs}). \quad (1)$$

When 633 nm light impinges on a nanogap, a strong LSPR is excited and the localized electric field is strongly enhanced. This generates SPPs propagating along the long-narrow gaps with much smaller wavelengths than the excitation wavelength.[50] The decreased wavelength may satisfy the equation (1) for the gap-height (H=150 nm). Smaller gap-widths contribute to stronger LSPR,[18] while large gap-widths lead to weak LSPR and SPPs, which may also result in a weak resonance and low field enhancement in the gap. However, for much smaller gap-widths, even though it can greatly decrease the wavelength, a significant amount of light is reflected by the upper surface of the two gold nanowires. Thus, the amount of light that can interact with the two closed edges of gold is insufficient to excite strong SPP waves. The SPPs that can reach the gold mirror is then too weak to form a standing wave. This relationship explains why neither a smaller gap nor a larger gap can form effective standing waves and why the maximum is obtained with a 5 nm gap-width and enables a mechanistic study of the electric field dependence

on gap-width for the high-ratio nanogaps.

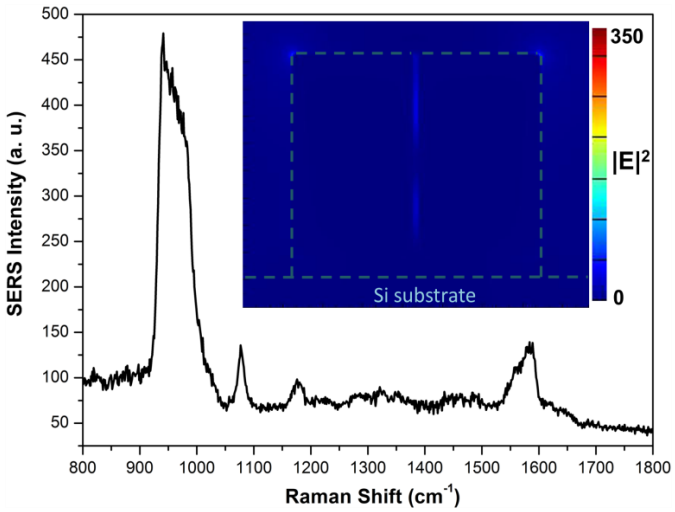

Figure 3.9 FDTD simulation of the 5 nm-gap residing on a silicon substrate without a gold mirror, and the corresponding SERS spectrum, which shows a weak characteristic signal of PATP and an overtone band of the silicon substrate.

3.3.4 Fabrication of 2D and 3D nanogap arrays

Based on the individual 1D nanogap, in order to integrate nanogap devices with required geometries over a large area, a surface patterning technique is introduced to produce 2D patterned nanogap arrays in the horizontal plane. As illustrated in Figure 3.1b, the patterned epoxy substrate was replicated from a photoresist template via soft lithography. The gold/aluminum/gold was successively deposited at a glancing angle on the unilateral sides of the shaped epoxy replica and then embedded the entire structure in more epoxy for sectioning. Due to the low adhesion between gold and the epoxy substrate, they tended to separate by the shear force during sectioning. However, the angular deposition fabricated discrete “L” shaped sandwich films, so that the epoxy on both sides of the films can interconnect and thus weakened the effect of the shear force caused by the diamond knife during sectioning. The epoxy block was sectioned parallel to the substrate into 150 nm-thick slabs containing arrays of gold/aluminum/gold sandwich nanowires. The slabs were transferred onto a silicon wafer bearing a gold mirror. After removal of aluminum and epoxy, a 2D, linear nanogap array was constructed with a higher level of

integration than that of a single nanogap (Figure 3.10a). Using this method, different lithographic masks will provide a wide variety of design freedom for making 2D patterned plasmonic and electric devices with required geometries over a large area. The packing density of the 2D nanogap array is increased along the horizontal direction compared with 1D linear nanogap. In general, a closer array leads to a larger hot spot density and a higher throughput. In practice, the resolution of conventional lithography techniques limits the period of stripes. Therefore, it remains a challenge to integrate more nanogaps on the same area with a higher throughput and improve their electric field enhancement without resorting to laborious direct-writing techniques.

To address this challenge, we explored the construction of 3D nanogaps along the vertical direction analogous to multistory construction, which is difficult for conventional nanogaps made by planar lithography. Likewise, nanoskiving is a process that usually focusses on the 1D or 2D nanostructures contained in one individual slab,[32, 37, 38] thus it might constrain the fabrication of 3D nanostructures. Nevertheless, different from most nanofabrication strategies, which usually yield a fixed structure on a substrate, the sectioned slabs are quasi-copies with free-standing and transferrable properties, thus we can position a second slab onto the original one using a “Perfect Loop” tool (Electron Microscope Sciences) to guide the second nanogap array over the first nanogap array in the desired orientation and position as illustrated in Figure 3.1c. The alignment of the two nanogap-arrays varying with the stacking angle (α) defines the shape of the nanogrids. After removal of the sacrificial spacer and epoxy, 3D packed nanogap grids were constructed (Figure 3.10b, c). In this way, more nanogaps can be packed on the same area by occupying vertical space, requiring only a simple stacking process with no special infrastructure. Moreover, the linear nanogaps in the 3D structures are able to interlock with each other into a highly stable 3D woodpile configuration in comparison with loosely packed 2D structures assembled by metallic nanoparticles[51]. To our knowledge this is the first report on the stacking of nanogap arrays along the vertical direction.

In the 2D nanogap array, the gap density is largely increased, but the electric field enhancement remains unchanged compared to the 1D nanogap, because the individual nanogaps are too far from each other to couple. Nevertheless, in the 3D nanogap grids, two types of hotspots were acquired. One is the linear gap as mentioned above; the other is the "two-story" gap at the crossing point where upper and lower linear nanogaps are stacked angularly. Manipulating the position of the second slab generates differently-shaped nanogap grids, such as a square grid and a diamond grid (Figure 3.10b, c). To explore the electric field enhancements in these unconventional plasmonic structures, SERS measurements were performed on linear nanogaps and crossing points of the nanogrids with different α (Figure 3.10d). The black dotted line shows the Raman spectra of PATP taken from the linear gap in the nanogap grid, and the intensity from the crossing point of $\alpha = 90^{o}$ shown by the black solid line is a factor of 2.5 greater than that from the linear gaps (C-S stretch at 1077 cm^{-1} was used for comparison). Notably, the crossing point of $\alpha = 45^{o}$ generates a signal, plotted by the red line, stronger by a factor of 4.5 compared to that from the linear gaps. This observation suggests that 3D-packed nanogap grids not only enlarge the gap density by extending into the vertical space, but also improve the electric field enhancement, which may originate from a strong and intense localized electromagnetic field (hot spots) at the crossing point. To a certain extent, smaller angle crossing points may generate the stronger electric field enhancement according to the corresponding SERS measurements.

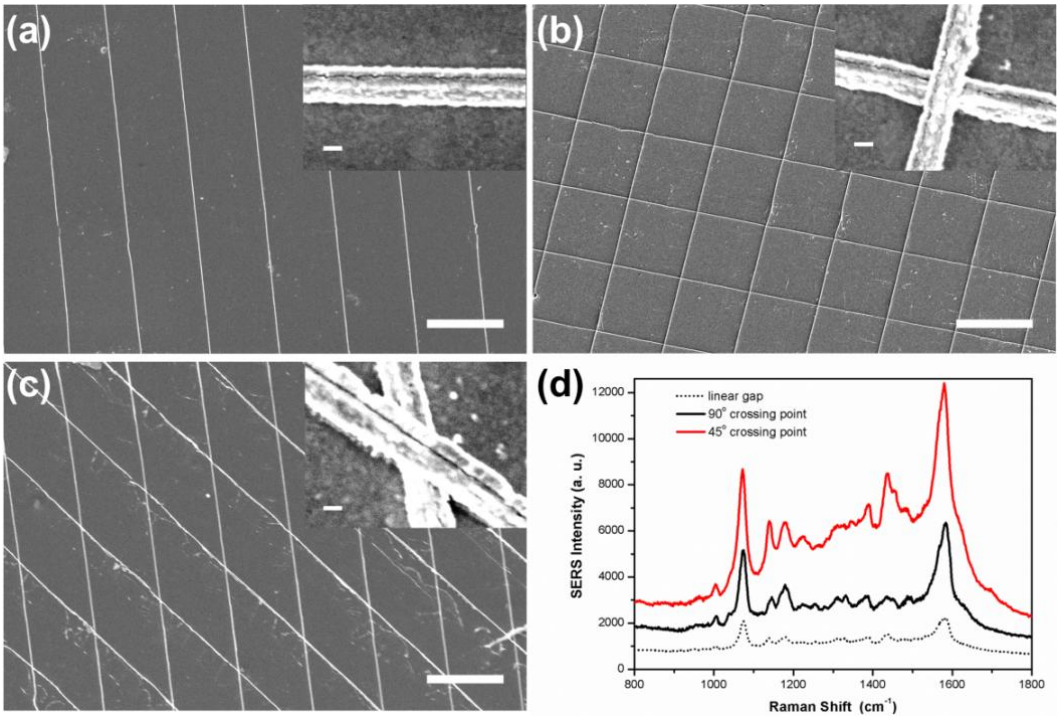

Figure 3.10 (a) SEM images of a linear nanogap array. (b, c) SEM images of a nanogap grid array with different stacking angles. Scale bar: 20 μm. Insets show magnified images. Scale bar: 100 nm. (d) SERS spectra obtained from the linear gap and the crossing point of b, c.

The 3D nanogaps are composed of two 1D nanogaps with different intersection angle α, which may range from 0^o to 90^o. Without consideration of the interaction of the two gaps, under non-polarized light (whose beam spot is 1 μm, which is much larger than the crossing point region, corresponding sketch shown in Figure 3.11), the total plasmonic performance (I_{3D}) at the crossing point region is the sum of either gap performance (I_{1D}) because of the doubled coupling region, which remains unchanged no matter what the stacking angle is ($I_{3D} = 2\ I_{1D}$). However, according to the corresponding SERS experiments, the crossing points in the 3D orthogonal nanogaps generated a greater signal enhancement, $I_{3D\text{-}90^\circ} = 2.5I_{1D}$; the crossing point of $\alpha = 45^o$ generates a much stronger signal, $I_{3D\text{-}45^\circ} = 4.5I_{1D}$. The additional enhancement should be attributed to the interaction of the two linear gaps as.

$$I_{add\text{-}90^\circ} = 2.5I_{1D} - 2I_{1D} = 0.5I_{1D},\ I_{add\text{-}45^\circ} = 4.5I_{1D} - 2I_{1D} = 2.5I_{1D} \quad (2)$$

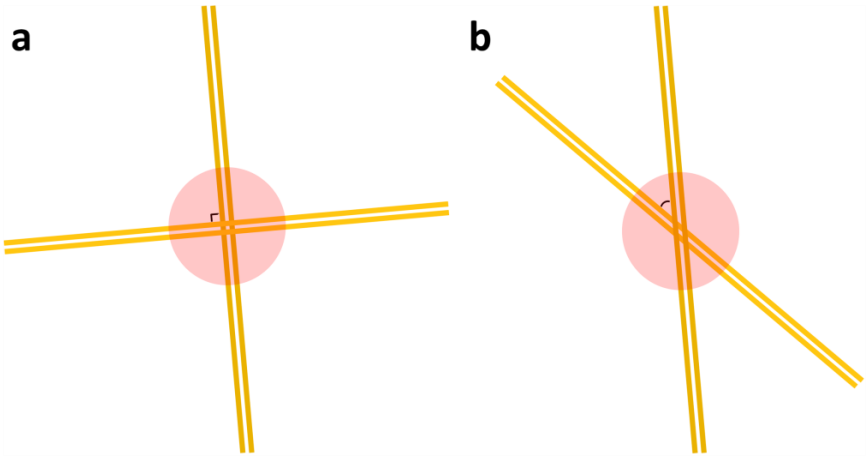

Figure 3.11. Sketches of the relationship of the laser beam used in the SERS measurements and the orthogonal a) and skew b) 3D nanogaps.

FDTD simulations were performed upon the different-angled 3D nanogaps (Figure 3.12a-c). The strongest electric-field enhancement happens at the outside corners of the crossing points; the lower nanogaps also generate a strong electric-field enhancement which is weaker than the corners but much stronger than the corresponding 1D gap. However, the upper nanogaps perform really slight electric-field enhancement. For the orthogonal 3D gaps, the local highest electric-field intensity is approximately 700; the local highest electric-field intensity for 45^{o} case reaches up to 6000, comparing to the local highest electric-field intensity for the corresponding 1D nanogaps of nearly 400. These comparisons could corroborate the experimental data interpretation. Moreover, when α decreased to 30^{o}, the electric-field enhances extremely sharply with a local highest electric-field intensity of approximately 20000, indicating that decreasing the intersection angle will tremendously enhance the electric-field at the crossing points. We attribute the huge field enhancement to the adiabatic nanofocusing caused by the SPP propagation toward the tapered tip (acute-angled region of the crossing point).[52] This propagation causes accumulation of the SPP energy at the tip and giant increase of the local fields. Sharper tips generate stronger accumulation of the energy, thus smaller α contributes to stronger electric-field. As a reference, a simulation for two 30^{o}-stacked nanowires with doubled wire-width but no inset gaps shows a strong field enhancement

at the acute corners of the crossing point with a local highest electric-field intensity of about 2000, which is still much weaker than the homological ones with nanogaps inset (Figure 3.12d). We infer that the presences of nanogaps and the smaller α are both vital to the huge field enhancement. The sub-10 nm gaps provide strong SPP which could propagate towards the sharp tip to accumulate energy and enormously enhance the local field. When α is definitely 0^{o}, which means the upper and lower nanogaps completely overlapped, the sharp tip disappears and SPP could not accumulate, lowering the electric-field to a common level (Figure 3.13).

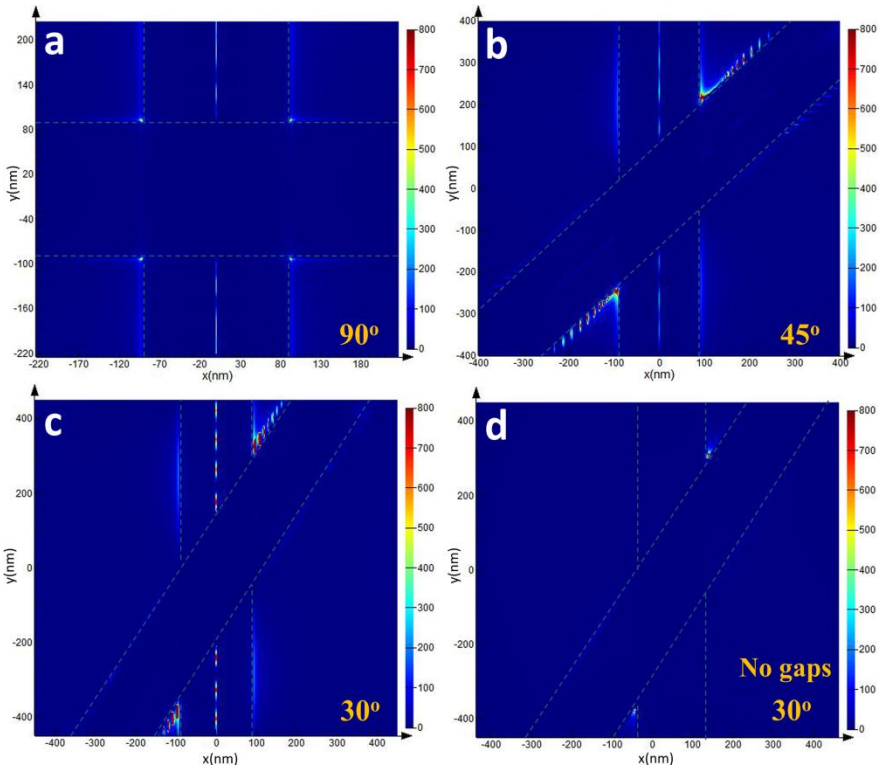

Figure 3.12 a-c) FDTD simulations of the electric-field distribuation in the 3D stacked nanogaps with different α. d) FDTD simualtion of two 30^{o}-stacked nanowires with doubled wire-width but no inset gaps. The scale represents $|E|^2$.

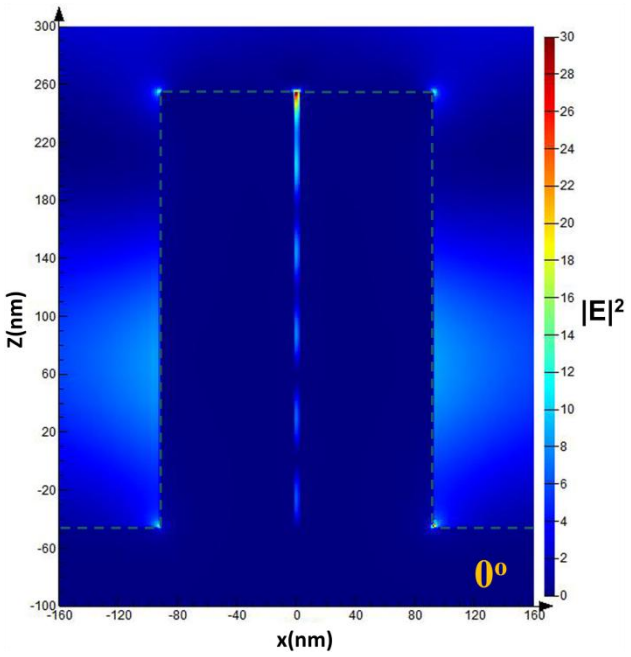

Figure 3.13 FDTD simulation of the electric-field distribution in the cross-section of a 0^{o}-stacked nanogap (*i.e.*, a doubled-height 1D nanogap), showing weak electric-field intensity. The scale bar represents $|E|^2$.

3.4 Conclusion

In this chapter, 1D, 2D and 3D plasmonic gaps with tunable, sub-10 nm gap-widths are fabricated by nanoskiving. The gap-widths can be controlled with nanometer precision via the thickness of sacrificial spacer films. As the hot spots of each nanogap extend uniformly along macroscopic lengths, these nanogaps are robust to local defects or contaminants, facilitating more reproducible SERS spectroscopy. This reproducibility enables a systematic investigation of the dependence of electric field enhancement on gap-width, with the surprising result that it is non-monotonic in the range between 2 and 8 nm with a maximum at 5 nm, which we attribute to the formation of a standing wave. In agreement with FDTD simulations, the maximum SERS signal is obtained for this gap width. The surface patterning technique could be extended to fabricate a 2D patterned nanogap array on a horizontal plane with a higher integration. Furthermore, by stacking nanogaps along the vertical direction, 3D nanogap grids are easily constructed. The

construction of 3D nanogap grids not only enlarges the gap density, but also improves the electric field enhancement at the crossing points. For a smaller stacking angle, the electric-field is tremendously enhanced, which result from the adiabatic nanofocusing caused by the SPP propagation toward the tip. Such structures will facilitate the control of plasmonic interactions and contribute to applications in nano-optics as well as nano-electronics[53-55]. We also expect that the 3D nanogap arrays based on nanoskiving and stacking of nanogaps along the vertical direction will broaden the scope of fabricating 3D complex nanostructures in a simple and efficient way and improve our understanding of local electric fields.

Bibliography

1. A. M. Michaels, J. Jiang, and L. Brus, Ag Nanocrystal Junctions as the Site for Surface-Enhanced Raman Scattering of Single Rhodamine 6G Molecules, *J. Phys. Chem. B* **2000**, 104, 11965–11971.

2. P. K. Jain, X. H. Huang, I. H. El-Sayed, and M. A. El-Sayed, Noble Metals on the Nanoscale: Optical and Photothermal Properties and Some Applications in Imaging, Sensing, Biology, and Medicine, *Acc. Chem. Res.* **2008**, 41, 1578−1586.

3. B. Ai, Y. Yu, H. Möhwald, and G. Zhang, Responsive Monochromatic Color Display Based on Nanovolcano Arrays, *Adv. Opt. Mater.* **2013**, 1, 724−731.

4. B. Ai, Y. Yu, H. Möhwald, L. Wang, and G. Zhang, Resonant Optical Transmission through Topologically Continuous Films, *ACS Nano* **2014**, 8, 1566–1575.

5. M. N. Sanz-Ortiz, K. Sentosun, S. Bals, and L. M. Liz-Marzán, Templated Growth of Surface Enhanced Raman Scattering-Active Branched Gold Nanoparticles within Radial Mesoporous Silica Shells, *ACS Nano* **2015**, 9, 10489–10497.

6. G. Bodelón, V. Montes-García, C. Fernández-López, I. Pastoriza-Santos, J. Pérez-Juste, and L. M. Liz-Marzán, Au@pNIPAM SERRS Tags for Multiplex Immunophenotyping Cellular Receptors and Imaging Tumor Cells, *Small* **2015**, 11, 4149–4157.

7. J. Kumar, X. Wei, S. Barrow, A. M. Funston, K. G. Thomas, and P. Mulvaney, Surface Plasmon Coupling in End-to-End Linked Gold Nanorod Dimers and Trimers, *Phys. Chem. Chem. Phys.* **2013**, 15, 4258– 4264.

8. L. Gunnarsson, E. J. Bjerneld, H. Xu, S. Petronis, B. Kasemo, and M. Käll, Interparticle coupling effects in nanofabricated substrates for surface-enhanced Raman scattering, *Appl. Phys. Lett.* **2001**, 78, 802–804.

9. H. Wang, C. S. Levin, and N. J. Halas, Nanosphere Arrays with Controlled Sub-10-nm Gaps as Surface-Enhanced Raman Spectroscopy Substrates, *J. Am. Chem. Soc.* **2005**, 127, 14992–14993.

10. D. R. Ward, N. K. Grady, C. S. Levin, N. J. Halas, Y. P. Wu, P. Nordlander, and D. Natelson, Electromigrated Nanoscale Gaps for Surface-Enhanced Raman Spectroscopy, *Nano Lett.* **2007**, 7, 1396–1400.

11. T. Brintlinger, A. A. Herzing, J. P. Long, I. Vurgaftman, R. Stroud, and B. S. Simpkins, Optical Dark-Field and Electron Energy Loss Imaging and Spectroscopy of Symmetry-Forbidden Modes in Loaded Nanogap Antennas, *ACS Nano* **2015**, 9, 6222– 6232,

12. L. D. Qin, S. L. Zou, C. Xue, A. Atkinson, G. C. Schatz, and C. A. Mirkin, Designing, fabricating, and imaging Raman hot spots, *Proc. Natl. Acad. Sci. U.S.A.* **2006**, 103, 13300–13303.

13. X. Chen, H.-R. Park, M. X. Pelton, Piao, N. C. Lindquist, H. Im, Y. J. Kim, J. S. Ahn, K. J. Ahn, N. Park, D.-S. Kim, and S.-H. Oh, Atomic layer lithography of wafer-scale nanogap arrays for extreme confinement of electromagnetic waves, *Nat. Commun.* **2013**, 4, 2361.

14. M. Danckwerts, and L. Novotny, Optical Frequency Mixing at Coupled Gold Nanoparticles, *Phys. Rev. Lett.* **2007**, 98, No. 026104.

15. Z. Dong, M. Asbahi, J. Lin, D. Zhu, Y. M. Wang, K. Hippalgaonkar, H.-S. Chu, W. P. Goh, F. Wang, Z. Huang, and J. K. W. Yang, Second-Harmonic Generation from Sub-5 nm Gaps by Directed Self-Assembly of Nanoparticles onto Template-Stripped Gold Substrates, *Nano Lett.* **2015**, 15, 5976−5981.

16. H. Xu, and M. Kall, Surface-Plasmon-Enhanced Optical Forces in Silver Nanoaggregates, *Phys. Rev. Lett.* **2002**, 89, No. 246802.

17. Y. Pang, and R. Gordon, Optical Trapping of a Single Protein, *Nano Lett.* **2012**, 12, 402−406.

18. M. Chirumamilla, A. Toma, A. Gopalakrishnan, G. Das, R. Proietti Zaccaria, R. Krahne, E. Rondanina, M. Leoncini, C. Liberale, F. De Angelis, and E. Di Fabrizio, 3D Nanostar Dimers with a Sub-10-nm Gap for Single-/Few-Molecule Surface-Enhanced Raman Scattering, *Adv. Mater.* **2014**, 26, 2353−2358.

19. X. S. Chen, C. Ciraci, D. R. Smith, and S. H. Oh, Nanogap-Enhanced Infrared Spectroscopy with Template-Stripped Wafer-Scale Arrays of Buried Plasmonic Cavities, *Nano Lett.* **2015**, 15, 107−113.

20. V. T. Cong, E. O. Ganbold, J. K. Saha, J. Jang, J. Min, J. Choo, S. Kim, N. W. Song, S. J. Son, S. B. Lee, and S. W. Joo, Gold Nanoparticle Silica Nanopeapods, *J. Am. Chem. Soc.* **2014**, 136, 3833−3841.

21. Y. Naitoh, T. Ohata, R. Matsushita, E. Okawa, M. Horikawa, M. Oyama, M. Mukaida, D. F. Wang, M. Kiguchi, K. Tsukagoshi, and T. Ishida, Self-Aligned Formation of Sub 1 nm Gaps Utilizing Electromigration during Metal Deposition, *ACS Appl. Mater. Interfaces* **2013**, 5, 12869−12875.

22. S. J. Barrow, A. M. Funston, D. E. Gómez, T. J. Davis, and P. Mulvaney, Surface Plasmon Resonances in Strongly Coupled Gold Nanosphere Chains from Monomer to Hexamer, *Nano Lett.* **2011**, 11, 4180–4187.

23. S. Shaw, and L. Cademartiri, Nanowires and Nanostructures that Grow like Polymer Molecules, *Adv. Mater.* **2013**, 25, 4829–4844.

24. H. Duan, H. Hu, H. K. Hui, Z. Shen, and J. K. W. Yang, Free-standing sub-10 nm nanostencils for the definition of gaps in plasmonic antennas, *Nanotechnology* **2013**, 24, 18530110.1088/0957- 4484/24/18/185301.

25. H. Choo, M.-K. Kim, M. Staffaroni, T. J. Seok, J. Bokor, S. Cabrini, P. J. Schuck, M. C. Wu, and E. Yablonovitch, Nanofocusing in a metal–insulator–metal gap plasmon waveguide with a three-dimensional linear taper, *Nat. Photonics* **2012**, 6, 838−844.

26. M. Melli, A. Polyakov, D. Gargas, C. Huynh, L. Scipioni, W. Bao, D. F. Ogletree, P. J. Schuck, S. Cabrini, and A. Weber-Bargioni, Reaching the Theoretical Resonance Quality Factor Limit in Coaxial Plasmonic Nanoresonators Fabricated by Helium Ion Lithography, *Nano Lett.* **2013**, 13, 2687−2691.

27. H. Im, K. C. Bantz, S. H. Lee, T. W. Johnson, C. L. Haynes, and S.-H. Oh, Self-Assembled Plasmonic Nanoring Cavity Arrays for SERS and LSPR Biosensing, *Adv. Mater.* **2013**, 25, 2678−2685.

28. J. M. Hoffmann, H. Janssen, D. N. Chigrin, and T. Taubner, Enhanced infrared spectroscopy using small-gap antennas prepared with two-step evaporation nanosphere lithography, *Opt. Express* **2014**, 22, 14425−14432.

29. H. Ni, M. Wang, T. Shen, and J. Zhou, Self-Assembled Large-Area Annular Cavity Arrays with Tunable Cylindrical Surface Plasmons for Sensing, *ACS Nano* **2015**, 9, 1913– 1925.

30. L. Qin, S. Park, L. Huang, and C. A. Mirkin, On-Wire Lithography, *Science* **2005**, 309, 113–115.

31. T. Ozel, G. R. Bourret, and C. A. Mirkin, Coaxial lithography, *Nature Nanotech.* **2015**, 10, 319-324.

32. H. Im, K. C. Bantz, N. C. Lindquist, C. L. Haynes, and S.-H. Oh, Vertically Oriented Sub-10-nm Plasmonic Nanogap Arrays, *Nano Lett.* **2010**, 10, 2231−2236.

33. T. Li, W. Hu, D. Zhu, Nanogap Electrodes, *Adv. Mater.* **2010**, *22*, 286–300.

34. Y. Fang, N. H. Seong, and D. D. Dlott, Measurement of the Distribution of Site Enhancements in Surface-Enhanced Raman Scattering, *Science* **2008**, 321, 388–392.

35. A. V. Zaretski, B. C. Marin, H. Moetazedi, T. J. Dill, L. Jibril, C. Kong, A. R. Tao, and D. J. Lipomi, Using the Thickness of Graphene to Template Lateral Subnanometer Gaps between Gold Nanostructures, *Nano Lett.* **2015**, 15, 635−640.

36. Q.-Y. Lin, Z. Li, K. A. Brown, M. N. O'Brien, M. B. Ross, Y. Zhou, S. Butun, P.-C. Chen, G. C. Schatz, V. P. Dravid, K. Aydin, and C. A. Mirkin, Strong Coupling between Plasmonic Gap Modes and Photonic Lattice Modes in DNA-Assembled Gold Nanocube Arrays, *Nano Lett.* **2015**, 15, 4699−4703.

37. A. Klinkova, H. Therien-Aubin, A. Ahmed, D. Nykypanchuk, R. M. Choueiri, B. Gagnon, A. Muntyanu, O. Gang, G. C. Walker, and E. Kumacheva, Structural and Optical Properties of Self-Assembled Chains of Plasmonic Nanocubes, *Nano Lett.* **2014**, 14, 6314−6321.

38. L. Le Thi Ngoc, M. Jin, J. Wiedemair, A. van den Berg, and E. T. Carlen, Large Area Metal Nanowire Arrays with Tunable Sub-20 nm Nanogaps, *ACS Nano* **2013**, 7, 5223−5234.

39. X. Liu, Y.-Z. Long, L. Liao, X. Deng, and Z. Fan, Large-Scale Integration of Semiconductor Nanowires for High-Performance Flexible Electronics, *ACS Nano* **2012**, 6, 1888−1900.

40. V. Abramova, A. S. Slesarev, and J. M. Tour, Meniscus-Mask Lithography for Fabrication of Narrow Nanowires, *Nano Lett.* **2015**, 15, 2933–2937.

41. Q. Xu, B. D. Gates, and G. M. Whitesides, Fabrication of Metal Structures with Nanometer-Scale Lateral Dimensions by Sectioning Using a Microtome, *J. Am. Chem. Soc.* **2004**, 126, 1332−1333.

42. Q. Xu, J. Bao, F. Capasso, and G. M. Whitesides, Surface Plasmon Resonances of Free-Standing Gold Nanowires Fabricated by Nanoskiving, *Angew. Chem. Int. Ed.* **2006**, 45, 3631−3635.

43. Q. Xu, R. M. Rioux, M. D. Dickey, and G. M. Whitesides, Nanoskiving: A New Method to Produce Arrays of Nanostructures, *Acc. Chem. Res.* **2008**, 41, 1566−1577.

44. D. J. Lipomi, M. A. Kats, P. Kim, S. H. Kang, J. Aizenberg, F. Capasso, and G. M. Whitesides, Fabrication and Replication of Arrays of Single- or Multicomponent Nanostructures by Replica Molding and Mechanical Sectioning, *ACS Nano* **2010**, 4, 4017–4026.

45. D. J. Lipomi, R. V. Martinez, and G. M. Whitesides, Use of Thin Sectioning (Nanoskiving) to Fabricate Nanostructures for Electronic and Optical Applications, *Angew. Chem. Int. Ed.* **2011**, 50, 8566−8583.

46. P. Pourhossein, and R. C. Chiechi, Directly Addressable Sub-3 nm Gold Nanogaps Fabricated by Nanoskiving Using Self-Assembled Monolayers as Templates, *ACS Nano* **2012**, 6, 5566−5573.

47. P. Pourhossein, and R. C. Chiechi, Fabricating Nanogaps by Nanoskiving, *J. Vis. Exp.* **2013**, 75, e50406.

48. L. M. Tong, H. X. Xu, and M. Käll, Nanogaps for SERS applications, *MRS Bull.* **2014**, 39, 163–168.

49. N. Mohri, S. Matsushita, M. Inoue, and K. Yoshikawa, Desorption of 4-Aminobenzenethiol Bound to a Gold Surface, *Langmuir* **1998**, 14, 2343–2347.

50. E.-S. Kwak, J. Henzie, S.-H. Chang, S. K. Gray, G. C. Schatz, and T. W. Odom, Surface Plasmon Standing Waves in Large-Area Subwavelength Hole Arrays, *Nano Lett.* **2005**, 5, 1963-1967.

51. M. Chen, I. Y. Phang, M. R. Lee, K. W. Yang, and X. Y. Ling, Layer-By-Layer Assembly of Ag Nanowires into 3D Woodpile-like Structures to Achieve High Density "Hot Spots" for Surface-Enhanced Raman Scattering, *Langmuir* **2013**, 29, 7061−7069.

52. M. I. Stockman, Nanoplasmonic Sensing and Detection, Sc*ience* **2015**, 348, 287-288.

53. S. Kim, J. H. Jin, Y. J. Kim, I. Y. Park, Y. Kim, and S. W. Kim, High-harmonic generation by resonant plasmon field enhancement, *Nature* **2008**, 453, 757–760.

54. M. W. Knight, H. Sobhani, P. Nordlander, and N. J. Halas, Photodetection with Active Optical Antennas, *Science* **2011**, 332, 702–704.

55. H. Song, Y. Kim, Y. H. Jang, H. Jeong, M. A. Reed, and T. Lee, Observation of molecular orbital gating, *Nature* **2009**, 462, 1039–1043.

Chapter 4

Fabrication of Gold Nanowire Devices with Bisecting Microfluidic Channels by Nanoskiving

4.1 Introduction

Devices based on nanowires are emerging as ultrasensitive sensors that produce signals for the detection of biologic and chemical species from drug molecules, proteins and DNA to gas, pH and ethanol.[1-7] Nanowires together with ultrahigh sensitivity to surface changes is quite advantageous for sensing applications and could revolutionize many aspects of sensing and detection due to their large surface area to volume ratio and the similar size of nanowires with species being sensed. Much of the work on nanowire sensors have been studied by measuring the change of an electrical signal resulting from reactions or effects of species on the surface of the nanowires.[8-11] In general, nanowires serve as the most basic components of integrated circuitry: field effect transistor (FET), combining with microfluidic systems for sensing applications. The detection can be made at extremely low concentrations. In 2001, Si nanowires were first used to as chemical and biological sensors followed by many subsequent studies.[3] Through the optimization of

*Parts of this chapter have been published in: ACS Nano, 2016, 10, 2852-2859. The fabrication and position of the gold nanowires were performed in my lab. I would like to thank Gerard A. Kalkman, Yanxi Zhang, Enrico Monachino, Klaus Mathwig, Machteld E. Kamminga, Parisa Pourhossein, Pieter E. Oomen, Sarah A. Stratmann, Antoine M. van Oijen, and Elisabeth Verpoorte for the fruitful collaboration. I would like to give special thanks to Gerard A. Kalkman who made a great contribution for this work; Machteld E. Kamminga who kindly provided images in her Master thesis as references in my thesis.

device performance, real-time detection of various biological species at low concentrations has been achieved.[4,12,13]

However, the most of nanowires in these devices are just several micrometers in length. They have to be placed on the floor of a microchannel that confines them to a surface and does not take advantage of their discrete nature; there is little functional difference between a thin, photolithographically patterned stripe and a nanowire lying on a flat surface. In microfluidic devices viscous forces tend to dominate, leading to laminar flow. The flow profile in this case is zero at the solid/liquid interface and at a maximum in the center of the channel. The mass transport to the nanowire surface positioned on the floor of channels occurs mainly by diffusion that limits the further improvement of the sensitivity and detection time of the nanowire sensors. Therefore, in microfluidic configuration, the sensitivities of the nanowire sensor are unlikely to exceed the near femtomolar range on the order of minutes. Additionally, ultrafast detection (<100 s) at fetomolar concentrations also is difficult to achieve in practice.[14] Failure of detection may be due to the limit of the system. Thus, it is very important to fabricate long nanowires that can be suspended away from the floor of channel to the central place for sensing the highest rate of flow.

Comparison to the conventional lithography and gas-phase or solution-phase synthesis for the fabrication of nanowires, Nanoskiving, a simple and fast method, fabricates nanowires inside a host matrix (usually a cross-linked polymer[15]) that can be manipulated one or several at a time.[16,17] It can be used to form nanowires directly from thin films embedded in polymer matrices.[18] The simplest case, sectioning thin metal films, produces metallic nanowires with control over all three dimensions that can be millimeters long.[19] These high-aspect-ratio nanowires can be transferred and positioned in the center of the channel.

In sufficiently small channels with large surface-to-volume ratios, flow is near-zero over a large portion of the channel. Therefore, when structures are anchored to a surface in the channel for flow interaction in regions which are near or at zero flow, measurements

will yield results which are not fully representative of the flow profile. A common example of this problem arises in the *in situ* measurement of rates of flow. Planar lithography confines metallic features to two dimensions and anchors them to a surface, requiring two sensing elements and a heating element to measure flow resistively.[20] Micro-electro-mechanical systems can measure flow mechanically *e.g.*, using external optics,[21] but at the expense of sensitivity and the simplicity of resistive measurements. Another example of an experiment requiring flow in a passive microfluidic system is the study of flow elongation in which long DNA molecules are confined to a microfluidic channel and pulled taut by flow for visualization by single-molecule fluorescence.[22-24] The visualization is performed using total internal reflection fluorescence (TIRF) microscopy. In comparison to other single-molecule imaging techniques, such as atomic force microscopy, optical traps and magnetic tweezers, to immobilize and stretch out only one DNA molecule at-a-time for studying, a number of DNA molecules can be studied at the same time in a flow cell. If DNA molecules are attached to the surface of the bottom of a channel, they are placed in a region of near-zero flow and require high flow rates to achieve elongation. Usually, glass coverslips serve as the bottom of the channel to immobilize DNA molecules via biotin-streptavidin-biotin linkage. Light passes from the glass into water to generate a thin evanescent field of about 100 nm by the total internal reflection of the incoming light at the glass-sample interface. The evanescent field excites the fluorescent molecule resulting in high-contrast fluorescence images of single-molecule with high signal-to-noise ratio. Both of these examples-one active and one passive-would benefit from the nanoscale objects being elevated from the surface and held in the center of the channel where the flow is the highest. However, to do so requires the ability to place discrete, three-dimensional nano-objects at arbitrary positions inside of a microchannel, exposing the entire surface-area to the fluid environment.

In this chapter, millimeter-long gold nanowires fabricated by nanoskiving were integrated into microfluidic devices. The fabrication process of the devices is extraordinarily simple. The channels are fabricated independently followed by placing the

nanowires one-at-a-time or in arrays. Meantime, the fabrication enables control over the rotation, position, and spacing of the nanowires. To demonstrate the utility of integrating discrete nanowires into microfluidic channels, two device architectures were designed, one active and one passive. The active device demonstrates a two-terminal, hot-wire anemometer that samples flow in the center of the channel in which the entire surface area of the wire is in contact with the fluid being measured. The passive device uses the nanowires as substrates for the attachment of long DNA molecules for the study of elongation.

4.2 Experimental section

4.2.1 Fabrication of gold nanowires

A 200 nm-thick film of gold was deposited onto a clean silicon wafer through a Teflon mask by thermal evaporation. Epofix epoxy prepolymer was used to adhere and embed the gold features to form blocks of cured epoxy. After trimming the top of the prepared block to the width of diamond knife (2 mm Diatome Ultra 35^{o}) in a trapezoid shape using a razor blade, the block was sectioned using an ultramicrotome (Leica EM UC-6) to produce 200 nm-thick slabs that floated onto the surface of water. The resulting slabs containing gold nanowires were transferred from the water onto the appropriate substrate (e.g., etched glass). The epoxy matrix was removed by oxygen plasma dry etching for 15 min at 1 mbar.

4.2.2 Fabrication of devices

HF etching of glass: A prefabricated 4” square borofloat wafer coated with chromium and photoresist (Telic, USA, MED027021P) was exposed to a UV light source through a semitransparent mask. Developer (AZ 351 B Developer, AZ Electronic Materials, Germany) was used to remove the exposed photoresist. Chrome etch (Chrome Etch 18, OSC-OrganoSpezialChemie, Germany) was used to remove the chrome layer beneath. The exposed glass was etched using HF. After etching the unexposed photoresist and chrome

were removed using acetone and chrome etch.

Fabrication of PDMS channel: A 40 µm-high SU-8 master was fabricated on a glass borofloat wafer (10 cm diameter, 0.7 mm thick). The wafer was cleaned following standard wet cleaning protocols and dried on a hot plate. A spin-coater was used to coat the wafer with a 40 µm-thick layer of SU-8 50 (Microchem). After a baking step to evaporate the solvent in the SU-8, the wafer was exposed to UV light through a semi-transparent mask to cross-link the exposed SU-8. Developer (md-Dev 600, Micro Resist Technology, Germany) was used to remove the unexposed SU-8. Poly(dimethylsiloxane) (PDMS) prepolymer (Sylgard 184, Dow Corning, prepolymer and curing agent in 10:1 w/w ratio) was placed under a vacuum for 30 min to remove any bubbles, and then poured over the wafer and cured in oven for 3 hours at 60 ^{o}C. After curing, the desired patterns were cut from the PDMS slab using a sharp razor blade. To create fluid inlets and outlets, a biopsy puncher with a diameter of 1.2 mm was used.

Procedure of fabricating devices: After etching glass to form a channel, a sand blaster (Sandmaster FG 2-94) was used to create two holes on both sides that were positioned approximately 2 mm from the center of channel for contact wires. Next, two contact wires were added (0.1 mm tin wires) and the glass was mounted on a microscope slide using epoxy glue for easy handing and mechanical stability. An epoxy section containing a 200 nm × 200 nm gold nanowire was transferred over the center of the channel of glass substrate. The epoxy matrix was then etched using oxygen plasma. Two holes were punched by hand in the PDMS top part on both sides of the channel using a 3 mm-diameter biopsy puncher, approximately 0.5 mm from the sides of the channel. The glass and PDMS parts were exposed to oxygen plasma and contacted with each other to irreversibly bond them. A custom-built aligner was used to align the two parts prior to bonding. In the last step the gold nanowire was connected to the contact wires by adding silver paste into the two holes of PDMS part.

Resistance versus flow measurement: The fluid inlet of the nanowire device was connected to a 10 mL syringe with a diameter of 15.8 mm, and the fluid outlet was

coupled to a waste beaker. Polyethylene tubing (PE 60, 0.76 mm inner diameter, 1.22 mm outer diameter, Bioseb) was used to make the fluid connections. The inlet rates of the flow were set manually by a syringe pump (Spritzenpumpe LA-100, Landgraf Laborsysteme HLL GmbH). The used fluid was ethanol. The device was connected to a Keithley 2400 SourceMeter. After the ethanol flow was injected into microfluidic channel, the I-V plots of the gold nanowire under a series of voltages (0.5 V, 1.0 V, 1.5 V, and 2.0 V) were recorded and the resulting current was measured over time at different rates of fluid flow.

4.2.3 Construction of flow cell for DNA stretching

Glass coverslips (60 mm in length, 24 mm in width, and 0.13-0.16 mm in thickness) were successively cleaned in 2% Hellmanex III (Hellma Analytics), 100% ethanol (Avantor), and 1 M KOH (Sigma-Aldrich) followed by depositing a 2 nm chromium adhesion layer and a layer of 10 nm gold on the surface of the glass. Two stripes of 50 µm–thick double-sided tape were attached on each slide to form a 40 mm × 4 mm channel. HF etching was performed to excavate a 60 µm-wide and 20 µm-deep channel in a borofloat glass (Telic, 0.7 mm in thickness, 5 mm in width, and 45 mm in length). After the 400 nm × 400 nm gold nanowires were positioned on the bottom surface, the etched slide was placed on the two tape stripes so that the etched channel is in center. Then epoxy was used to glue two homemade ports on the top of inlet/outlet holes for supporting the polyethylene tubing. A syringe pump was connected to the inlet tube to control the buffer flow.

The gold-coated glass coverslips were incubated with 10 mM cysteamine in ethanol for at least 2 hours, functionalizing the gold surface with primary amines via the formation of a self-assembled monolayer. After rinsing by ethanol, the modified gold-coated coverslips were incubated with 0.3 mg/mL PEG-biotin in PBS (pH=8.2) for 1 hour to functionalize them with biotin. Subsequently, they were incubated with 0.2 mg/mL streptavidin in PBS (pH=8.2) for 30 minutes to bind the biotin resulting in the gold surface modified with surface-bound streptavidin and then constructed into a flow cell. Finally, forked

lambda-phage DNA molecules, biotinylated at the 5' end of the fork (3), were flowed into the chamber in 20 mM Tris (pH=7.5), 2 mM EDTA, 50 mM NaCl, 1 mg/mL bovine serum albumion (BSA), and 0.025% Tween20. Excess DNA molecules were removed by washing with the same buffer. 100 nM SYTOX Orange (Invitrigen) was used to stain the DNA molecules. The Sytox-stained DNA molecules were excited with a 532 nm solid-state laser (Coherent Sapphire 532-200 CW) at 25 Wcm^{-2} in epifluorescence mode. The resulting fluorescent signal was collected through a 100x oil-immersion TIRF objective (Olympus, 1.49 NA) and recorded on an EM-CCD camera (Hamamatsu). For immobilizing DNA molecules on gold nanowires, the modifications of the suspended gold nanowires in the flow cell were performed in the similar ways. The only difference is that, after functionalized with amine groups, the nanowires were incubated with 0.3 mg/mL NHS-biotin in PBS (pH=8.2).

4.2.4 Microscopy imaging

Scanning electron microscope images of the gold nanowire were acquired using a field emission SEM (Jeol JSM 7000F) operating at 5 kV. A thin layer of gold was sputtered on the surface to avoid charging artifacts.

4.3 Results and Discussion

4.3.1 Fabrication

High-aspect-ratio gold nanowires were fabricated by depositing a 200 nm-thick gold film which was then embedded in a block of epoxy, and sliced into thin sections (200 nm in thickness) perpendicular to the plane of thin film by Nanoskiving. Both the width and height of the nanowire were 200 nm to provide enough mechanical strength to keep intact nanowire integrated into the device. The length of the nanowire (defined by the Teflon mask) was 1.5 mm. Figure 4.1 shows a schematic of the microfluidic device architecture. By HF etching and soft lithography, the glass bottom part and the PDMS top part were fabricated, each containing channel structure. Two holes were made on both

sides of the channel through the top or bottom parts for connecting the gold nanowire to electrodes. The sections containing the gold nanowires were transferred from the water and positioned over 30 µm-deep channels etched in glass substrates, and then the epoxy matrix was ashed by oxygen plasma to yield free-standing nanowires spanning the glass channel. The PDMS part with also 30 µm-deep channel was sealed to the glass part to form a closed channel. The holes in the PDMS part were placed on the same position with the holes of the glass part, and then filled a drop of silver paste to connect the gold nanowire with contact wires. The total dimensions of the top and the bottom parts of the devices are roughly 2 cm × 1 cm. The length of the channels is 1 cm. The designed width of glass and PDMS are 60 µm and 80 µm, respectively. The PDMS channels have a depth of 20-40 µm.

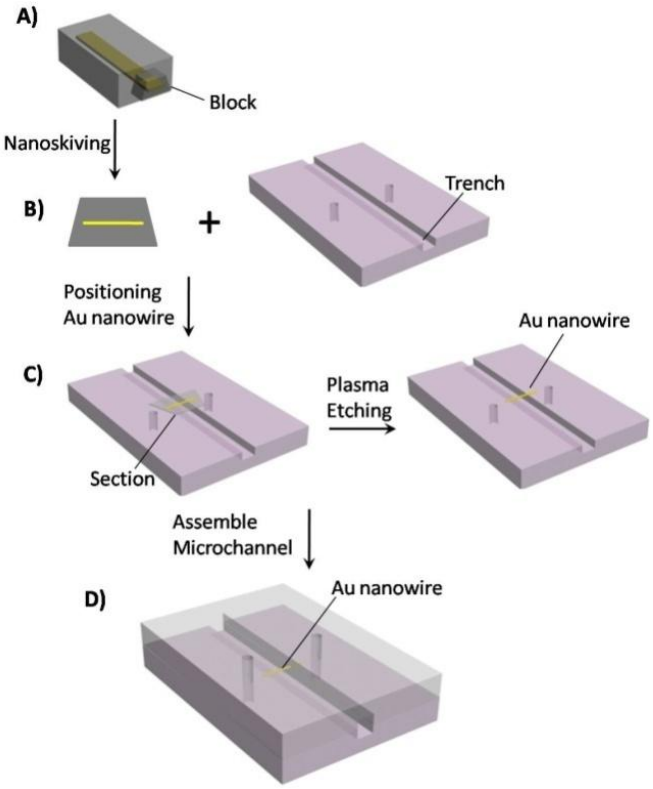

Figure 4.1 Schematic illustration of a microfluidic device integrated by a millimeter-long gold nanowire. A) Epoxy block containing a strip of gold are mounted in an ultramicrotome. B) The block is sectioned to produce slabs containing gold nanowires that can be transferred onto a glass substrate with a trench. C) The slabs are positioned over the trench of the glass substrate, and epoxy matrix is removed by oxygen plasma to yield a free-standing gold nanowire. D) A schematic of an intact microfluidic device.

After placing the gold nanowire on the glass substrate, its position can be controlled to suspend it perpendicularly over the glass channel. Figure 4.2 shows SEM images of 200 nm × 200 nm gold nanowires spanning the entire width of around 70 μm-wide trench in glass. SEM images taken from both top-down view and tilted-view indicate that the nanowires are still intact after manipulation and don't make contact with the surface of the glass channels. The glass and PDMS parts are bonded through their surfaces in contact with each other with the alignment of the channels to form the intact device.

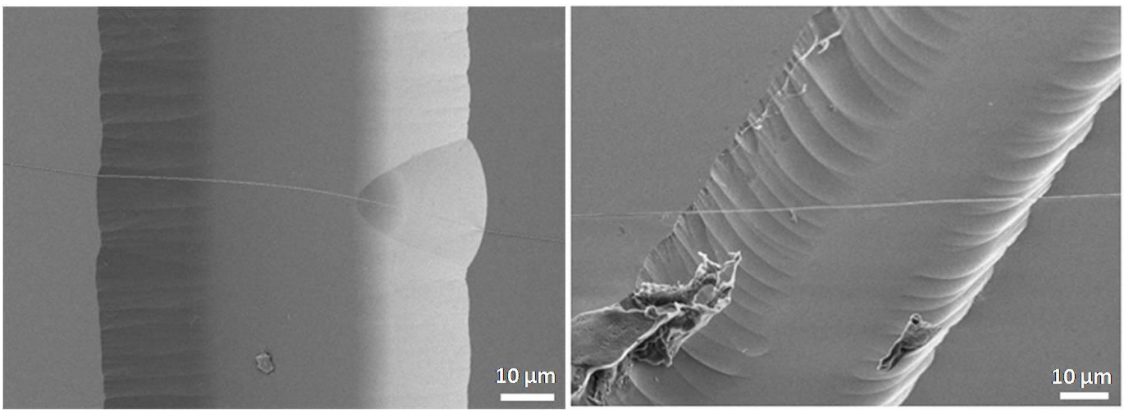

Figure 4.2 SEM images of a 200 nm × 200 nm gold nanowire fabricated by nanoskiving suspending over a glass trench with a dimension of 70 μm in width, 30 μm in depthcarved from the substrate The images are taken at 90° (left) and 45° (right) angles.

An optical microscope image of the intact device bonding the PDMS part and filling silver paste is shown in Figure 4.3. It is clear to see the gold nanowire is spanning the channel between two silver pads. The actual width of the glass and PDMS channel was measured to be about 68 μm and 93 μm, respectively. The difference may be induced by too long exposure of substrates in the process of HF etching and photolithography. The width of the PDMS channel is deliberately made to be a little larger than the glass channel, facilitating the alignment of the two and also protecting the nanowire from being broken. Before the final device is constructed, several steps should be done such as positioning the gold nanowires, bonding the glass and PDMS, and adding contact wires, *etc*. Integrity test of the device should be performed prior to usage. An advantage of this device is that the test can be simply figured out by a multimeter to know whether it is

intact or not (shown in Figure 4.4).

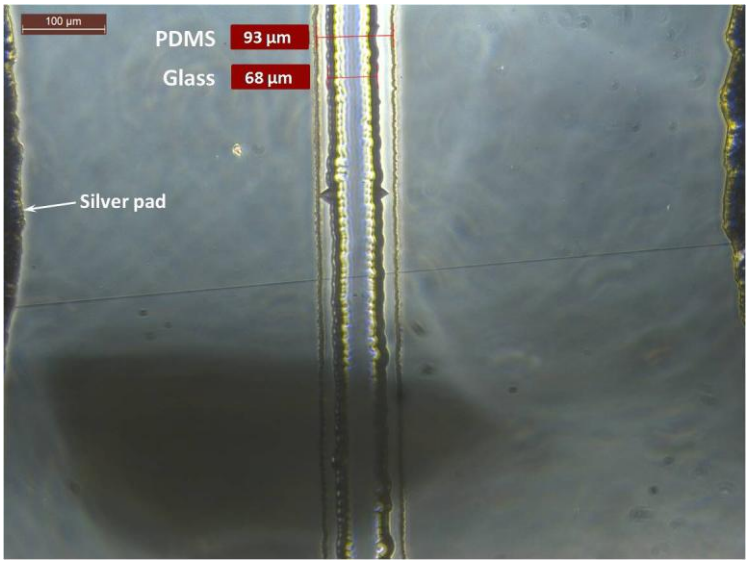

Figure 4.3 An optical microscopy image of a completed device. The width of the glass and PDMS channels are 68 and 93 µm, respectively. The horizontal black line in the center is a gold nanowire connected with two silver pads.

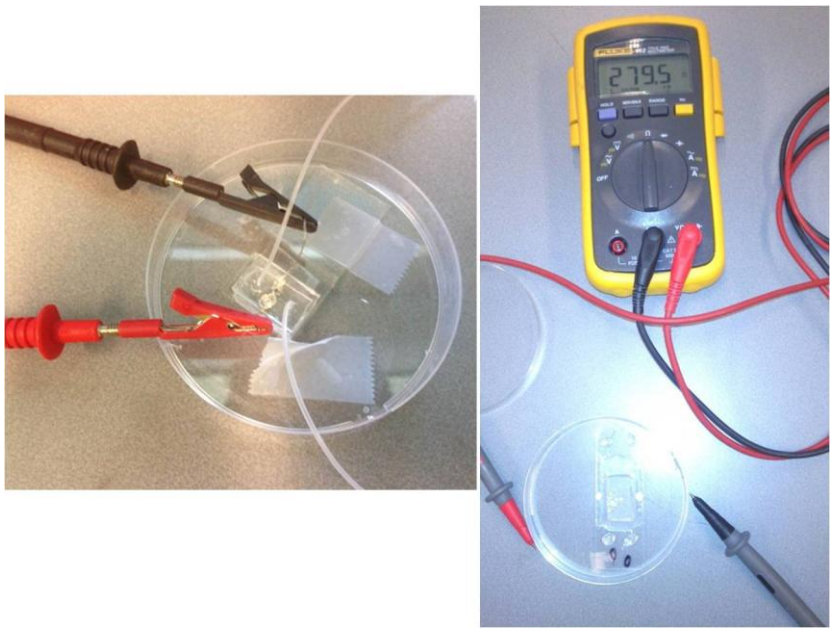

Figure 4.4 Images of intact microfluidic devices for flow sensing. A multimeter was used to measure the resistance of gold nanowires so to test the integrity of the nanowire.

4.3.2 Flow sensor

In microfluidic devices, based on the principle of heat dissipation the rate of flow can be sensed by measuring changes of resistivity affected by changes of temperature as the liquid flows pass a metallic conductor. Normally, to measure the rates of flow, heating and sensing elements (*e.g.*, thin strips of metal) are placed at the bottom of microchannel where flow is near zero that can avoid physically changing the flows by the bulky elements. High-aspect-ratio nanowires, however, are small enough that they will not disrupt flow and so can be placed in the center of the channel. Exploring the temperature dependence of resistivity of the gold nanowires fabricated by nanoskiving is useful for measuring flow rates. A 200 nm × 200 nm gold nanowire was placed on a glass substrate and connected to two contact wires. A multimeter was used to measure the resistance of the nanowire. The glass substrate was placed on a hot plate with a digital temperate display. The temperature was set to different values and the resistance was recorded when temperature was stabilized. The nanowire resistance was then calculated from the resistance measurement, $\rho=R\times A/L$. The temperature coefficient of resistivity (TCR), α, given by equation (1), describes linear relationship between temperature and resistivity. It can be explained as the change in resistivity per unit of temperature.

$$\alpha=\Delta\rho/\rho_0\Delta T \qquad (1)$$

Where $\Delta\rho=\rho-\rho_0$ is difference between the final and initial resistivity and $\Delta T=T-T_0$ is difference between the final and initial temperature. The temperature in this experiment is probably an over estimation of the real temperature of the nanowire since the temperature sensor in the hot plate is located closer to the heat element that the nanowire. Figure 4.5 shows a plot of the resistivity versus temperature for the gold nanowire. It can be seen that the resistivity has a linear dependence on temperature. The TCR for gold nanowire is found to be 2.47×10^{-3}/K. This value is in agreement with the value for bulk gold (3.9×10^{-3}/K).

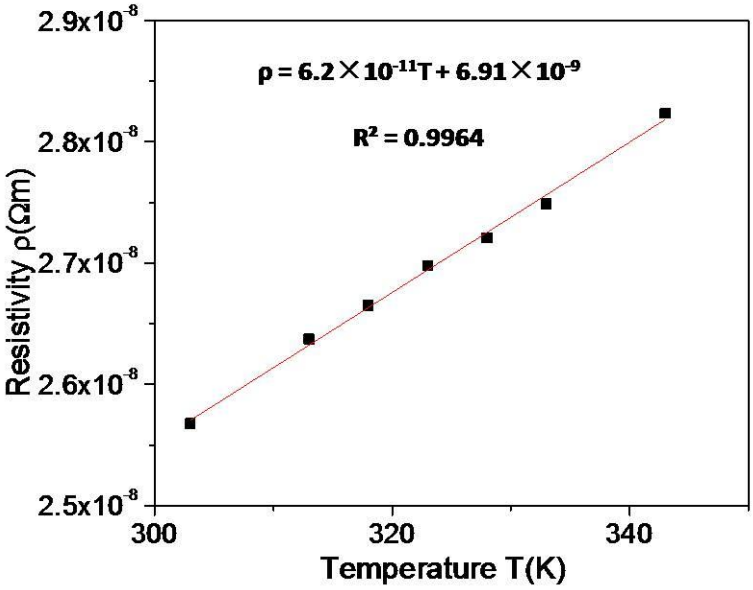

Figure 4.5 The resistivity of a gold nanowire plotted against temperature.

Integrating the gold nanowire fabricated by nanoskiving into microfluidic channel, a simple hot-wire anemometer was constructed using only a single gold nanowire as the heating and sensing element. Ethanol was continually injected into the channel using a syringe pump, and the current response monitor as a function of flow-rate at 0.5 V, 1.0 V, 1.5 V, and 2.0 V. Figure 4.6 shows the raw current curves with the change of the rates of flow at different voltages. Joule heating causes the resistance of the nanowire to increase, which is counteracted by the transport of heat away from the wire by the liquid. Higher rates of flow cool the wire more, and higher voltages give higher sensitivity. Thus, the current at a fixed voltage rises to a plateau as the rate of flow is increased. In order to relate the conductance of the nanowire to flow rates, the raw data were re-plotted as relative conductance G/G_0 versus flow rate, where G is the conductance at a plateau and G_0 is the conductance at zero flow. These data are shown in the left plots of Figure 4.7 over a range of 0 mL/min to 30 mL/min with increases of 10 mL/min in each step. Data acquired for a nanoskived nanowire placed in the bottom of a channel are shown in red for comparison. These plots clearly show that G/G_0 varies with the rate of flow when the nanowire is freely suspended in the channel, but not when it is place on the floor.

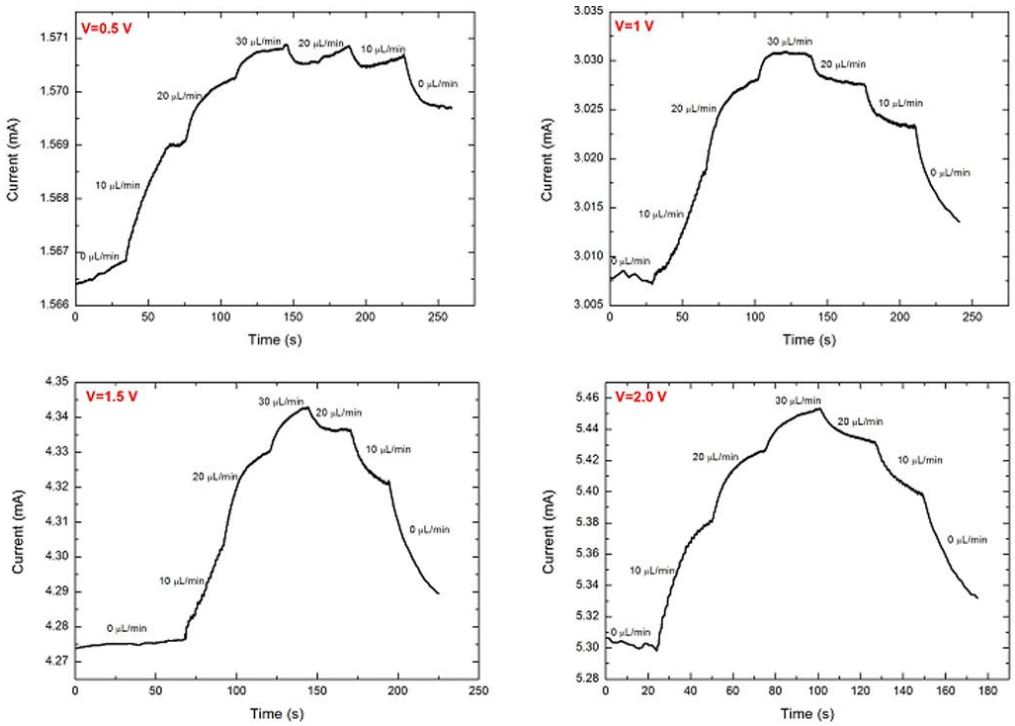

Figure 4.6 The current passed the nanowire centered in the microfluidic channel response to the different rates of flow over time at different voltages: 0.5V, 1.0 V, 1.5 V and 2.0 V.

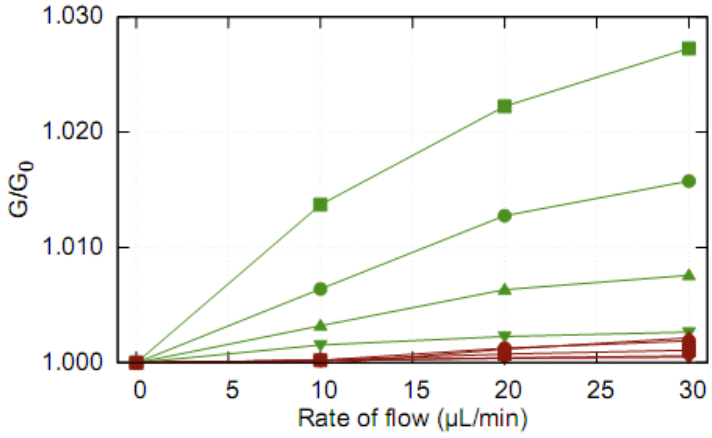

Figure 4.7 Plots of flow sensor data from hot-wire anemometers formed by bisecting microfluidic channels with gold nanowires (green) and placing the wires on the floor of the channel (red). The data show the conductance versus rate of flow at 2.0 V (squares), 1.5 V (circles), 1.0 V (triangles), 0.5 V (upside-down triangles), and 0 V (exes).

Increasing voltage increases the sensitivity for the suspended nanowire, but not sufficiently to detect the rate of flow when the nanowire is placed on the bottom of the channel. Ramping the flow rate up and then back down has no effect on the initial value of G/G_0, indicating that there is no hysteresis associated with this approach.

4.3.3 DNA stretching

In order to visualize DNA molecules by fluorescence imaging, one end of long, linear DNA molecules is usually tethered to a planar surface and stretched-out by a laminar flow.[25,26] However, while the other end is loosed within the flow, the fluctuations of the stretched DNA molecules are significant because of the low rate of flow close to the surface in a laminar, Poiseuillie flow. Since the flow profile has maximum at the center of the flow cell, DNA molecules move only slightly above surface in the low velocity regime. The fluctuations are undesired, because they disturb the precise measurements, *i.e.* the localization of molecules, which is a key in single-molecule studies. Furthermore, DNA molecules and protein bound to them are susceptible to non-specific interactions with the surface.[25,27,28] If many DNA molecules attach to a suspended nanowire, they can form a curtain that enables recording several single-molecule events at the same time and the study of DNA-protein interactions at a high local DNA concentration. The formation of DNA curtains usually needs a passivating layer that is defined by planar lithography. By binding DNA molecules to a gold nanowire fabricated by nanoskiving in the center of microfluidic channel (Figure 4.1), the DNA molecules sense a more uniform flow and higher rate of flow than they attach to a surface. The elevated nanowire will result in better stretched DNA molecules with less fluctuation. Furthermore, the microfluidic channel simplifies the formation of curtains by eliminating the lithography steps and the need for passivating a surface.

In the successive steps for binding DNA molecules on gold-coated glass coverslips, the wettability of the surface of gold is different. Contact angle measurements are performed to confirm that the modifications of gold surface are done in each step. Figure 4.8 shows

the contact angles of water on the modified surface of gold. When the surface is modified with amine groups, the contact angle is 60.7±2.0^{o}, and the contact angle of the PEGylated surface is 34.8±2.0^{o}. These values are in close proximity with those in literature (58.4±1.7^{o} for the surface of amine groups and 35.8±1.0^{o} for PEGylated sureface).[29]

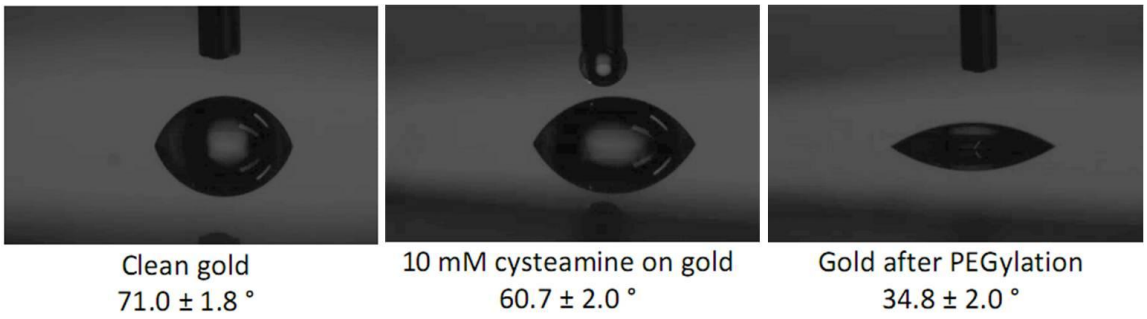

Figure 4.8 Contact angles of gold surface after each modified step.

Before DNA molecules were coupled to the gold nanowires using standard Au-S chemistry to attach biotin-streptavidin followed by the introduction of biotinylated DNA, as shown in Figure 4.9, by specifically coupling one end of linear λ phage DNA (48.5 kilobases of double-stranded DNA; contour length 16.3 μm) to a thin layer of gold surface, DNA molecules were stretched by flow. The DNA molecules contain a biotinylated arm

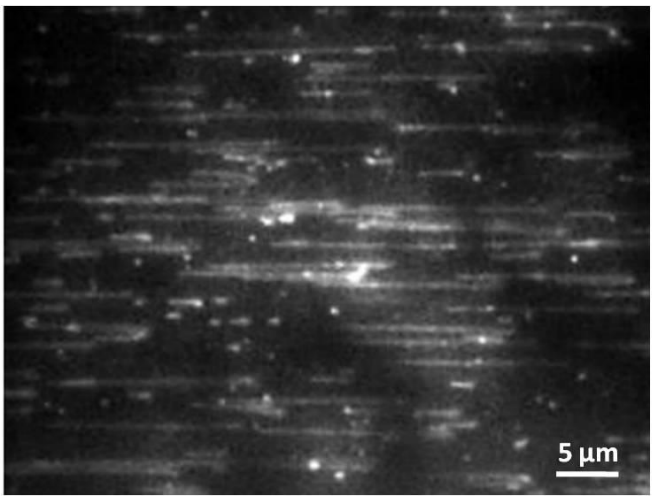

Figure 4.9 A fluorescence image of flow-stretched DNA molecules stained with SYTOX orange. The DNA molecules are bound to random positions on the surface of gold. Flow is coming in from the left to right.

and are tethered *in situ* to the biotin-streptavidin functionalized gold-coated coverslips that are constructed into a flow cell. The DNA molecules are bound to random positions on the bottom of the flow cell. There are image artifacts due to non-specific binding and the signal intensity is low. However, it is demonstrated that the DNA molecules did bind to the gold surface and the functionalization is successful. It is critical to successfully bind DNA molecules on gold nanowires.

When the λ phase DNA molecules were coupled to the gold nanowire, a curtain of DNA can be stretched by flow. The DNA density on the nanowire was controlled by the DNA concentration and the time of incubation. At sufficiently low densities, single molecules could easily be resolved. A gold nanowire was placed on the surface of a glass substrate, as shown in Figure 4.10A, it is clearly visible that DNA molecules bind to the nanowire.

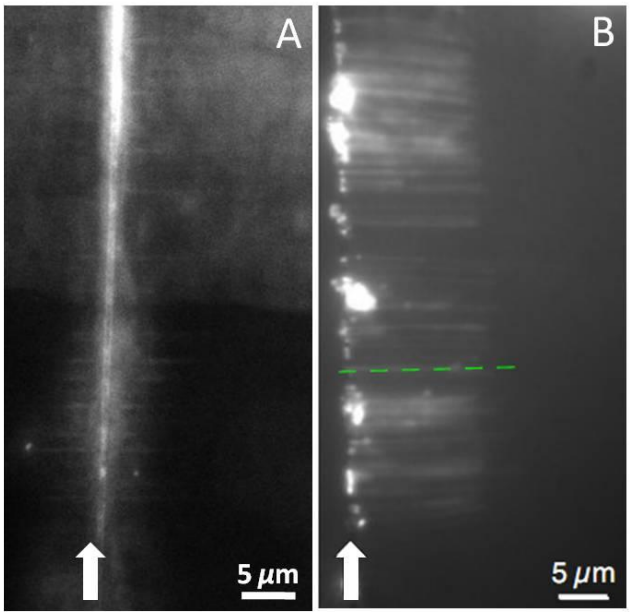

Figure 4.10 Fluorescence images of immobilized DNA molecules elongated by flow stained with SYTOX orange. A) The DNA molecules are bound to a gold nanowire that is position on the bottom of a microfluidic channel. B) The DNA molecules are bound to a gold nanowire bisecting the microfluidic channel at the midpoint. The position of the nanowires is indicated with white arrows. A curtain of DNA molecules extends outward from the direction of flow (from left to right).

However, there is significant background from non-specific binding and lower signal

intensity. This visualization works well. Based on this demonstration, after DNA molecules are bound to a gold nanowire bisecting the microfluidic channel at the midpoint, DNA molecules arrange along the nanowire to form a curtain in the direction of flow (shown in Figure 4.10B). The signal intensity is slightly higher and more uniform than in the randomly-bound surface case because of the elimination of background signal to a certain extent from the separation of the nanowire from the floor of the channel. At low rates of flow, the total DNA extension is less than contour length. At high rates of flow, the hydrodynamic force increased the mean extension of the DNA molecules.

4.4 Conclusion

In microfluidic devices, nanowire sensors are constrained to the walls of the channel, where the rate of flow is near zero. The lowest rate of flow limits the detection of biological and chemical species, or measurements of flow. Positioning a nanowire in the center of a microfluidic channel, where the rate of flow is the highest, allows experiments to be performed. However, fabricating the discrete, millimeter-long nanowires is necessary to place them in the center of the channel. In this work nanoskiving is used to fabricate high-aspect-ratio gold nanowires, which can be placed directly onto a channel to sense the highest flow rate. The gold nanowire is suspended in a microfluidic channel, so it is sensitive enough to serve as both the heating and sensing element to measure the change in resistivity. Binding DNA molecules to the gold nanowires similarly exposes the entire surface of the nanowire-DNA assembly to the carrier liquid, eliminating background signal from non-specific binding in fluorescence experiments and forming a curtain of DNA molecules along the nanowires. Because the rate of flow within the channel is highest away from the walls of the channel, flow-elongating the DNA molecules can reach maximum at low rates of flow.

Bibliography

1. F. Patolsky, and C. M. Lieber, Nanowire nanosensors, *Materials Today* **2005**, 8, 20-28.

2. W. Wang, C. Chen, K. Lin, Y. Fang, and C. M. Lieber, Label-free detection of small-moleule-protein interactions by using nanowire nanosensors, *Proc. Natl. Acad. Sci. USA* **2005**, 102, 3208-3212.

3. Y. Cui, Q. Wei, H. Park, and C. M. Lieber, Nanowire nanosensors for highly sensitive and selective detection of biological and chemical species, *Science* **2001**, 293, 1289-1292.

4. J. Hahm, and C. M. Lieber, Direct ultrasensitive electrical detection of DNA and DNA sequence variations using nanowire nanosensors, *Nano Lett.* **2004**, 4, 51-54.

5. S. Chen, N. Jokilaakso, P. Björk, A. E. Karlström, and S.-L. Zhang, A two-terminal silicon nanoribbon field-effect pH sensor, *Appl. Phys. Lett.* **2010**, 97, 264102.

6. A. Kolmakov, Y. Zhang, G. Cheng, and M. Moskovits, Detection of CO and O_2 using Tin Oxide Nanowire Sensors, *Adv. Mater.* **2003**, 15,997-1000.

7. Q. Wan, Q. H. Li, Y. J. Chen, T. H. Wang, X. L. He, J. P. Li, and C. L. Lin, Fabrication and ethanol sensing characteristics of ZnO nanowire gas sensors, *Appl. Phys. Lett.* **2004**, 84, 3654-3656.

8. C. M. Lieber, Nanoscale science and technology: Building a big future from small things, *MRS Bull* **2003**, 28, 487-491.

9. L. Samuelson, Self-forming nanoscale devices, *Materials Today* **2003**, 6, 22-31.

10. M. Law, H. Kind, B. Messer, F. Kim, and P. Yang, Photochemical sensing of NO_2 with SnO_2 nanoribbon nanosensors at room temperature, *Angew. Chem. Int. Ed.* **2002**, 41, 2405-2408.

11. Z. Fan, and J. G. Lu, Gate-refreshable nanowire chemical sensors, *Appl. Phys. Lett.* **2005**, 86, 123510.

12. G. Zheng, F. Patolsky, Y. Cui, W. U. Wang, and C. M. Lieber, Multiplexed electrical detection of cancer markers with nanowire sensor arrays, *Nat. Biotechnol.* **2005**, 23, 1294-1301.

13. A. Kim, C. S. Ah, H. Y. Yu, J.-H. Yang, I.-B. Baek, C.-G. Ahn, C. W. Park, M. S. Jun, and S. Lee, Ultrasensitive, label-free, and real-time immunodetection using silicon field-effect transistors, *Appl. Phys. Lett.* **2007**, 91, 103901.

14. P. R. Nair, M. A. Alam, Performance limits of nanobiosensors, *Appl. Phys. Lett.* **2006**, 88, 233120.

15. R. L. Mays, P. Pourhossein, D. Savithri, J. Genzer, R. C. Chiechi, and M. D. Dickey, Thiol-containing polymeric embedding materials for nanoskiving, *J. Mater. Chem. C* **2013**, 1,

121-130.

16. Q. Xu, R. M. Rioux, M. D. Dickey, and G. M. Whitesides, Nanoskiving: A new method to produce arrays of nanostructures, *Acc. Chem. Res.* **2008**, 41, 1566-1577.

17. D. J. Lipomi, R. V. Martinez, and G. M. Whitesides, Use of thin sectioning (nanoskiving) to fabricate nanostructures for electronic and optical applications, *Angew. Chem. Int. Ed.* **2011**, 50, 8566-8583.

18. B. Wiley, D. J. Lipomi, J. Bao, F. Capasso, and G. M. Whitesides, Fabrication of surface Plasmon resonators by nanoskiving single-crystalline gold microplates, *Nano Lett.* **2008**, 8, 3023-3028.

19. Q. Xu, B. D. Gates, and G. M. Whitesides, Fabrication of metal structures with nanometer-scale lateral dimensions by sectioning using a microtome, *J. Am. Chem. Soc.* **2004**, 126, 1332-1333.

20. L. Schöler, B. Lange, K. Seibel, H. Schäfer, M. Walder, N. Friedrich, D. Ehrhardt, F. Schönfeld, G. Zech, and M. Böhm, Monolithically integrated micro flow sensor for lab-on-chip applications, *Microelectronic Engineering* **2005**, 78-79, 164-170.

21. M. S. Cheri, H. Latifi, J. Sadeghi, M. S. Moghaddam, H. Shahraki, and H. Hajghassem, Real-time measurement of flow rate in microfluidic devices using a cantilever-based optofluidic sensor, *Analyst* **2014**, 139, 431-438.

22. D. Dulin, J. Lipfert, M. C. Moolman, and N. H. Dekker, Studying genomic processes at the single-molecule level: Introducing the tools and applications, *Nat. Rev. Genet.* **2013**, 14, 9-22.

23. B. Hua, K. Y. Han, R. Zhou, H. Kim, X. Shi, S. C. Abeysirigunawardena, A. Jain, D. Singh, V. Aggarwal, S. A. Woodson, and T. Ha, An improved surface passivation method for single molecule studies, *Nat. Meth.* **2014**, 11, 1233-1236.

24. A. Robinson, and A. M. van Oijen, Bacterial replication, transcription and translation: Mechanistic insights from single-molecule biochemical studies, *Nat. Rev. Micro.* **2013**, 11, 303-315.

25. A. Granéli, C. C. Yeykal, T. K. Prasad, and E. C. Greene, Organized arrays of individual DNA molecules tethered to supported lipid bilayers, *Langmuir* **2006**, 22, 292-299.

26. N. A. Tanner, J. J. Loparo, S. M. Hamdan, S. Jergic, N. E. Dixon, and A. M. van Oijen, Real-time single-molecule observation of rolling-circle DNA replication, *Nucleic Acids Research* **2009**, 37, e27-e27.

27. T. Fazio, M.-L. Visnapuu, S. Wind, and E. C. Greene, DNA curtains and nanoscale curtain rods: High-throughput tools for single molecule imaging, *Langmuir* **2008**, 24, 10524-10531.

28. T. Ha, I. Rasnik, W. Cheng, H. P. Babcock, G. H. Gauss, T. M. Lohman, and S. Chu, Initiation and re-initiation of DNA unwinding by the Escherichia coli rephelicase, *Nature* **2002**, 419,

638-641.

29. D. Janssen, R. de Palma, S. Verlaak, P. Heremans, and W. Dehaen, Static solvent contact angle measurements, surface free energy and wettability determination of various self-assembled monolayers on silicon dioxide, *Thin Solid Films*, **2006**, 515, 1433-1438.

Chapter 5

Perfect Transfer and Control of Nanostructures Fabricated by Nanoskiving

5.1 Introduction

Nanoscience exploits unique properties of nanoscale structures not found in bulk materials, requiring nanostructures with specific geometries and the interactions of multiple structures in well-defined arrays. The more elements there are in a nanostructured system, however, the more challenging it is to create the desired geometry. Thus, fabrication requires manipulating and addressing nanostructures individually and/or in ensembles and interfacing them with the macro world. A particularly challenging configuration is heterostructures that are stacked vertically. The fabrication of these devices require the controlled transfer of ensembles of nanostructures from the substrate on which they are prepared to a target substrate with control over orientation without affecting previously-transferred structures.[1,2] Existing methods for transferring nanostructures have focused mainly on transfer printing,[3-7] and the transfer of two-dimensional materials such as graphene,[8-11] and MoS_2.[12-14] Transfer printing utilizes an elastomeric stamp as mediator for the heterogeneous integration of nanostructures from a source

*This chapter has been published in: Nanoscale Horiz., 2016, DOI: 10.1039/C6NH00099A.

substrate to a target surface. However, multiple transfer steps are difficult because the stamp must adhere to a structure on the source substrate and release it to the target without perturbing previously-transferred structures. To separate the stamp from the target surface chemical adhesion must be controlled while optimizing pressing force. Additionally, the use of a stamp requires planar and hard source and target substrates. Free-standing films are an alternative for the transfer of polymer nano-sheets and inorganic, ultrathin layers.[15-17] However, despite the substantial development of transfer methods, there is no robust, generalizable approach available for easily transferring, stacking and precisely manipulating nanostructures on surfaces.

There are many approaches to fabricating nanostructures by various lithographic and self-assembly processes that immobilize nanostructures on as-prepared substrates into useful geometries. Conventional techniques for nanofabrication, such as electron beam lithography, focuses-ion beam milling, photolithography, etc., can generate arbitrary patterns in materials to produce nanostructures. However, they require specialized facilities and are constrained by the limitations of planar lithography; they are not suitable for non-planar surfaces and have a low tolerance for organic materials, for example. Random assembly processes circumvent some of these limitations, but suffer from low yields and lack control over orientation.

Nanoskiving is a flexible technique for nanofabrication that is a form of edge lithography based on sectioning thin structures with an ultramicrotome.[18,19] It is facile, compatible with a wide variety of materials, including organics, requires no special facilities or clean rooms. Nanostructures fabricated by nanoskiving are embedded in polymeric slabs that, after sectioning with a diamond knife, float into a water bath and can be collected simply by dipping virtually any substrate in the water. Although the nanostructures within each slab are precisely defined, there is no inherent control over the orientation of the slabs with respect to each other.

Thus, after drying, the nanostructures are fixed arbitrarily on the substrate, precluding further manipulation or transfer.

There are two methods that afford some control over the orientation of the slabs before the water has evaporated. One is the direct, physical manipulation with, for example, a hair. A more sophisticated approach combines physical manipulation with alignment by magnetic fields.[20] This latter method requires the embedding of nickel into the epoxy matrix along with the nascent nanostructures. The nickel then serves as a sacrificial ferromagnet that moors the entire epoxy slab to the magnetic field created by rare-earth magnets positioned below. This approach, therefore, requires that the materials of interest be incorporated alongside the nickel, which is co-embedded in epoxy matrix and etched out in the last step (after sectioning, transfer and drying). To maximize the strength of the interaction with the external magnetic field, the dimensions of nickel strips in epoxy slabs should be as large as possible, however, a film that is too thick will damage the diamond knife. It is also necessary to slow the evaporation of the very small volume of water that supports the section during positioning, which must take place on a hydrophilic substrate to minimize capillary forces. Thus, when positioning successive sections, the epoxy matrix of the previous section (because it is hydrophobic) has to be removed. Thus, magnetic mooring is generally limited to relatively simple nanostructures (e.g., wires) and the positioning of one or two consecutive slabs. This technique also must take place in relatively close proximity to the microtome because the sections must remain floating on water between fabrication and positions. This is, of course, a common problem for any sort of nanofabrication that is highly dependent on equipment, regardless of the simplicity of that equipment.

In this work, we describe an on-demand transfer approach using a film of polymer as carrier layer and aluminum as sacrificial layer to transfer and manipulate sections that are fabricated by nanoskiving. Using this method, several

sections can be prepared one-at-a-time and stored on a sacrificial surface. When the sections are needed, they can be transported and transferred onto a target substrate under ambient conditions. This transfer process is simple and fast and protects the nanostructures, keeping them intact and uniform without introducing defects, cracks, and residues. And no other materials (e.g., nickel for magnetic positioning) must be co-embedded. Position the sections does not depend on the wettability of substrates, which are not constrained in composition or topology. By successively stacking nanostructures (one-dimensional nanowires are used in this work), various two-dimensional (2D) or three-dimensional (3D) structures and even heterostructures can be constructed, improving the range of applications of nanoskiving. Virtually any structure fabricated by nanoskiving should be compatible with this transfer "perfect transfer" method.

5.2 Experimental section

5.2.1 Procedure of sectioning

A 100 nm-thick gold film was deposited through a mask on a silicon wafer passivated with tridecafluoro-1,1,2,2,-tetrahydrooctyl)trichlorosilane to form rectangular gold features before Epofix epoxy prepolymer was used to cover the entire wafer. After curing the epoxy, the gold features were cut using a jeweler's saw into small pieces and was then embedded with more epoxy prepolymer to form epoxy blocks. A prepared block was placed in the ultramicrotome (Leica EM UC-7), and its top was trimmed to the width of the diamond knife (4 mm Diatome Ultra 35^{o}). The diamond knife was utilized to section the block to 100 nm at 1 mm/s to produce epoxy sections containing the gold structures. Finally, the resulting sections were collected from the surface of the water in the boat to an aluminum substrate that is generated by thermal deposition of aluminum on silicon or glass substrates.

5.2.2 Preparation of two-dimensional colloidal crystals

Hexagonal close-pack monolayers of PS nanospheres (1 μm and 700 nm) were prepared by the interface method. In brief, 0.1 mL of 5% PS spheres dispersion in a mixture of deionized water and absolute ethanol (v/v=1:1) was dropped onto the surface of water in a petri dish by a syringe, and then 20 μL of 8% SDS aqueous solution was dropped into water along the edge of the plate. Finally, the PS nanospheres assembled into close-packed monolayers and then were lifted onto the as-prepared substrates.

5.2.3 Fabrication of nanocrescent arrays

The nanospheres with diameter of 1 μm were etched using ICP-RIE system (Oxford Plasma Technology Type 80Plus) with a mixture of O_2 (40 sccm) and CF_4 (10 sccm), 30 W RF power to ignite the plasma and provide anisotropic etching, and 300 W ICP power to help sustain the plasma and provide relatively more isotropic etching. The etching process was applied at a work pressure of 10 mTorr and a temperature of 10 ^{o}C. The etching duration is 100 s, leading to non-close-packed nanosphere arrays. A gold nanomesh was then produced by evaporating 5 nm Ag and 10 nm Au on the silicon substrate. After the gold was deposited, the PS nanospheres were removed by toluene with mild sonication. A metal-assisted chemical etching process was applied to fabricate the arrays of silicon cylindrical nanoposts. The gold nanomesh-covered silicon substrates were immersed into an etching mixture consisting of HF (49%), H_2O_2 (30%) and ethanol (5:1:1 of HF: H_2O_2: ethanol). The etching duration is 15 min. Using a PDMS mold as an intermediate, these arrays of nanoposts were replicated from silicon to epoxy. A 50 nm-thick gold film was deposited only partially around the epoxy nanoposts by shadow evaporation. The substrate was placed at a 45^{o} angle from the source of evaporation. This structure was embedded in more epoxy to form a block that was then sectioned to yield epoxy slabs containing the array of nanocrescents.

5.2.4 Fabrication of nanohole arrays

After the monolayer of 700 nm PS nanospheres was transferred onto aluminum substrate,

the same conditions of etching were performed on these nanospheres. The etching duration is 80 s. A 30 nm-thick film of gold was then deposited on the nanospheres and the substrate. After the samples were immersed into toluene with slight ultrasonication to remove the PS nanospheres, gold nanohole arrays were generated.

5.2.5 Fabrication of nanowire arrays

Photoresist was patterned using photolithography with a stripe-patterned mask, and then the patterned silicon surface was passivated with PFS. Using soft lithography, the patterns were replicated in epoxy through a PDMS mold. After the patterned epoxy substrate was obtained, a 100 nm-thick layer of gold was deposited on the patterned epoxy substrate at a glancing angle of 45^{o}. This structure was embedded in more epoxy to form a block, and then the block was sectioned to yield epoxy slabs containing the array of nanowires.

5.2.6 Procedure of transfer

Polystyrene (Mw: 280000 g/mol) was dissolved into toluene to form 100 mg/mL solution that was spin-coated (2000 rpm for 60s) on the section-covered aluminum substrate or the surface of gold nanohole arrays. Then the PS film was scored around the edge using a razor blade. A drop of HCl solution was used to cover the top of the sample. After 2 minutes, the PS-section or PS-nanoholes assembly was separated from the substrate by the penetration of HCl through the PS film to etch aluminum. The assembly was picked up using tweezers and transferred onto a target substrate. Thus, the position of the section or the gold nanohole arrays can be precisely controlled under a light microscope. Finally, the assembly was baked for 20 minutes at 60 ^{o}C to remove water residue and attach section or structures on the target substrate, before removing the sacrificial PS by rinsing with toluene. The epoxy matrix was etched by oxygen plasma to release nanostructures on the substrate.

5.2.7 Characterization

Scanning electron microscope (SEM) images were performed using a JEOL FESEM 6700F electron microscope with electron energy of 3 kV. Electrical measurements were performed using Keithley 2400 source meter. A Maya 2000PRO optics spectrometer, and a model DT 100 CE remote UV/vis light source (Ocean Optics) was used to measure transmission spectra. Optical microscope images were captured with a camera mounted on the microscope (Olympus microscope BX51). Photographs were taken with a Canon A590 camera.

5.3 Results and Discussion

The epoxy sections containing gold nanostructures were produced by nanoskiving and then transferred onto aluminum substrates. To extend the field of application and simplify operation for nanoskiving, Figure 5.1 shows the process by which the sections can be transferred and positioned from a source substrate to a target substrate. A layer of PS is spin-coated onto the section-covered aluminum substrate, and then HCl solution is used to etch aluminum to release PS-section assembly. Since the polystyrene (PS) layer coats the whole surface of aluminum, it blocks the penetration of HCl below the PS layer. And, since the exposure of aluminum is necessary to induce the penetration, the PS layer must be cut around the edge. After waiting for several minutes, the PS-section assembly can be detached from the substrate and floated on the surface of water droplet. The self-standing assembly is robust enough that it can be readily picked up using tweezers and easily transferred onto a target substrate without affecting the embedded epoxy slab and/or nanostructures. The target substrate is covered with enough water to wet the PS/section assembly. After that, the assembly is baked for 30 minutes at 60 ^{o}C to remove water residue and enhance the adhesion of the section with the target substrate. The assembly can also be baked for an addiontal 20 minutes at 130 ^{o}C to eliminate wrinkles. The adhesion of the epoxy section is sufficient such that, during subsequent dissolution of the PS layer by toluene, the section remains in-place on the target substrate.

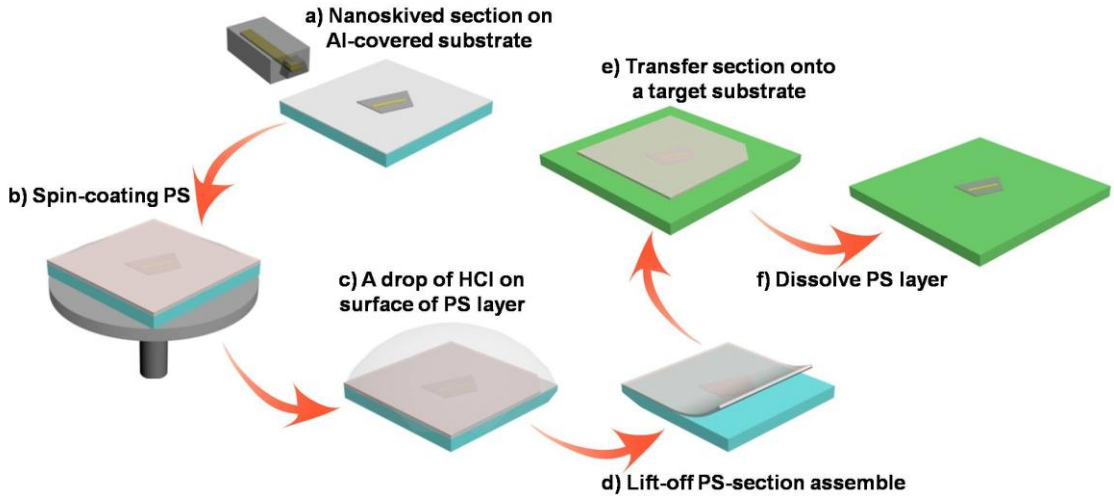

Figure 5.1 A schematic of transfer process of sections. A layer of PS was spin-coated on a section-covered aluminum substrate. Then a drop of HCl is used to etch aluminum. So the polymer/section assembly can be lifted off and transferred onto arbitrary substrates. The last step is dissolving the PS with organic solvent.

Figure 5.2 shows photographic images of the transfer process. Despite the coating of PS layer, sections are still visible by eye, enabling precise control of sections under an optical microscope (Figure 5.2b) (Guides on the target substrate and/or the epoxy section can be used for further precision.) Aluminum is gradually etched as HCl penetrates the PS film, releasing the PS/epoxy-slab assembly, which can be lifted off with tweezers. (If the embedded nanostructures are acid sensitive, aluminum can be etched with NaOH instead.) The assembly can be dried by wicking the HCl solution away with a filter paper. The transfer of the assembly keeps the epoxy sections intact and uniform without wrinkles and cracks (in the epoxy slab) even after the assembly is transferred onto a target substrate, baked and the PS layer is dissolved with toluene (Figure 5.2g). Sections prepared by nanoskiving can be transferred one-at-a-time or picked up from the water boat in ribbons of several sections. Both individual sections and ribbons can be transferred in a PS assembly. Since the nanostructures tend to be confined to the center of each slab, transferring ribbons allows arrays of (~5-10) individual 2D and 3D structures to be fabricated in parallel on a target substrate.

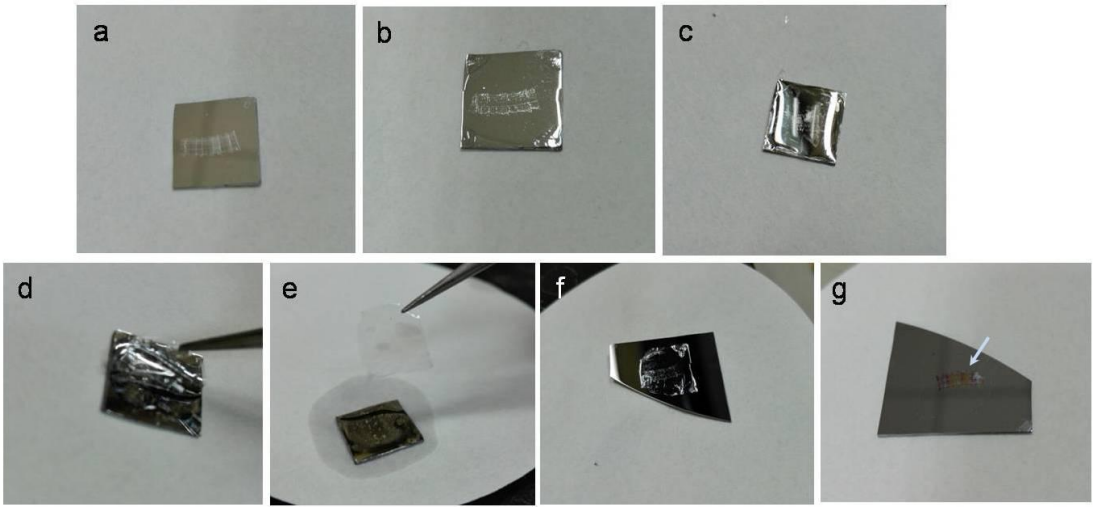

Figure 5.2 Photographs of a transfer procedure. (a) Sections fabricated by nanoskiving were collected on an aluminum substrate. (b) A layer of PS was spin-coated on the sections-covered substrate. (c) A droplet of HCl was dropped on the surface of PS layer. (d) Polymer-sections assembly can be lifted-off with the etching of aluminum. (e) The polymer-sections assembly can be readily picked using tweezers. (f) The assembly was transferred onto a silicon substrate followed by baking for 30 min at 60 ^{o}C. (g) PS layer was dissolved by toluene.

To demonstrate that the nanostructures are not damaged by the transfer or release, sections containing gold nanowires were transferred to a glass substrate. Two ends of gold nanowires were then connected with electrodes to form electrical contacts. As shown in Figure 5.3, the I-V data for a typical gold nanowire are linear, indicating ohmic behavior and confirming that the gold nanowire is intact. This example also serves to highlight the gentle nature of the transfer process. Transfer methods based on sacrificial films usually employ high surface energy or strongly adhesive carrier polymers. These transfer processes work by overcoming the adhesion of the film with substrate without detaching from the structure that is to be transferred, utilizing a difference in the adhesive force between polymer-structure and structure-substrate. The forces involved in this process could easily damage delicate (e.g., soft, organic) structures fabricated by nanoskiving which, even when embedded in an epoxy section, can be damaged by only a slight mechanical force. In addition to the gentle release and lack of reliance on adhesives, the PS layer can serve as a protective layer to enhance the stability and mechanical

strength of epoxy sections.

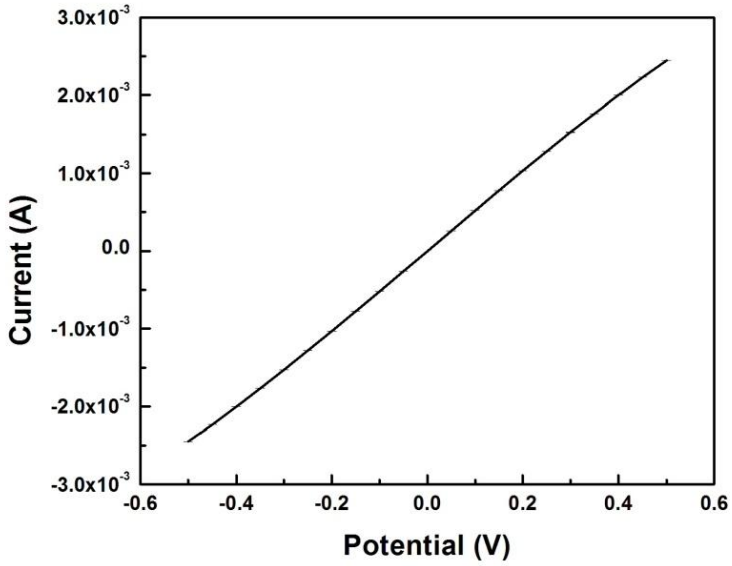

Figure 5.3 The linear plot of current against voltage for a gold nanowire embedded in an epoxy section that was transferred from the source substrate to a glass substrate using this process.

This process can perfectly transfer sections onto arbitrary substrates, including onto pre-existing nanostructures for heterogenous integration of various nano/micro-structures into 2D or 3D structures. The flexible polymer films and the gentle operations can maintain the integrity of not only nanostructures embedded in sections, but also the original structures on substrates. Figure 5.4A and B show SEM images of gold nanowire array over nanocrescent arrays and gold nanohole arrays. Nanocrescent arrays were fabricated by the combination of soft lithography and nanoskiving and gold nanohole arrays were generated by colloidal lithography. After a PS film containing epoxy sections with embedded nanowire arrays is lightly placed on them, the gentle dissolution of PS has no deleterious effect on the existing structures. Further, by aligning nanowire arrays, gold nanogrids were constructed with intersection angle of 45^{o} and 90^{o} (Figure 5.4C and D). These structures can be made by magnetic mooring as well, but perfect-transfer extends the scope of target substrates; sections can be transferred onto gold, ITO, and even non-planar surface, for example (Figure 5.4 E, F and G). And many sections can be

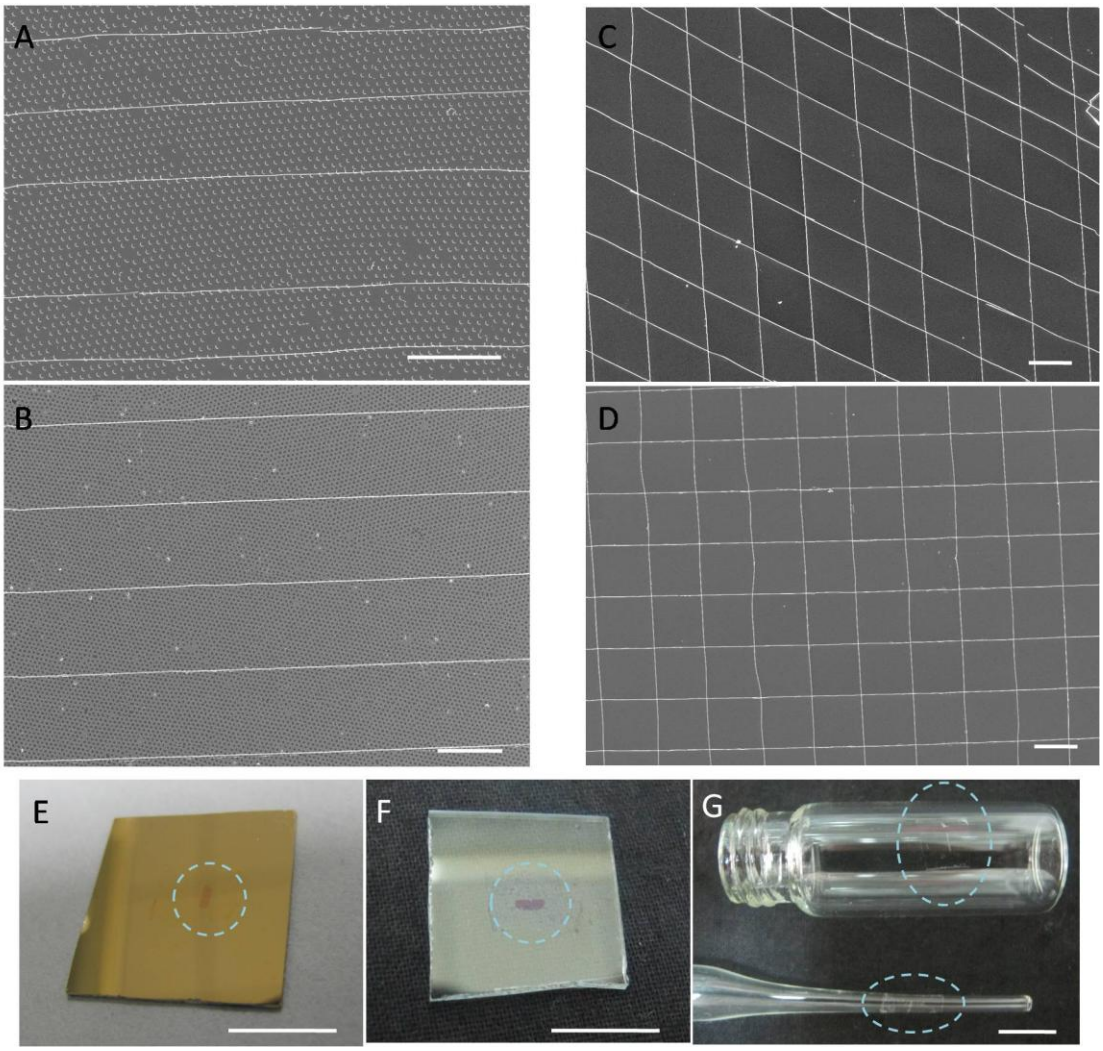

Figure 5.4 Nanostructures embedded in epoxy sections can be transferred onto arbitrary substrates, including onto existing structures. (A, B, C, D) SEM images of gold nanowire arrays over nanocrescent arrays (A) and nanohole arrays (B), and gold nanogrids with intersection angle of 45^{o} (C) and 90^{o} (D). Scale bar: 10 μm. Meantime, sections can be transferred onto gold (E), ITO (F), and non-planar surfaces (G). Scale bar: 1 cm.

all-at-once at the ultramicrotome and stored on aluminum substrates for on-demand release and transfer. The PS-section-aluminum assemblies are sufficiently robust for shipping as well, facilitating cross-lab collaboration

Before release, sections can be accurately controlled and positioned onto a place, irrespective of the hydrophobicity of the target substrate are regardless of whether the epoxy matrix of the previous section is etched or not. As shown in Figure 5.5, nanowires embedded in sections can easily be align to form 2D or stacked 3D structures by rotating successive sections containing arrays of parallel nanowires before dissolution of the PS layer and etching of the epoxy matrices. When nanowires are periodically stacked with orthogonal arrangements, they can form rectangular, ordered 3D structures (Figure 5.5A). If the intersection angle is changed to 60^{o}, the nanowires form equilateral triangles (Figure 5.5B) or other geometric shapes. Individual nanowires can also be assembled parallel to each other with equal (or non-equal) spacing (Figure 5.5C), which is a more flexible method for creating parallel nanowire assemblies than sectioning stacked films by nanoskiving. Three is presumably no limit to how many nanostructure-containing epoxy sections can be oriented and stacked by perfect-transfer.

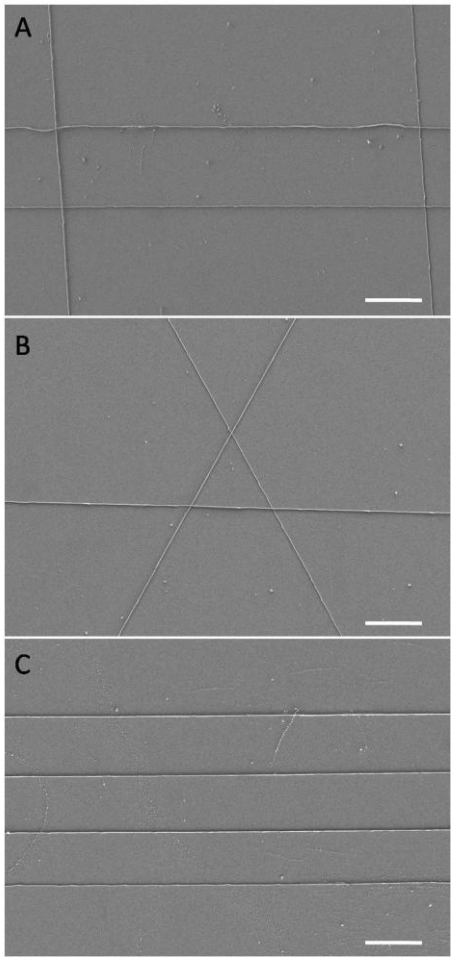

Figure 5.5 SEM images of the assemblies of gold nanowires through the process of transfer and manipulation. Gold nanowires were successively stacked to construct 2D or 3D structures, including (A) rectangular, (B) equilateral triangle, and (C) parallel structures. Scale bar: 10 μm.

This process is not limited to nanostructures formed by nanoskiving; it can transfer structures formed by various methods and combinations of methods. The only restriction is that the nano/microassemblies be placed on an aluminum substrate. Subwavelength nanohole arrays patterned in metal have extraordinary optical transmission,[21] they have become one of the most extensively studied plasmonic structures for applications in spectroscopy,[22,23] biosensing,[24,25] and color filtering.[26] They are not formed by nanoskiving, but are compatible with perfect-transfer. Large-area gold nanohole arrays were fabricated on an aluminum substrate by colloidal lithography with 380 nm diameter and 700 nm periodicity and then PS layers were spin-coated on top of them. After

releasing the PS layers, the nanohole arrays could be transferred to a target substrate as described above. An SEM image of a periodic gold nanohole array, post-transfer, is shown in Figure 5.6A. There is no discernable difference between the as-prepared and transferred arrays; importantly the periodicity and size and unaffected. To demonstrate this preservation, the optical transmission spectra of the nanohole arrays were measured before and after the transfer process (Figure 5.6B). The nanohole array exhibits two main peaks at wavelength of 517 nm and 1260 nm, demonstrating that the perfect transfer process can maintain the integrity of even any nanostructures.

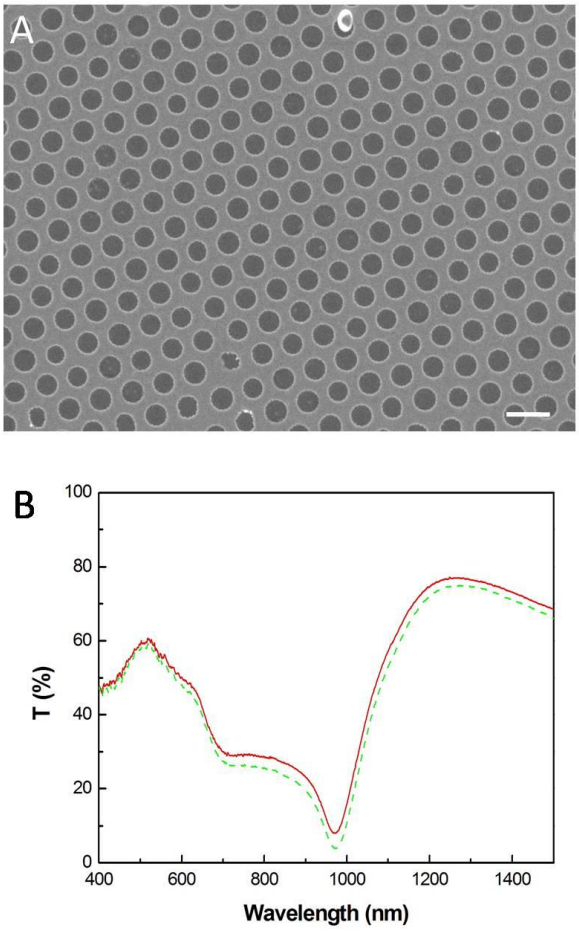

Figure 5.6 (A) SEM image of a gold nanohole array transferred from aluminum surface to glass substrate. Scale bar: 1 μm. (B) Transmission spectra of nanohole arrays before (red solid line) and after (green dashed line) the transfer.

5.4 Conclusion

A “perfect transfer” method was demonstrated that uses a polymer film as a carrier layer and aluminum as sacrificial layer to transfer and manipulate sections that are fabricated by nanoskiving and nanohole arrays formed by self-assembly. This method affords precise control over orientation and allows structures to be stacked to produce arrays and/or 2D and 3D structures. It is simple, fast, non-damaging, does not rely on strong adhesives or high surface energies and places no constraints on the target substrate. Nanostructures transferred by this method remain intact and uniform and are free of defects, cracks, and residues (introduced by the transfer process). Many sections can be prepared one-time by ultramicrotome and saved to be released and transferred on-demand. This method, to some extent, circumvents the dependence of nanofabrication technology on specialized, expensive equipment; stored sections can be shipped to other laboratories or used in-house, away from the ultramicrotome. No other materials (e.g., nickel for magnetic positioning) are required and the deleterious influence of capillary forces on the precise orientation of epoxy sections is eliminated. The perfect-transfer process is compatible with any nanostructures that can be placed on an aluminum substrate and should enable the fast and easy preparation of a wide variety of nanostructures that are otherwise laborious or impossible to fabricate.

Bibliography

1. E. J. Smythe, M. D. Dickey, G. M. Whitesides, and F. Capasso, A technique to transfer metallic nanoscale patterns to small and non-planar surfaces, *ACS Nano* **2009**, 3, 59-65.

2. G. F. Schneider, V. E. Calado, H. Zandbergen, L. M. K. Vandersypen, and C. Dekker, Wedging transfer of nanostructures, *Nano Lett.* **2010**, 10, 1912-1916.

3. M. A. Meitl, Z.-T. Zhu, V. Kumar, K. J. Lee, X. Feng, Y. Y. Huang, I. Adesida, R. G. Nuzzo, and J. A. Rogers, Transfer printing by kinetic control of adhesion to an elastomeric stamp, *Nat. Mater.* **2006**, 5, 33-38.

4. J.-H. Ahn, H.-S. Kim, K. J. Lee, S. Jeon, S. J. Kang, Y. Sun, R. G. Nuzzo, and J. A. Rogers, Heterogeneous three-dimensional electronics by use of printed semiconductor nanomaterials, *Science* **2006**, 314, 1754-1757.

5. M. C. McAlpine, H. Ahmad, D. Wang, and J. R. Heath, Highly ordered nanowire arrays on plastic substrates for ultrasensitive flexible chemical sensors, *Nat. Mater.* **2007**, 6, 379-384.

6. A. Javey, S. Nam, R. S. Friedman, H. Yan, C. M. Lieber, Layer-by-layer assembly of nanowires for three-dimensional multifunctional electronics, *Nano Lett.* **2007**, 7, 773-777

7. X. Liang, Z. Fu, and S. Y. Chou, Graphene transistors fabricated via transfer-printing in device active-areas on large water, *Nano Lett.* **2007**, 7, 3840-3844.

8. L. B. Gao, G. X. Ni, Y. P. Liu, B. Liu, A. H. C. Neto, and K. P. Loh, Face-to-face transfer of wafer-scale graphene films, *Nature* **2014**, 505, 190-194.

9. X. Li, W. Cai, J. An, S. Kim, J. Nah, D. Yang, R. Piner, A. Velamakanni, I. Jung, E. Tutuc, S. K. Banerjee, L. Colombo, and R. S. Ruoff, Large-area synthesis of high-quality and uniform graphene films on copper foils, *Science* **2009**, 324, 1312-1314.

10. X. Li, Y. Zhu, W. Cai, M. Borysiak, B. Han, D. Chen, R. Piner, L. Colombo, and R. S. Ruoff, Transfer of large-area graphene films for high-performance transparent conductive electrodes, *Nano Lett.* **2009**, 9, 4359-4363.

11. S. J. Kim, T. Choi, B. Lee, S. Lee, K. Choi, J. B. Park, J. M. Yoo, Y. S. Choi, J. Ryu, P. Kim, J. Hone, and B. H. Hong, Ultraclean patterned transfer of single-layer graphene by recyclable pressure sensitive adhesive films, *Nano Lett.* **2015**, 15, 3236-3240.

12. K. K. Liu, W. J. Zhang, Y. H. Lee, Y. C. Lin, M. T. Chang, C. Su, C. S. Chang, H. Li, Y. M. Shi, and H. Zhang, Growth of large-area and highly crystalline MoS_2 thin layers on insulating substrates, *Nano Lett.* **2012**, 12, 1538-1544.

13. A. Gurarslan, Y. Yu, L. Su, Y. Yu, F. Suarez, S. Yao, Y. Zhu, M. Ozturk, Y. Zhang, and L. Cao, Surface-energy-assisted perfect transfer of centimeter-scale monolayer and few-layer MoS2

films onto arbitrary substrates, *ACS Nano* **2014**, 8, 11522-11528.

14. Y. C. Lin, W. J. Zhang, J. K. Huang, K. K. Liu, Y. H. Lee, C. T. Liang, C. W. Chu, and L. J. Li, Wafer-scale MoS_2 thin layers prepared by MoO_3 sulfurization, *Nanoscale* **2012**, 4, 6637-6641.

15. W. Cheng, M. J. Campolongo, S. J. Tanb, and D. Luo, Freestanding ultrathin nano-membranes via self-assembly, *Nano Today*, **2009**, 4, 482-493.

16. T. Fujie, Y. Okamura, and S. Takeoka, Ubiquitous transference of a free-standing polysaccharide nanosheet with the development of a nano-adhesive plaster, *Adv. Mater.* **2007**, 19, 3549-3553.

17. S. Zhao, C. Hu, X. Chen, J. Zhou, Y. Jiao, K. Zhang, and Y. Fu, Transfer of inorganic thin films by soluble polymer layer for arbitrary surface coating, *Soft Matter* **2012**, 8, 937-941.

18. Q. Xu, R. M. Rioux, M. D. Dickey, and G. M. Whitesides, Nanoskiving: A new method to produce arrays of nanostructures, *Acc. Chem. Res.* **2008**, 41, 1566-1577.

19. D. J. Lipomi, R. V. Martinez, and G. M. Whitesides, Use of thin sectioning (Nanoskiving) to fabricate nanostructures for electronic and optical applications, *Angew. Chem. Int. Ed.* **2011**, 50, 8566-8583.

20. D. J. Lipomi, F. Ilievski, B. J. Wiley, P. B. Deotare, M. Loncar, and G. M. Whitesides, Integrated fabrication and magnetic positioning of metallic and polymeric nanowires embedded in thin epoxy slabs, *ACS Nano* **2009**, 3, 3315-3325.

21. T. W. Ebbesen, H. J. Lezec, H. F. Ghaemi, T. Thio, and P. Wolff, Extraordinary optical transmission through sub-wavelength hole arrays, *Nature* **1998**, 391, 667-669.

22. A. G. Brolo, E. Arctander, R. Gordon, B. Leathem, and K. L. Kavanagh, Nanohole-enhanced Raman scattering, *Nano Lett.* **2004**, 4, 2015-2018.

23. J. A. Hutchison, D. M. O'Carroll, T. Schwartz, C. Genet, and T. W. Ebbesen, Absorption-induced transparency, *Angew. Chem. Int. Ed.* **2011**, 50, 2085-2089.

24. A. G. Brolo, R. Gordon, B. Leathem, and K. L. Kavanagh, Surface Plasmon sensor based on the enhanced light transmission through arrays of nanoholes in gold films, *Langmuir* **2004**, 20, 4813-4815.

25. A. Lesuffleur, H. Im, N. C. Lindquist, and S.-H. Oh, Periodic nanohole arrays with shape-enhanced plasmon resonance as real-time biosensors, *Appl. Phys. Lett.* **2007**, 90, 243110.

26. T. Xu, Y.-K. Wu, X. Luo, and L. J. Guo, Plasmonic nanoresonators for high-resolution colour filtering and spectral imaging, *Nat. Commun.* **2010**, 1, 59.

Summary

One-dimensional nanowires possess unique characteristics so that they can play an important part as functional units in the fabrication of electronic, optical and sensing devices. Nanowires have high surface-to-volume ratio and large tolerance for mechanical deformation to be integrated into micro/nanoscopic systems for various applications. Although a number of approaches have been developed for the fabrication of nanowires, such as nanolithographic techniques, anisotropic crystalline growth, template-directed synthesis, vapor-liquid-solid phase growth, etc, they have issues with high-costs, the control of size, the fabrication of ultra-long nanowires, or the manipulation of single-wire. Nanoskiving is a cost-effect technique of nanofabrication that can simply and fast produce a number of high-aspect-ratio (>10000:1) nanowires directly from sectioning thin film. All three dimensions of these nanowires can be controlled according to practice. Meantime, each nanowire embedded in a polymeric slab is able to be transferred onto any substrate with accurate manipulation and alignment. Thus, gold nanowires fabricated by nanoskiving in this thesis, are expected as building blocks to be integrated into functional structures for applications.

First, nanogap electrodes composed of two millmeter-long gold nanowires were fabricated by nanoskiving in **Chapter 2**. Here, a sacrificial layer of aluminum is applied to form air-gaps to achieve metal/insulator/metal junctions. The width of the gaps can be precisely controlled by the thickness of aluminum spacer. It breaks the limitation of molecule-gap focused on the order of their length scale. For these air-nanogap junctions with different width of gap, the electrical measurements demonstrate that the current density through the junctions depends exponentially on the bias, and linearly on the width of the gap. These data indicate that the mechanism of charge transport is tunneling. Comparing to existing methods, we offer an exceedingly simple approach to fabricate air-gap electrodes that are directly addressable, requiring no addition lithography steps. No special equipment is needed to fabricate them—only an ultramicrotome that is much cheaper than conventional infrastructure. They can be made in large number with short

time consuming (at the rate of about one per second). In addition to providing control over all three electrode dimensions, many identical air-gap electrodes can be produced at a time, thus eliminating the need to image each individual electrode.

Following the fabrication of the air-gap electrodes, 1D, 2D and 3D plasmonic ultralong-gaps with tunable, sub-10 nm gap-widths were fabricated using the same method in **Chapter 3**. As the hot spots of each nanogap extend uniformly along macroscopic lengths, these nanogaps are robust to local defects or contaminants, facilitating more reproducible SERS spectroscopy. This reproducibility enables a systematic investigation of the dependence of electric field enhancement on gap-width, with the surprising result that it is non-monotonic in the range between 2 and 8 nm with a maximum at 5 nm. In agreement with FDTD simulations, the maximum SERS signal is obtained for this gap width. The surface patterning technique could be extended to fabricate a 2D patterned nanogap array on a horizontal plane with a higher integration. Furthermore, by stacking nanogaps along the vertical direction, 3D nanogap grids are easily constructed. The construction of 3D nanogap grids not only enlarges the gap density, but also improves the electric field enhancement at the crossing points. For a smaller stacking angle, the overlapping areas between gaps in a plane increase, and this generates stronger electric field enhancement. The 3D nanogap arrays based on nanoskiving and stacking of nanogaps along the vertical direction will broaden the scope of fabricating 3D complex nanostructures in a simple and efficient way.

In microfluidic devices, nanowire sensors are constrained to the walls of the channel, where the rate of flow is near zero. The lowest rate of flow limits the detection of biological and chemical species, or measurements of flow. Positioning a nanowire in the center of a microfluidic channel, where the rate of flow is the highest, allows experiments to be performed. However, fabricating the discrete, millimeter-long nanowires is necessary to place them in the center of the channel. In **Chapter 4**, the high-aspect-ratio gold nanowires can be placed directly onto a channel to sense the highest flow rate. The gold nanowire is suspended in a microfluidic channel, so it is sensitive enough to serve as

both the heating and sensing element to measure the change in resistivity. Binding DNA molecules to the gold nanowires similarly exposes the entire surface of the nanowire-DNA assembly to the carrier liquid, eliminating background signal from non-specific binding in fluorescence experiments and forming a curtain of DNA molecules along the nanowires. Because the rate of flow within the channel is highest away from the walls of the channel, flow-elongating the DNA molecules can reach maximum at low rates of flow.

In **Chapter 5**, a perfect transfer method is developed to use a film of polymer as carrier layer and aluminum as sacrificial layer to transfer and manipulate sections that are fabricated by nanoskiving. This transfer process is simple and fast, and keeps nanostructures embedded in sections intact and uniform without defects, cracks, and residues. Furthermore, a number of sections can be prepared one-at-a-time by ultramicrotome and saved to be used many times. This method, to some extent, circumvents the dependence of nanofabrication technology on specialized, expensive equipment. During positioning nanostructures, other materials (e.g., nickel for magnetic positioning) are not required. Meantime, the manipulation does not depend on the wettability of substrates and can eliminate the effect of capillary force. By successively stacking nanostructures, various 2D or 3D structures can be constructed that can improve the range of applications of nanoskiving. In addition, this process is applicable to other structures or arrays of structures as well.

Samenvatting

Eendimensionale nanodraden bezitten unieke eigenschappen waarmee zij een belangrijke rol kunnen spelen als functionele componenten bij de vervaardiging van elektronische-, optische- en detectieapparatuur. Nanodraden hebben een grote oppervlakte-volume verhouding en sterke tolerantie voor mechanische vervorming, wat ze uitermate geschikt maakt voor integratie in micro/nanoscopische systemen voor diverse toepassingen. Hoewel verschillende methoden ontwikkeld zijn voor het vervaardigen van nanodraden, zoals nanolithografische technieken, anisotropische kristallijne groei, matrijsgestuurde synthese, damp-vloeistof-vaste fase groei, etc, kampen deze technieken met tekortkomingen zoals hoge kosten, de controle op afmetingen, de fabricatie van lange nanodraden, of de manipulatie van enkele nanodraden. Nanoskiving is een kostenefficiënte nanofabricagetechniek waarmee snel en eenvoudig meerdere nanodraden met grote hoogte-breedteverhouding (> 10.000:1) geproduceerd kunnen worden. Nanodraden worden rechtstreeks gefabriceerd door een dunne (metalen)film in plakken te snijden waarbij alle drie de dimensies relatief eenvoudig beïnvloed kunnen worden. Elke nanodraad is ingebed in een plak matrixpolymeer en kan vervolgens met hoge nauwkeurigheid en uitlijning op elke ondergrond overgedragen worden. Verwacht word dat de in dit proefschrift gefabriceerde gouden nanodraden geïntegreerd gaan worden als bouwstenen in functionele structuren voor specifieke toepassingen.

Allereerst werden nanospleet elektroden vervaardigd, bestaande uit twee millimeter lange gouden nanodraden, gebruikmakende van nanoskiving in **hoofdstuk 2**. Hiervoor werd een aluminium offerlaag aangebracht tussen twee goudlagen zodat, na verwijdering van het aluminium door etsen, een metaal/isolator (lucht)/metaal verbindingen gerealiseerd werd. De afstand van de lucht-nanospleten kan nauwkeurig worden geregeld door de dikte van de aluminium tussenlaag te variëren. Bovendien zijn deze nanospleten zijn ordes van grootte langer dan molecuul gebaseerde nanospleten. Elektrische metingen van lucht-nanospleet juncties met variërende diktes van de

nanospleten, tonen aan dat de stroomdichtheid door de juncties exponentieel afhankelijk zijn van de bias en lineair afhankelijk zijn over de afstand van de spleet. Deze gegevens tonen aan dat het mechanisme van ladingstransport tunneling is. In vergelijking met bestaande methoden, bieden wij een zeer eenvoudige benadering voor het fabriceren van luchtspleet elektroden die direct adresseerbaar zijn, zonder gebruik van lithografie stappen. Er is geen speciale apparatuur nodig en alleen een ultramicrotoom, welke vele malen goedkoper is dan conventionele fabricage infrastructuren. Tevens kunnen nanodraden gemaakt worden in een kort tijdbestek (met een snelheid van ongeveer één per seconde). Naast het leveren van controle over de drie dimensies van de elektroden, worden meerdere identieke luchtspleet elektroden tegelijk geproduceerd, in tegenstelling tot lithografie technieken.

Na het vervaardigen van de luchtspleet elektroden, werden extreem lange 1D, 2D en 3D plasmonische nanospleten met controleerbare sub-10 nm spleetbreedtes gefabriceerd in **hoofdstuk 3**. Omdat de hot spots van elke nanospleet uniform verspreid zijn over macroscopische lengtes, zijn deze nanospleten bestand tegen lokale gebreken of verontreinigingen, wat beter reproduceerbare SERS spectroscopie mogelijk maakt. Deze reproduceerbaarheid maakt een systematisch onderzoek mogelijk van de afhankelijkheid van elektrische veldversterking op de spleetbreedte, met het verrassende resultaat dat deze niet-monotoon is in het bereik tussen 2 en 8 nm met een maximum bij 5 nm. Tevens word, in overeenstemming met FDTD simulaties, het maximale SERS signaal verkregen voor deze spleetbreedte. De oppervlak patroonvormingstechniek kan worden uitgebreid voor het fabriceren van een 2D nanospleet matrix patroon op een horizontaal vlak, met een hogere integratie. Verder kunnen 3D nanospleet roosters eenvoudig geconstrueerd worden door het stapelen van nanospleten langs de verticale richting. De constructie van 3D nanospleet roosters vergroot niet alleen de spleetdichtheid, maar verbetert ook de versterking van het elektrische veld op de juncties. Voor een kleinere stapelhoek, zal de overlappende gebieden tussen spleten in een vlak toenemen, en dit genereert hogere veldversterking. De 3D nanospleet matrixen gebaseerd op nanoskiving en het stapelen van nanospleten langs de verticale richting,

wordt de reikwijdte van het vervaardigen van complexe 3D structuren eenvoudig en efficiënt verbreed.

In microfluïdische apparaten worden doorgaans nanodraadsensoren beperkt tot de wanden van het kanaal, waarbij het debiet bijna nul is. De laage stroomsnelheid beperkt de detectie van biologische en chemische eenheden of metingen van de stroomsnelheid. Positioneren van een nanodraad in het midden van een microfluïde kanaal, waarbij het debiet het hoogst is, bied duidelijke voordelen. Het kanalen met millimeter lange nanodraden in het midden van het kanaal is hierbij noodzakelijk. In **hoofdstuk 4**, worden de gouden nanodraden met grote hoogte-breedteverhouding direct op een kanaal geplaatst om zo het hoogste debiet te kunnen meten. De gouden nanodraad wordt gesuspendeerd in een microfluïde kanaal, dus het is gevoelig genoeg om zowel te dienen als de verwarmings- en als detectieelement om de verandering in weerstand te meten. Door vervolgens DNA moleculen te binden aan de goud nanodraden word eveneens het gehele oppervlak blootgesteld aan de dragervloeistof. Hierdoor word het achtergrondsignaal van niet-specifieke binding in fluorescentie experimenten, en het vormen van een gordijn van DNA moleculen aan de nanodraden verminderd. Doordat het debiet middenin het kanaal het hoogste is, kan tevens stroom geïnduceerde verlenging van de DNA-moleculen gemaximaliseerd worden bij lagere stroomsnelheden.

In **hoofdstuk 5**, is een perfecte overdrachtsmethode ontwikkeld gebruikmakende van een polymeerfilm als drager, en aluminium als offerlaag, om secties vervaardigd door nanoskiving over te brengen en te manipuleren. Deze overdrachtsmethode is eenvoudig en snel, en houdt secties van nanostructuren ingebed in een drager intact en uniform zonder gebreken, scheuren, of residuen. Bovendien kan een aantal secties één-voor-één bereid worden met een ultramicrotoom en bewaard worden om later vele malen gebruikt te worden. Tot op zekere hoogte, omzeilt deze methode de afhankelijkheid van nanofabricage technologieën die afhankelijk zijn van gespecialiseerde en dure apparatuur. Tevens zijn overige materialen niet vereist tijdens het positioneren van de nanostructuren (bijvoorbeeld nikkel voor magnetische positionering). De manipulatie is

ook niet afhankelijk van de bevochtigbaarheid van de substraten en effecten zoals capillaire krachten worden geëlimineerd. Door nanostructuren achtereenvolgens te stapelen kunnen verschillende 2D- of 3D-structuren geconstrueerd worden wat de toepassingsmogelijkheden van nanoskiving verder kan verbeteren. Tot slot is deze werkwijze algeheel toepasbaar op andere structuren en matrixen voor de eenvoudige constructie van complexe componenten

Acknowledgements

Time flew in the past years although I still immerse myself in memories with pleasant, exciting, delightful, also anxiety moments. I have to say that this is an excellent experience in my life. I would like to gratefully acknowledge everyone who has given me help and support during my PhD period. After all, it is impossible that I am able to finish this project without the help and support. I am truly grateful for all the friends and colleagues I met.

First of all, I would like to express my deeply thanks to my supervisor Prof. Ryan C. Chiechi, who made my PhD studies in the Netherlands possible. Without his help and supports, this thesis would not have been accomplished. He is a brilliant man of wide learning, and his rigorous academic attitude for work and patience set up a good example for me. I learned a lot of science and how to find interesting point for a project from him. He always taught us in a friendly way no matter how stupid to understand one question. His laugh is still in my memory even I was back in China more than two years. I also would like to thank him for his training that have enriched me as an independent researcher and will definitely benefit me in my career. Ryan, it was great time for me to work with you in the first two years of my PhD period and thanks to you again for all your guidance and help.

I also would like to thank Prof. Kees Hummelen for his constructive suggestion in the group meetings.

I appreciate that the members of my reading committee Professor Jeff Th. M. de Hosson, Professor Jianting Ye, and Professor Hao Zhang spend your precious time and patience on my manuscript.

I would like to express my gratitude to Renate for all her help. She was always so nice to everyone and ready to help, both work and private things. And our technician Reinder, he has excellent ability to make tools, fix broken things, and provide support to all kinds of issues. And thank Alfred for his great help to the whole group.

Moreover, I take this opportunity to thank my colleagues in CBMD group who helped me greatly and I had good time with you. First, I need to thank Wenqiang for all of helps from the first day I was in Groningen to the end of my PhD both inside and outside of the lab. Next, I would like to give a special thanks to my colleague and co-promotor-like Parisa. She is very nice person with great knowledge and efforts for work. She is like a sister to teach me Nanoskiving and all other experiments that she knows and to give me a lot of help to integrate our group, when I was freshman to come to a strange country and face people with different language and skin. I have learned a lot from her working-hard and in doing good experiments. Davide, you are handsome (girls said), and thank you for your help in using evaporator, soft-lithography and revising my PPT for the Thursday Speaking. Thomas, thank you for translating the summary of this thesis into Dutch and best wishes to you for your defense in June. Thanks to Yanxi for all kinds of help after I left Groningen and for being my paranymph. Olga, it's nice to work with you during the beginning of your PhD. I would like to gratefully acknowledge the support of our group members. Thanks to Mehrnoosh, Jenny, Difei, Thijs, Bouke, Aim, Dan, Jim, Piet.

I also would like to thank my collaborators from Prof. Antoine van Oijen's group: Sarah and Machteld, and Prof. Elisabeth Verpoorte's group: Arno and Pieter.

在此，我还要感谢我的硕士生导师张刚教授一直以来对我的关心和指导，能够来到格罗宁根大学学习，是您提供的机会。

接下来我要感谢在格罗宁根的朋友们。首先是我刚刚到荷兰时候，经常聚在一起找家里感觉的朋友们，虽然刚开始大家做的东西都很难吃，但还是乐此不疲的享受。艳萍，娜娜，秋艳，朱蕾，洪浩，面团，然然，李明，杨朔和静祎，佳伟和孙鹤，金涛和林林，谢谢你们。

再者就是黄楼的战友们，你们让我学到了很多知识（虽然颜色各异）和见识，斗地主扎金花的技术也是你们培养的。强哥像大哥一样带着我一一引荐，领我入会，让我成为这个帮会的一员，是我坚实的靠山。作为帮中老大，子璘和考拉特别照顾我这个小弟，你们离开时候我分了好多你们的家产，对了，还有你们的小团子健康快乐哦。小铮铮，真正的师姐，怀念一起述说吉大，一起咖啡时间八卦的日子。飞哥，飞嫂和可爱的鲁子儿，喜欢听你正直的扯犊子，无论何时，打牌必应。斌哥，有了你从此去超市不用骑车了，八卦你跟你的妹子们，是我们的乐趣。凯哥，娟娟和小格格小荷荷，未来的院士，你要多注意自己的言行，不然很容易让人看到你内心的放荡。家文，蓓蓓和 Robin，从你那里开阔了视野，体会到了骚的味道。谢谢你们带给我的快乐。

格罗宁根足球队的队友们，让我在格村最后的半年焕发了第二春，每周末有了新的期待。张涛，军哥，飞哥，凯哥，国伟，杨朔，小泉，袁涛，李军，虎哥，田才，峥哥，刘庆，张峰，谢谢你们。其中，跟张涛，田才组成的酒吧小分队也是 happy 无限。

铮铮和阿阳，佳佳，大赵和坤坤，家文和蓓蓓，我们一起形成的这伙人的聚会给我的生活带来更多的精彩，人多八卦多，爱八卦的女人多，八卦更多，哈哈，谢谢你们。

对边哥一家，文君，超哥和小刘，小明，中涛夫妇，陈辉林师兄，徐瑾，小孟，威哥，刘允，尹旺等等在格村的朋友们一并谢过。

同时，对吉大超分子的多尺度组的各位师弟师妹，于也，紫薇，王立敏，艾斌，李元吉，谷盼盼，王增瑶，薛培宏，盛，树立，陈红旭，葛鹏，自博，赵晓欢，常玲霞等等表示感谢，谢谢大家对我的关照。

最后，最真挚的感谢给我的家人，感谢我的父母给予我生命，抚育我长大成人；特别感谢我的老婆，感谢她对我的爱，对我的理解和支持，异地不容易，但是我们坚持走下来，修成正果，爱你！